ESA/SCI(2017)4
March 2017

XIPE

X-ray Imaging Polarimetry Explorer

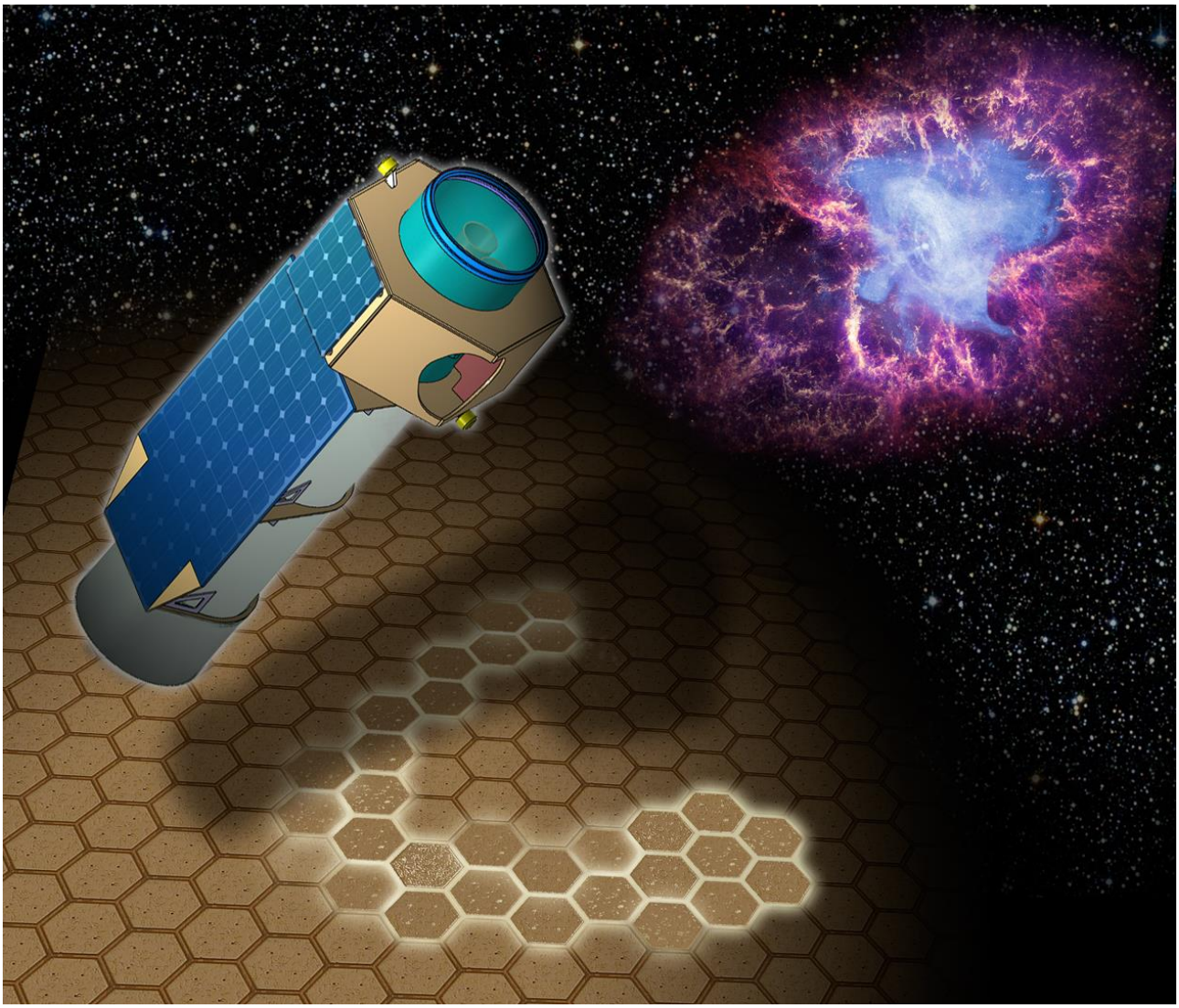

Assessment
Study Report

European Space Agency

The front page shows an artist's impression of the *XIPE* spacecraft together with one of its primary targets, the Crab nebula. The pixelized detector in the background illustrates how *XIPE* will measure the polarization of X-ray photons from the trajectories of the photoelectrons they produce.

XIPE **Assessment Study – Mission Summary**	
Key scientific goals	Obtain unique physical and geometrical information on basically all classes of X-ray sources through two still unexplored observables – the degree and angle of polarization. • **Particle acceleration processes**: map the magnetic field and locate acceleration regions in the Crab Nebula and other PWN, and in SNR; infer the magnetic field structure in jets, deriving jet composition in blazars and studying acceleration physics in GRBs. • **Emission in strong magnetic field**: derive vital information on accretion geometry and physical parameters in white dwarfs and neutron stars; constrain the equation of state of ultra-dense matter; understand the mechanism that triggers bursts in magnetars. • **Scattering in aspherical geometries**: definitely test if the black hole at the center of our Galaxy was active a few hundred years ago; constrain the geometry and origin of the X-ray emitting corona in AGN and Galactic accreting black holes. Study the geometry of wind flow in AGNs. • **Fundamental Physics**: observe vacuum birefringence in highly magnetized neutron stars; take advantage of General Relativistic effects to derive the spin of Galactic accreting black holes; search for Quantum Gravity signatures and Axion-like particles.
Reference core payload	The Payload consists of three identical X-ray telescopes with 4 m focal length and an instrument control unit. The mirrors have a total effective area of about 1500 cm^2 with an angular resolution better than 30". The Gas Pixel Detectors are designed as gas proportional counters but with a revolutionary readout, i.e. an ASIC CMOS chip developed to this aim. This readout allows us to measure the X-ray polarization of cosmic sources in the 2-8 keV energy range with high sensitivity by imaging the photoelectron track of each event. The energy resolution is 20% at 5.9 keV. The sensitivity (Current Best Estimate) is 1.2% for an intensity of $2x10^{-10}$ erg/s/cm^2 (10 mCrab) in 300 ks of net observing time (the requirement is 1.8%). Each Detector Unit comprises also a Filter and Calibration Wheel and the Back End Electronics that manages the ASIC, digitally convert the analogue signals, time-tag the events with a few μs resolution and perform the zero suppression. The Instrument Control Unit produces on-board a set of Quick Look data to be downloaded with high priority, used to monitor the on-going observations. It also formats and stores the data and sends them to the on-board data handling unit. The countries involved in the design and provision of the payload items are: Germany, Italy, Spain, United Kingdom, Poland. Involved in the study phase were also Sweden, Switzerland, the Netherlands, Finland and, to a small extent, also China.
Overall mission profile	*XIPE* is designed to be launched with a VEGA-C vehicle into an orbit of 550-630 km and <6° inclination. With this orbit, eclipses last about 35 minutes. The decay time is well above the nominal life time, extendable with a small amount of delta-v. Due to remaining spacecraft fragments the mission is planned to end by controlled re-entry. The baseline ground station is Kourou either for S/S or S/X telemetry band, albeit Malindi (or Singapore) is additionally available, if necessary, for additional downloading capability in case of particularly bright sources. The mission duration is 3+2 years. *XIPE* will perform consecutive slews and long exposure pointings while the observing plan includes also snapshot pointings for monitoring purposes. Target of Opportunities are also foreseen with a reaction time below 12 hours in working days and hours. The data policy foresees that 25% of the time is dedicated to a Core Program while the remaining 75% is dedicated to a competitive Guest Observing program.
Description of the spacecraft	The Spacecraft is composed by a Payload module and a Service module. The first hosts the focal plane, the second hosts the three mirrors. They are connected by a telescope tube maintained at a constant temperature of 20° C. Two industrial studies assessed the feasibility of the mission design with this satellite configuration. The Service Module surrounds the 3 mirrors. The focal plane platform will be accommodated at the other end of the telescope tube. The solar panel, of about 6.7 m^2, will be fixed and either configured as a single body-mounted panel or composed of two sections with one deployed after launch. The field of regard corresponds to ½ accessibility of the sky at any time. The spacecraft is 3-axis stabilized with reaction wheels. Science and housekeeping data are stored in a 228 Gbit memory. The dry mass at launch is 1430 kg, including contingency. The required power in the observation mode is 1050 W.

Foreword

Despite the many spectacular successes in the more than fifty years long history of X-ray Astronomy, our knowledge of X-ray emitting sources is still sorely incomplete. For almost all of them, in fact, and with the notable exception of the two brightest sources in the X-ray sky (the Crab Nebula and the accreting neutron star Sco X-1) we lack information on one fundamental characteristic of the radiation – polarization. Without knowing the polarization degree and angle, vital physical and geometrical information is missing, often leading to severe model degeneracies. Given that many X-ray sources are characterized by non-thermal emission processes and/or by radiation transferred in highly asymmetric systems, it is immediately clear that X-ray polarimetric observations would often be crucial, much more than at longer wavelengths. Indeed, as discussed in the Scientific Objectives section, almost all classes of X-ray sources are expected to benefit from polarimetric measurements. Key information on phenomena like e.g. particle acceleration, radiative transfer in strong magnetic fields (including vacuum birefringence, a QED effect predicted 80 years ago but still to be unambiguously verified) and in deep gravitational potential wells, and scattering in aspherical geometries, is encoded in the polarization of X-ray photons. X-ray polarimetry may even be used to test Quantum Gravity theories and to search for Axion-like Particles.

The only two currently available measurements, mentioned above, were obtained in the 1970s with non-imaging, narrow-band Bragg polarimeters. No X-ray polarimeters were part of the payload of space missions afterwards. Fortunately enough, highly efficient X-ray polarimeters based on the photoelectric effect have recently became available which, coupled with high throughput, long-heritage, focusing mirrors, result in a dramatic increase in sensitivity. The **X-ray Imaging Polarimetry Explorer (*XIPE*)** is designed to bring X-ray polarimetry into full maturity by providing astrophysically significant polarimetric measurements (time, spatially and spectrally resolved) for hundreds of targets. This will allow us to extend the observations to all classes of X-ray sources of interest, and to observe many sources in each of them, searching for correlations of the polarimetric properties with the main parameters of the class. Such an approach is crucial to fully understand the nature of these sources.

The *XIPE* proposal was submitted in response to the ESA call for M4 missions and selected, in June 2015, for a phase A study. The activities included an internal ESA study and two parallel industrial studies, which were completed in early 2017. These studies did not only confirm the feasibility and high Technology Readiness Level of *XIPE*, they also led to several improvements with respect to the original proposal. Among them: a larger effective area (30 mirror shells instead of the original 27), a longer focal length (4 meters instead of 3.5), a larger Field of Regard (50% of the sky instead of 30%). Scientific performances were correspondingly enhanced, and *XIPE* now has a better sensitivity over the whole band, an improved capability to observe transient phenomena and to perform coordinated observations with ground-based facilities.

The original Science Case has been revised, extended and sharpened by a Science Team, composed by more than 350 scientists worldwide, and structured in thematic Working Groups. Extensive simulations were performed to assess quantitatively the ability of polarization measurements to extract physical and geometrical information and to distinguish between competing models. One of the main results of this work is the confirmation that the baseline mission duration of 3 years is adequate, with some margin, to reach the main scientific goals. A possible extension of 2 years will permit to explore more challenging and/or uncertain science objectives, as well as to increase the statistical quality of the population studies. It is worth mentioning that a number of our targets need to be observed in a particular flux or spectral state. In the pessimistic case that no external facilities will be operating at the time of *XIPE* to provide the relevant triggers, a monitoring program of up to 12-14 sources, to be observed at regular cadence with very short exposures, is foreseen to assess their state. The 12 h repointing time will then allow us to go promptly to the target, if needed, as well as to point to unexpected, externally triggered events.

In summary, the studies have demonstrated that *XIPE* is a simple, mature and low risk mission fully able to achieve its ambitious science goals.

Authorship, acknowledgements

This report has been prepared by the *XIPE* Team listed below.

ESA Science Study Team (SST)		
Name	*Affiliation*	*City, Country*
Paolo Soffitta (Lead Scientist)	*INAF-IAPS*	*Rome, Italy*
Bellazzini Ronaldo	INFN	Pisa, Italy
Courvoisier Thierry	University of Geneva	Geneva, Switzerland
Goosmann Rene	Astronomical Observatory of Strasbourg	Strasbourg, France
Matt Giorgio	University Roma Tre	Rome, Italy
Reglero Victor	University of Valencia	Valencia, Spain
Santangelo Andrea	University of Tuebingen	Tuebingen, Germany
Tagliaferri Gianpiero	INAF-OA Brera	Milan, Italy
Vink Jacco	University of Amsterdam	Amsterdam, The Netherlands
Zane Silvia	MSSL/UCL	London, United Kingdome

The ESA Team supporting the activities is composed by:

ESA study team		
Andrea Santovincenzo (Study Manager)	ESA/ESTEC	Noordwjik, The Netherlands
Dave Lumb (Study Scientist)	ESA/ESTEC	Noordwjik, The Netherlands
Oosterbroek Tim (Payload Lead)	ESA/ESTEC	Noordwjik, The Netherlands
Jonan Larranaga (System Engineer)	ESA/ESTEC	Noordwjik, The Netherlands
Ivo Ferreira (System Engineer)	ESA/ESTEC	Noordwjik, The Netherlands
Jan-Uwe Ness (Science Ops Study Manager)	ESA/ESAC	Madrid, Spain
ESA Coordinator		
Luigi Colangeli	ESA/ESTEC	Noordwjik, The Netherlands

The XIPE SST is grateful to all XIPE Science Working groups, who made it possible to accurately refine the mission science objectives and prepare the detailed scientific sections of this Yellow Book. A list of all contributing scientists is available at: http://www.isdc.unige.ch/XIPE/science-team.html. The SST is particularly grateful to the Science Working groups leaders and chairs for their continued effort, together with F. Muleri and E. Bozzo for their dedication to the editing of the Yellow Book.

We are also grateful to all our instrument teams and all other members of the XIPE consortium (http://www.isdc.unige.ch/XIPE/consortium-members.html) for their precious contributions throughout the mission assessment study phase.

Table of contents

1 Executive summary

In its more than fifty years long history, X-ray astronomy has brought enormous progress to our understanding of the hot and energetic Universe. The physics of compact objects, astrophysical jets or explosive phenomena could not have been explored or, often, even been discovered without X-ray observations. In spite of these successes, however, large aspects of the physics of the X-ray sources remain unknown, since, for almost all of them, we are lacking information on one fundamental characteristic of the radiation – polarization. In fact, polarimetry adds two more observables, in addition to the direction, energy and arrival time of every photon: the degree and angle of polarization. The former gives direct insight into the emission mechanism and the geometry of the source, while the latter may often provide the only way to measure the orientation of the system (e.g. the magnetic dipole axis with respect to the rotation axis in binary pulsars), the orientation of the ionization cone with respect to the putative torus in AGNs or the orientation of the disk or corona in black-hole binaries. Without their measurement, our knowledge and understanding of most classes of X-ray sources is necessarily incomplete.

Indeed, since the beginning of X-ray Astronomy - with the discovery that many X-ray sources were characterized by non-thermal emission processes and/or by radiation transferred in highly asymmetric systems - it was immediately clear that polarimetry would be crucial, even more than at longer wavelengths. However, X-ray polarimetry is still an undeveloped astrophysical probe. Only two highly significant measurements exist so far. These were obtained in the 1970s with non-imaging, narrow-band Bragg polarimeters: a spatially-averaged measurement of the Crab Nebula, and a tight upper limit to the accreting neutron star Sco X-1. Since then no X-ray polarimeters were part of the payload of space missions. Fortunately, highly efficient X-ray polarimeters based on Gas Pixel Detectors (GPD) and using the photoelectric effect have recently become available. When coupled with high throughput focusing mirrors, these detectors allow for a dramatic increase in sensitivity. The **X-ray Imaging Polarimetry Explorer (*XIPE*)** is one of the missions exploiting this technique to bring X-ray polarimetry into full maturity *by providing astrophysically significant measurements for hundreds of targets, including the brightest objects of almost all classes of X-ray sources.*

Among the astrophysical processes for which X-ray polarimetric observations are crucial, **particle acceleration** plays a prominent role. This is most evident in the prototypical cosmic accelerator, the Crab pulsar wind nebula. Comparison of X-ray images with those at lower energies shows that the former bring direct evidence of freshly accelerated particles. As mentioned above, the Crab is the only source for which a high spatially-averaged X-ray polarization (19%) was measured in the early days. But *Chandra* images show a complex structure and therefore the total polarization is the sum of several distinct, highly polarized emitting regions that must be analyzed separately. *XIPE*, equipped with spatially resolved polarimetric capabilities, will perform such a detailed polarimetric map of the Crab nebula. *XIPE*'s imaging capability is also crucial for shell like supernova remnants, another well-established site of particle acceleration, as it can separate the thermalized plasma from non-thermal (synchrotron) components and thus locate the region of ordered magnetic field on the site of shock acceleration. This will provide unique direct evidence on the place where cosmic rays are accelerated, and determine how ordered the magnetic field is. Not less important, *XIPE* will also study the acceleration processes in jets in both Galactic and extragalactic sources: microquasars, blazars and radiogalaxies. Comparison with polarization at lower frequencies will allow us to understand the magnetic field structure in the jet. In those blazars in which X-rays are part of the high energy peak, polarimetry will constrain the composition of the jet (leptonic vs. hadronic) and, if leptonic emission will turn out to be dominant, it will also determine the origin of the seed photons of the Inverse-Compton emission. *XIPE*'s ability to repoint within 12 hours (down to 8 in the most favourable conditions) will allow us to search for polarimetric signatures in the afterglow of at least a few bright γ-ray bursts, a crucial information to understand particle acceleration, emission physics and magnetic fields in their expanding jets.

High levels of polarization are expected in aspherical geometries. **Strong magnetic fields** in accreting white dwarfs and neutron stars, which funnel the accreted plasma along the field lines, provide such geometries. Unique information on the geometry and physics of the accreting column and the magnetosphere can be obtained through X-ray polarimetry. Yet unknown key aspects of these systems will be unveiled: the geometry of the emission in accreting millisecond pulsars, necessary to measure the mass-to-radius ratio, and then constrain the equation of state of ultra-dense matter in neutron stars; the structure of the accreting column in

magnetized white dwarfs and neutron stars; the geometrical parameters of the magnetosphere in magnetars, crucial to understand the mechanisms that trigger their powerful outbursts. Most fascinating of all, however, is the possibility to observe vacuum birefringence in highly magnetized neutron stars, a QED effect predicted 80 years ago but yet to be unambiguously verified.

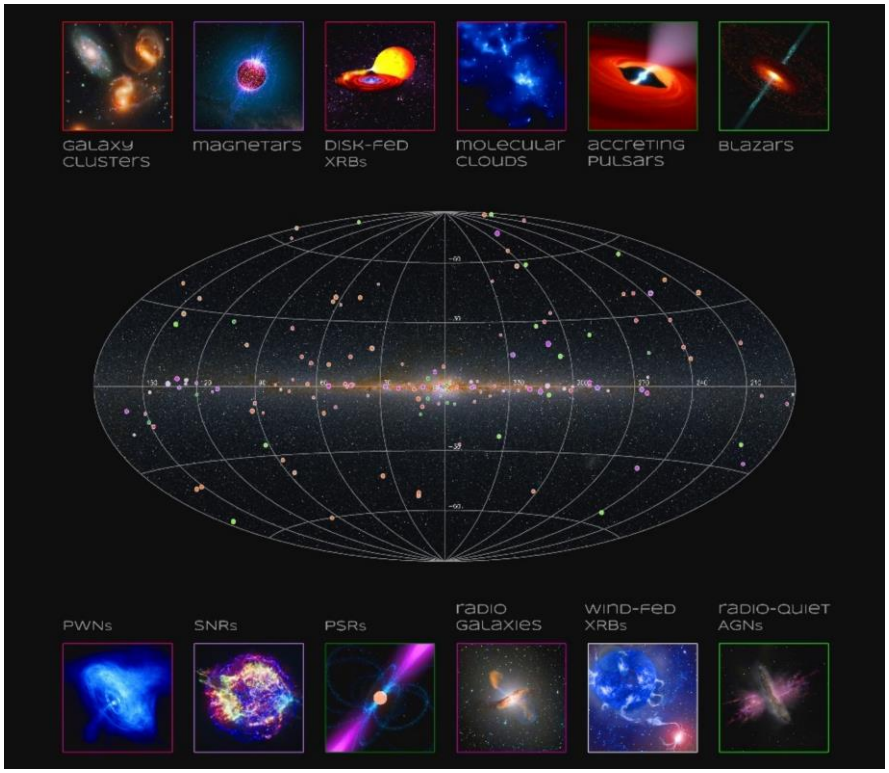

Figure 1-1 XIPE will provide a large number of polarization measurements for many classes of X-ray sources. At present, only the spatially averaged X-ray polarization measurement of the Crab nebula is available, together with a tight upper limit to the polarization of the accreting neutron star Sco X-1.

Scattering in aspherical geometries also produces high level of polarization. A case of peculiar interest is that of the molecular clouds around the supermassive black hole in the centre of our Galaxy. The polarization degree and angle will determine whether these X-ray bright clouds shine because they reflect the past activity of the presently quiet black hole at the Galactic centre, and therefore provide the ultimate proof that a few hundred years ago the centre of our Galaxy was millions times more active than now. The geometry of the X-ray emitting corona in Active Galactic Nuclei (AGN) and Galactic black holes can also be determined by *XIPE*. Broad band spectral measurements by *NuSTAR* provide the coronal physical parameters (temperature, optical depth) but their geometries, which are key to understand their nature and origin (disk perturbations, aborted jet, …), are virtually unknown. In Galactic Black Hole systems, when in soft state, a continuous change with energy of the polarization angle of the Comptonized disk thermal emission due to General Relativity (GR) effects is expected. The amplitude of the effect depends on the spin of the black hole, which can therefore be measured.

The above mentioned QED and GR effects are not the only examples of the use of X-ray polarimetry to probe **fundamental physics**. In fact, X-ray polarimetry provides a tool to test theories predicting birefringence effects as a function of energy and cosmic distance. Such effects are predicted by some Quantum Gravity theories and can be tested by observing distant polarized sources like blazars. This kind of observations, and even more the search for polarization in otherwise unpolarized sources like Clusters of Galaxies, will also enable the search for Axion-like Particles, one of the most elusive, even if least exotic, candidates to be the dark matter particle. While these measurements are admittedly challenging, they are potentially very rewarding and, at least partly, are by-products of observations that will be made for different purposes.

Although *XIPE* has been conceived and designed to address the specific scientific goals outlined above, it is well possible – indeed likely - that many breakthroughs will arrive from unexpected quarters. This is a general feature of many ambitious space projects, but even more so in the case of *XIPE*: as the first mission to survey the polarimetric properties of hundreds of targets belonging to all classes of X-ray sources, it has inevitably also an exploratory nature, with a great potential for discoveries and surprises. The nominal mission duration is three years, although the extension of the planned operations will not be limited by any technical payload or spacecraft constraint except extremely modest propellant volume. Given that the exposure time per target will

range from a few thousands seconds to ~1 Ms, with a typical value of 200-300 ksec, *XIPE* will be able to observe 150-200 targets during its nominal lifetime. This will allow us to reach our scientific goals with some margin on the minimum available exposure time. In particular, it will be possible to observe, for most classes of sources, several objects to search for differences and commonalities among them, and to explore correlations with system parameters. Moreover, there will be room to observe variable sources more than once, to search for changes in the polarimetric properties with the source state.

The observing program will include a Core Program (25% of the total available time), ensuring that the main scientific goals of the mission will be achieved, but all available *XIPE* Guest Observing exposure time will be competitively assigned through peer reviewed proposals. It is important to remark that some of the key *XIPE*'s targets will be transient, i.e. variable in flux and/or spectral state. For the case of γ-ray bursts or previously unknown transient sources, we expect to get alerts by missions dedicated to this science or featuring large field of view instruments that will be operating at the time of *XIPE*. For the most important 12-14 recurrent transient sources for which the location is already known, a dedicated monitoring program is being planned including a number of periodical short pointings (300-500 s) to verify the source status. A large fraction of the available observational time will still be at disposition for the world-wide scientific community in order to ensure that competitive new ideas will find their way into the observing program.

Early in 2017, when this document was being completed, the IXPE (Imaging X-ray Polarimeter Explorer) mission was selected by NASA in the Small Explorer (SMEX) program. The NASA SMEX program selects missions within tight budget and schedule constraints; IXPE is due for launch in 2020. While *XIPE* and IXPE are qualitatively similar in terms of instrumental set-up, as both of them plan to exploit the same technology (the GPDs) for spatially-resolved polarimetric measurements in the X-ray domain, *XIPE* provides two important improvements over IXPE:

a) The effective area of *XIPE* is almost a factor of two larger than that of IXPE. Therefore, to reach the same accuracy in the polarization measurements IXPE needs, for a given source, about twice the exposure time. This implies that the most demanding observations by *XIPE* require unrealistic exposure times with IXPE. More relevant, the *XIPE* observing program, based on a 3-years mission duration, would require about 6 years for IXPE to be completed. The nominal IXPE mission duration is 2 years; its in-orbit lifetime will depend on the actual orbital altitude, but the best current estimate is 4.3 years before re-entry. Therefore, it is likely that IXPE will not be able to perform an observing program as ambitious and articulated as *XIPE*'s. In particular, it will be difficult for IXPE to explore, within a certain class of X-ray sources, the correlations of the polarization properties with the various parameters, which of course would require the observation of several sources in the class. Moreover, an observing plan based on previous results, on a richer sample and on a longer time scale is more suited to set up campaigns of set up monitoring, possibly multi-frequency campaigns, extremely important in some cases, most notably for blazars. Needless to say, these studies are vital for a comprehensive understanding of the physics and geometry of X-rays sources.

b) The minimum time for repointing with IXPE is 48 hours, to be compared with the current <12 working hr requirement for *XIPE*. This requirement implies that if a request for a fast repointing arrives early during the nominal working hours of ESA (9:00 -18:00) from Monday to Friday, a repointing of the spacecraft could be completed in about 8 hours, a sufficiently short time to obtain a meaningful measurement of the polarization degree in bright GRB afterglows. With *XIPE*, we estimate that at least a handful of such observations can be performed. No such observations are possible with IXPE.

To summarize, while IXPE is expected to explore the polarization properties of the brightest sources of several X-ray classes, *XIPE* will extend the *exploratory phase* of X-ray polarimetric studies to fainter objects and therefore new classes. Based on IXPE's heritage, *XIPE* will built an optimized observing program able to bring the field to a *mature phase* by performing population studies and extending the observations to more challenging celestial targets (e.g., the GRB afterglows).

2 Scientific objectives

The linear polarization of electromagnetic radiation quantifies to which extent the electric field vector, ***E***, oscillates along a preferred direction. For a maximum polarization fraction P=100%, ***E*** would have a fixed direction (Fig. 2-1, top left). The angle between the northern direction of the sky and ***E*** defines the polarization position angle Ψ. Of course, astrophysical sources usually have much lower polarization fraction. As a rule of thumb, the net polarization fraction rises with the degree of geometrical asymmetry of the system while the polarization direction points out preferred axes in the source morphology, and such measurements can provide key unique information about cosmic phenomena.

Strong polarization up to a theoretical limit of P≈75% comes from synchrotron emission originating in ordered magnetic fields. In most synchrotron sources, such as pulsar wind nebulae (PWNe), supernova remnants (SNRs), or the jets in μ-quasars and active galactic nuclei (AGN), X-rays are emitted by the highest-energy electrons located at sites where the plasma is most strongly energized. The X-ray polarization is a unique tracer of the magnetic field at these locations. If the field is completely disordered on the probed spatial scales, the net polarization washes out and Ψ is basically undefined (Fig. 2-1, bottom left). The same holds true for thermal emission in regions of weak magnetic field.

Nonetheless, unpolarized radiation can acquire significant polarization by scattering. This is illustrated in Fig. 2-1 (right) where a beam of radiation induces dipole emission from scattering electrons. This is a key mechanism to decode the emission and reprocessing geometry inside a given source from its polarization properties. In non-spherical geometries the resulting radiation must withhold a net polarization.

Some X-ray sources harbour extreme physical conditions. According to theoretical prediction the very strong magnetic field in certain rotating neutron stars should cause quantum-electrodynamic vacuum birefringence that can only be verified by X-ray polarimetry. Furthermore, curved space-time around black holes in X-ray binaries and AGN rotates the polarization direction of X-rays emitted close to the event horizon. This gives us access to independent estimates of the black hole spin.

The two polarization observables (P, Ψ) can be taken as a function of wavelength and time. The *XIPE* mission would also spatially resolve a number of PWNe, SNRs and even AGN jets adding a dependence of (P, Ψ) on the position in the sky. In summary, (P, Ψ) are two more independent constraints on the morphology and physics of X-ray sources, in addition to established imaging, spectroscopic and timing information: without them, our knowledge of a source is inevitably incomplete.

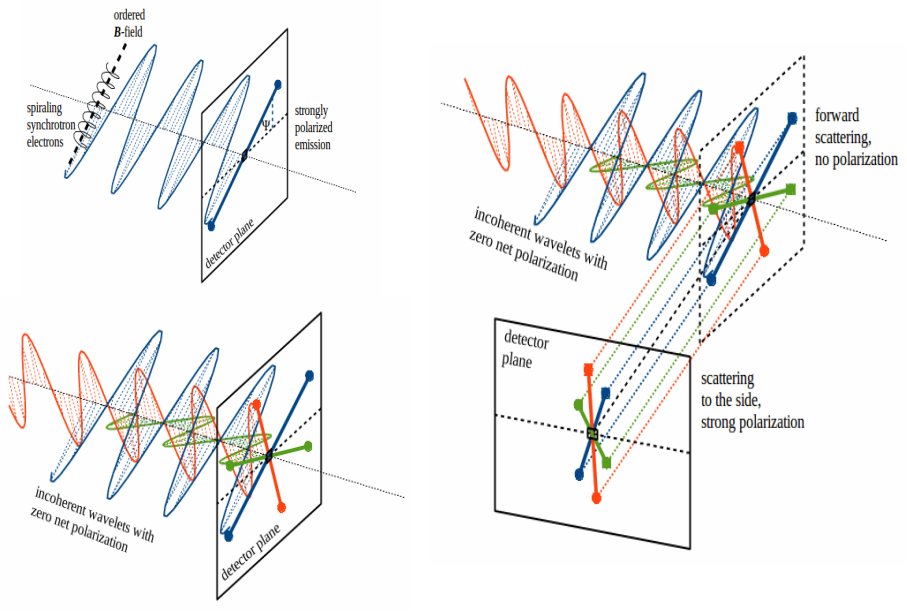

Figure 2-1 Polarization of coherent (top left), incoherent (bottom left) and scattered (right) radiation.

So far, the only X-ray polarimetric observations were taken in the 1970s using a non-imaging Bragg reflection polarimeter aboard OSO-8. A handful of the brightest Galactic X-ray sources were accessible to this instrument, which measured a significant net polarization of P=19% for the Crab nebula [274] and a tight upper limit of about 1% to the polarization of Scorpius X-1 [273] – not surprisingly, the brightest X-ray sources in the sky. Since then, the detector technology has greatly improved so that *XIPE* will be able to observe hundreds of galactic and extragalactic sources.

In the following, we lay out a number of astrophysical questions which can be solved with X-ray polarimetric information at the quality that *XIPE* can provide. We show that *XIPE* can make contributions to several fields of astrophysics and fundamental physics greatly supporting studies on almost all classes of X-ray sources and even enriching research on Quantum Gravity and Dark Matter. Finally, it is important to bear in mind that opening a new observational window leaves space for the yet unknown.

We often use the Minimum Detectable Polarization (MDP) defined as the minimum polarization degree that can be measured by *XIPE* at a significance level of 99% for a given source and exposure time (see Sect. 3).

2.1 Particle acceleration processes

Acceleration phenomena dominate the energy output of many X-ray sources, but the underlying acceleration mechanisms remains unclear. Fermi acceleration between magnetic mirrors on the up- and downstream sides of a shockwave (first-order) or between randomly moving magnetic mirrors (second order) plays an important role. The magnetic field and its level of turbulence is a key ingredient in the Fermi process as well as in reconnection events between neighbouring magnetised plasma tubes with opposite polarity. Reconnection triggers the change to a less energetic magnetic configuration efficiently accelerating particles. So far, a detailed knowledge of the magnetic field geometry, its level of turbulence and its strength on different spatial scales is most often missing leaving the acceleration mechanism unconstrained.

Progress requires a complete observational picture. Polarimetry at radio, infra-red and optical/UV wavelengths tells us about the structure and the level of turbulence of the magnetic field at different spatial scales – but X-ray polarimetry has the advantage to probe accelerated particles very close or even directly at the injection sites. The very short synchrotron relaxation time at X-ray energies reduces eventual depolarization effects along the line of sight and therefore allows us to probe the acceleration conditions at the shortest accessible spatial scales.

Imaging X-ray polarimetry is vital to understand the structure and turbulence level of the magnetic field in extended sources like Pulsar Wind Nebulae and Supernova Remnants. Without the polarization observables, our understanding of the acceleration mechanisms and matter interactions in such sources – the acceleration sites of the all-pervading cosmic rays - is necessarily incomplete.

In accreting compact objects, like radio galaxies and μ-quasars, X-ray polarimetry establishes the contribution of jets to the X-ray emission. In X-ray synchrotron-dominated blazars it probes the structure of the jet and constrains the acceleration mechanism, while in other blazars it provides answers to questions as fundamental as the composition of the jet (letponic vs. hadronic). If Inverse Compton is at work in a leptonic jet, *XIPE* conclusively determines the origin of the seed photons, which is the major missing piece to complete the puzzle of their Spectral Energy Distribution.

While challenging in terms of slewing time and/or faintness of the sources, *XIPE* observations of transient phenomena, like γ-ray bursts and tidal disruption events are nevertheless important and intriguing enough so that no efforts will be spared to get significant measurements for at least a few events.

2.1.1 Pulsar Wind Nebulae

XIPE will constrain the plasma dynamics inside the subcomponents of several young PWNe, verify if the relative orientation between rotational and magnetic axes of pulsars in evolved PWNe correlates with the nebula morphology, and test recent MHD models potentially solving the long-standing sigma-problem.

Pulsar Wind Nebulae (PWNe) are bubbles of relativistic particles and magnetic field formed by the interaction of the relativistic Pulsar Wind with the surrounding Supernova Remnant (SNR). They are among the most efficient particle accelerators in our Galaxy [189], [268] and emit synchrotron radiation in the X-ray band. At present, the Crab Nebula is the only astronomical source with a high-confidence X-ray polarimetric measurement of P=19.2±1.0%, [274]. Furthermore, past *INTEGRAL* results [57], [81] suggest a high level of soft γ-ray polarization.

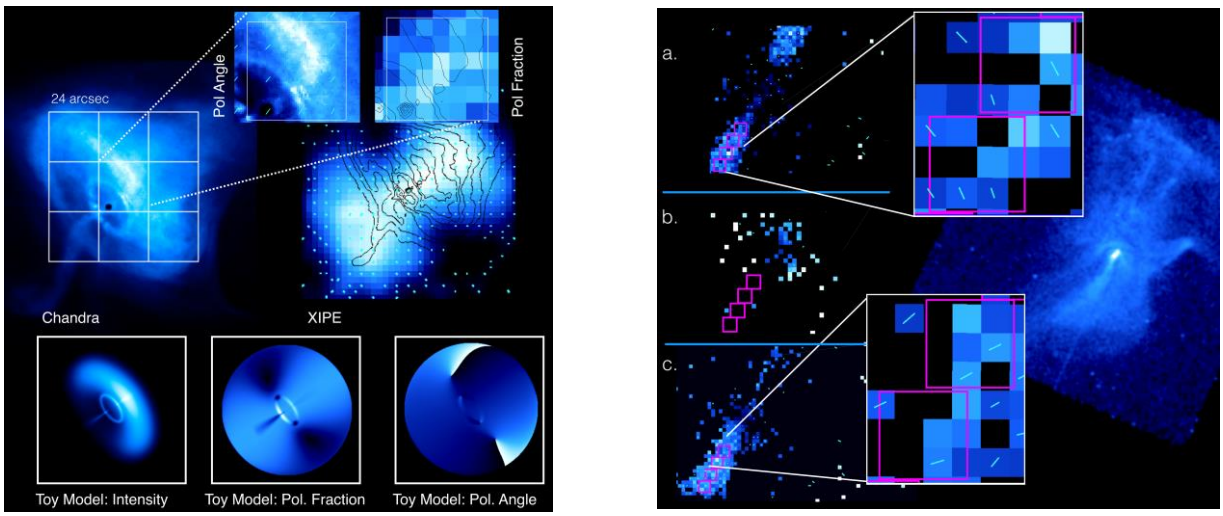

Figure 2-2 Left: Simulation of the Crab Nebula as seen by XIPE in 0.2 Msec. The toy model mimics the Chandra image for a given polarization angle and fraction. The reconstructed XIPE intensity image on the right is magnified on the top and shows the optimal reconstruction of the polarization characteristics inside 8×8 arcsec^2. The light blue lines show the reconstructed direction. Their size scales with polarisation degree. This demonstrates XIPE's capability to discriminate between different hypotheses). Right: Simulations of the PWN MSH 15-52 as seen by XIPE in 2 Msec. The images a, b, and c show the expected intensity map when applying three different polarization models to the Chandra intensity map and using the spectrum reported by [10]. The toy models consist of a jet and torus structure for the B-field, with an ordered toroidal component plus (a.) a fully ordered radial B-field, (b.) a fully disordered B-field and (c.) a fully ordered perpendicular B-field. Image (a.) and (c.) include a magnified sub-panel to show the reconstructed direction of the polarization.

The magnetic field in PWNe can be probed by optical and radio polarimetry. It is well-ordered with *P* as high as 60%, i.e. close to the theoretical limit. X-rays are produced close to where the synchrotron electrons are accelerated. Therefore, they provide a much cleaner view of the sites of active particle acceleration than optical observations, which moreover suffer from depolarizing foreground effects. Detailed morphological studies with *Chandra* revealed a complex structure of PWNe, such as, e.g., the torus-plus-jet structure in the Crab Nebula [272], quite different from the morphology observed at longer wavelengths. In general, young pulsars show an axial symmetry around what is believed to be the pulsar rotation axis [143], [123], [58], [28].

Spatially-resolved observations with *XIPE*, at its angular resolution of ≤30", will determine the magnetic field orientation and the level of turbulence in the torus, the jet, and at various distances from the pulsar (see Fig 2-2, left). This is of special interest because the polarized emission is more sensitive to the plasma dynamics in PWNe than the total synchrotron emission [31]. Knowing how the level of turbulence changes with distance from the shock could test recent MHD scenarios invoking the conversion of magnetic energy into particle energy inside the radiation region [204]. Moreover, comparing X-ray to optical polarization for the inner bright features [182] may clarify if particle acceleration sites and mechanism(s) at different energies coincide [233], [193].

The sigma-problem: from a magnetically to a kinetically dominated wind. Since the first MHD description of the plasma flow in the Crab Nebula [119], the low level of magnetization immediately upstream of the pulsar wind's termination shock remained unexplained. This defines the so-called sigma problem. To reproduce the Crab Nebula's morphology, recent 3D MHD modelling [204] predicts energy equipartition between the accelerated particles and the magnetic field at the shock front. Kink instabilities would cause the magnetic field to become progressively more tangled. Dissipation thus would happen in the bulk of the nebula, i.e. in the emitting region, rather than in the non-radiative cold pulsar wind. The expected level of X-ray polarization in such a scenario is lower than for alternative models. X-ray polarimetry offers the best possible tool to investigate this scenario, which, if proven correct, would solve the sigma-problem and additionally provide new insights into the relativistic plasma dynamics of PWNe. The potential of *XIPE* to describe the magnetic structure of the Crab nebula is illustrated in Fig. 2-2 (left) featuring a toy model of the nebula morphology to simulate a 0.2 Msec *XIPE* observation.

Probing the morphology of the pulsar wind: jets, tori, and sub-structures. Differently from young pulsars, more evolved systems rather show a "crushed" morphology that is due to the interaction between the PWN and the host SNR. Still, a wide diversity in morphology and time variability is found within both classes of young and evolved systems; PWNe around pulsars with similar characteristics may show striking differences when compared with each other. A likely explanation for this relies on the relative orientation between the spin and magnetic dipole axes. If this relative orientation evolves systematically with PWN morphology, it would also cause a systematic evolution of the polarization position angle and fraction. *XIPE* simulations of three different scenarios (see Fig 2-2, right, for a simulated 2 Msec *XIPE* observation of MSH 15-52) show its outstanding response to different values of (P, Ψ). The polarization features are convolved with the detailed *Chandra* image and reflect three different toy models. The observational errors are below 0.1% and by more than 10σ within the instrument PSF of *XIPE*. Interestingly, recent observations have measured an apparent helical motion in some jets (or misaligned outflows), which might be related to kink instabilities or pulsar precession [64], [161]. Resolving the jet's magnetic structure with *XIPE* will allow us to distinguish between the two hypotheses. As precession can be related to oblateness, this also provides a scheme to identify certain pulsars as potential sources of gravitational waves.

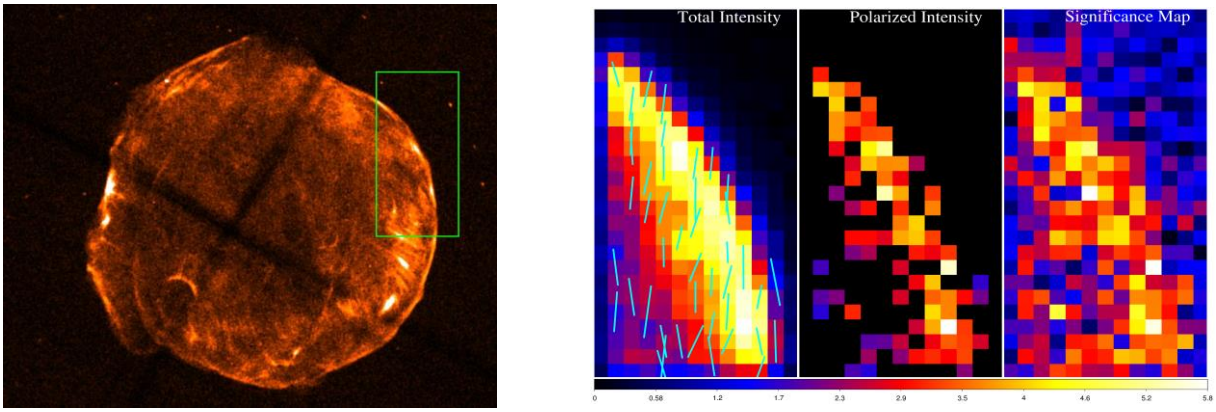

Figure 2-3 End to end simulation of a portion of Tycho's SNR, using a theoretically calculated polarisation maps as input for XIPE Monte Carlo simulations including the instrument responses in the 4-6 keV continuum band. Left: Chandra image of the Tycho SNR. Right: the total intensity, polarised intensity (polarised fraction times intensity – only pixels with a detection significance >3σ are shown), and significance map obtained from the Monte Carlo simulations.

2.1.2 Supernova Remnants

XIPE will be able to image in spatial detail the turbulence level of magnetic fields and thereby constrain theories of diffusive shock acceleration in SNRs and their contribution to Galactic cosmic rays.

Young supernova remnants (SNRs) are relativistic particle accelerators and the most likely sources of Galactic cosmic rays. X-ray synchrotron emitting regions in SNRs have been identified in several sources (see [97] for a review), proving that electrons are accelerated up to 10-100 TeV. At such energies, the time scale of radiation loss is very short so that X-ray synchrotron emission only occurs in regions of active particle acceleration: the SNR shock fronts.

The X-ray synchrotron emitting regions can be very narrow, their widths being a measure of the average strength of the magnetic field. In some cases, like for Cas A, Tycho's SNR and Kepler's SNR, the filaments are arc seconds wide and can only be resolved by the *Chandra* satellite. The filament widths indicate magnetic field strengths of 100-500 μG ranging well above the Galactic field strength of ~5 μG and indicating strong magnetic field amplification [19]. Irrespective of the magnetic field strengths, X-ray synchrotron emission can only occur for fast shocks (>3000 km/s). It requires small mean free paths for the relativistic electrons and therefore very turbulent magnetic fields.

XIPE can explore the turbulence level of the magnetic field, which plays a crucial role in theories of diffusive shock acceleration, and determines whether protons, accelerated under the same conditions as electrons, can

be accelerated up to energies beyond 100 TeV [34]. The latter is needed to explain the processes in collisionless shocks which otherwise cannot be studied in laboratories [146].

Polarized X-ray emission could be detected from Tycho's SNR with the sensitivity and angular resolution of *XIPE* and would provide unique constraints on models of diffusive shock acceleration with efficient magnetic field amplification in SNRs. The left panel of Fig. 2-3 shows the 4-6 keV X-ray image of Tycho's SNR constructed from a 1 Ms *Chandra* observation. Most of the emission in the 4-6 keV band is expected to be of synchrotron origin. The rectangular region was selected in the observed *Chandra* image to produce a simulated *XIPE* image of the polarized emission within the frame of the diffusive shock acceleration model.

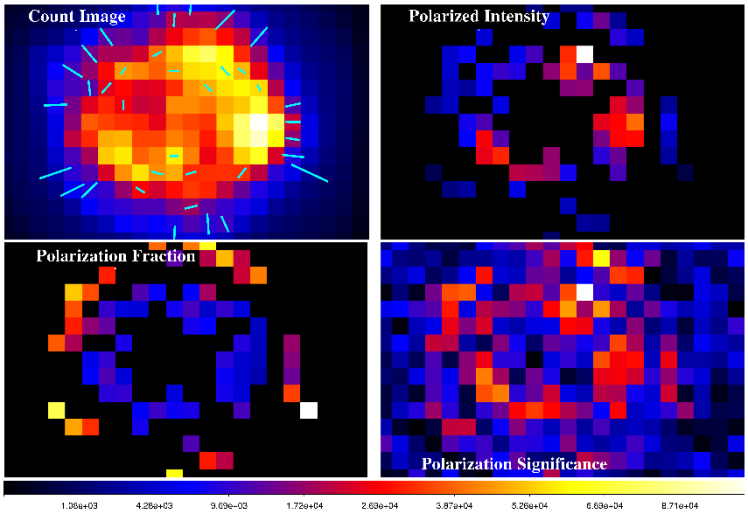

Figure 2-4 Modelling the XIPE view of the synchrotron filament structure in Cas A, showing its ability to map the polarization structure (see text).

The simulated three panels on the right show the total intensity in 4-6 keV, the polarized intensity (being the product of the total intensity and the degree of polarization), and the degree of linear polarization (indicated in the colour bar) respectively, convolved with the angular resolution of *XIPE*. To test the ability of *XIPE* to image the narrow filaments seen in the 4.1-6.1 keV continuum band of Cas A, we again constructed simulated *XIPE* observations (see Fig. 2-4). In Cas A there are also interior filaments associated with the reverse shock [98]. As an educated guess, we assumed a polarization fraction of 20% for the outer shock filaments and of 4% for the interior continuum emission. To assess the effects of blending, due to the PSF, we assigned a tangential polarization angle to the interior and a radial orientation to the outer filaments. Remarkably, even though the narrow outer rim cannot be resolved with *XIPE*, the images for the polarization fraction / polarized intensity show that the rims can be detected thanks to its distinct polarization pattern. The interior of the SNR has a lower polarization degree in the simulations, but given the higher brightness the polarization can be detected also here (see the bottom-right panel for polarization detection significance).

Apart from Tycho's SNR and Cas A, both of which fit *XIPE*'s field of view, the satellite can observe other X-ray synchrotron emitting shell-type SNRs. This will allow us to assess the polarization properties as a function of magnetic field strength and SNR size. SN 1006 and RX J1713.7-3946 are obvious other targets, but e.g. Kepler's SNR, RCW 86 and G1.9+0.3 also ought to be observed.

2.1.3 Jets in Blazars and radio-loud Active Galactic Nuclei

XIPE, in conjunction with observations at longer wavelengths, determines the jet structure and the acceleration mechanism in HSP blazars. In LSP and ISP blazars, XIPE discriminates between leptonic and hadronic models and determines the origin of the seed photons in leptonic jets. It images the structure of the magnetic field inside the X-ray emitting regions of Centaurus A and M87, the closest radio galaxies to Earth.

Blazars are a very peculiar type of Active Galactic Nuclei (AGN, powered by efficient accretion onto the supermassive Black Hole, SMBH, residing at the center of galaxies). They are defined by strong variability of non-thermal radiation from radio to γ-rays. Their Spectral Energy Distribution (SED) is composed of two broad peaks, the lower energy one being due to synchrotron radiation. Blazars are then subdivided into high (HSP), intermediate (ISP) and low (LSP) synchrotron peaked sources, depending on whether the synchrotron emission peaks in X-rays, the optical or the IR band, respectively. The remarkable properties of blazars include superluminal apparent motion – as high as 40c or more [115], [139] – substantial changes in flux and linear

polarization on time scales as short as minutes, and extremely variable high-energy luminosities that can exceed those at lower energies by several orders of magnitude.

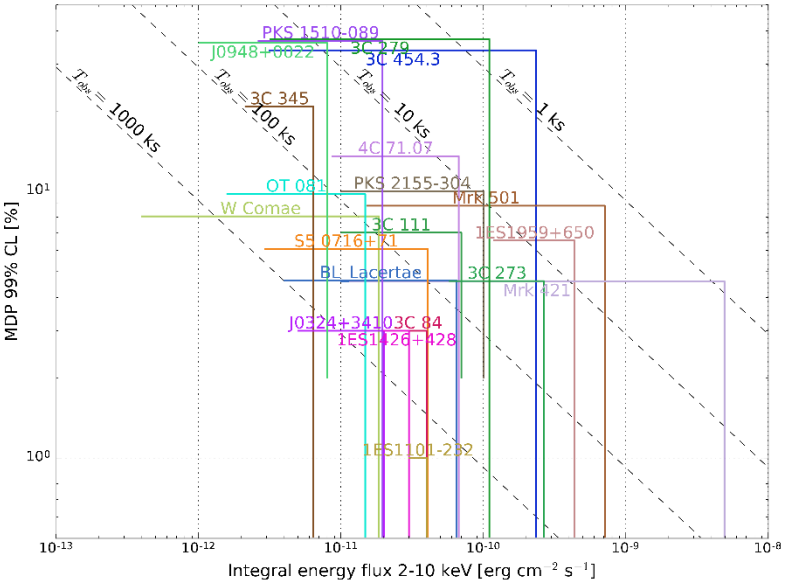

Figure 2-5 XIPE sensitivity plot: integration times to reach a given MDP for a point-like source with a corresponding total flux in the range [2,10] keV. The coloured right-angle wedges symbolize the range of observed total flux as a function of observed range of optical polarization degree for a given blazar or NLSy1 source. The polarization fraction was taken here as an upper limit of the expected X-ray polarization degree. This upper limit represents a realistic prediction of the actual polarization degree of HSP BL Lacs, e.g. the objects 1ES1959+650, Mrk 421, and Mrk 501. Their linear polarization can be measured by XIPE in integration times between a few tens and a few hundreds of ks.

These phenomena rely on relativistic jets of highly energized, magnetized plasma that are propelled along the rotational axes of the SMBH-disk system (e.g., Blandford & Payne 1982). They are believed to be physically similar in all kinds of jetted astrophysical objects, either associated with supermassive black holes (as in AGN and tidal disruption events) or with stellar-mass black holes in micro-quasars and gamma ray bursts. AGN jets pointing within less than about 10º of our line of sight beam their radiation and shorten the variability time scales to give blazars their extreme properties.

Given their brightness and expected high polarization degree, *XIPE* can obtain significant polarimetric measurements in many blazars within modest exposure times (see Fig. 2-5). Among the many problems that *XIPE* can help to solve, we name: the role of magnetic fields in jet launching and collimation; the jet composition (leptonic, e-e$^+$, versus hadro-leptonic, e-p$^+$, or simply hadronic); the dominant mode of particle acceleration; and the actual process of high-energy emission. It is important to point out that many of the measurements described in this section require coordinated polarimetric observations at longer wavelengths. Indeed, blazar science is the only case in which such observations are crucial. Radio, mm-wave, IR and optical coordinated polarimetric campaigns on blazars already exist, many of them lead by members of the *XIPE* consortium (e.g., [4], [5], [6], [11], [12], [131], [139], [215]). It will be a straightforward possibility for *XIPE* to join these efforts.

HSP. The X-ray synchrotron emission case. The optical synchrotron emission from blazars is polarized, typically between ~3% and ~30%. A perfectly ordered ***B***-field in the optical emission region would result in polarization fractions of ~70-75%.

Hence, the observations indicate a partially disordered magnetic field over the size of the dominant optical emission region. In HSP BL Lac objects (e.g. 1ES1959+650, Mrk 501, and Mrk 421), the X-ray emission is dominated by the high-energy end of the synchrotron component and is therefore expected to yield a similar polarization fraction. The X-ray polarization may be even stronger if the X-ray emission regions are smaller than the optical ones as suggested e.g. in [156] and [290], [291]. Therefore, HSP BL Lacs offer the chance to measure the relative size of the X-ray emitting regions with respect to the optical and radio ones as well as the magnetic field properties in the most energetic blazar zone.

XIPE also has the potential to measure fast polarization angle swings by more than 180° like those frequently observed in blazars in the optical, e.g. [132]. If such rotations happen always in the same sense, they can be directly associated to the underlying helical magnetic field, which could be measured in the innermost regions of the jet with *XIPE* observations in the case of HBLs, see [129].

HSP. Turbulent blazar models: constraining the particle acceleration mechanism. In an effort to explain the superposition of erratic variability and systematic trends in blazars, [156] proposed that the erratic aspect

of blazars is caused by turbulence in the jet which, combined with shocks, can explain the observed fluctuations in polarization and red-noise power spectra of flux variations (e.g., [45], [46], [2]).

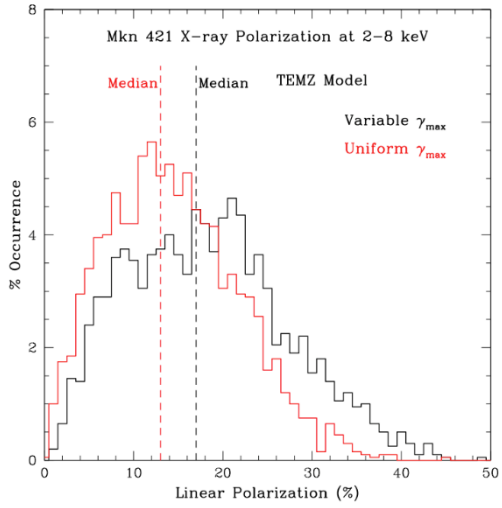

Figure 2-6 Histogram of time-variable X-ray polarization from Mrk 421 expected for two different versions of a turbulent jet model [156]: maximum electron energy dependent on magnetic field direction relative to the shock front (black) and independent of field direction (red). A single-zone model (e.g., magnetic reconnection) predicts X-ray polarization similar to optical, with median ~6%.

The model predicts that for a given value of the observed optical polarization in HSP blazars the median X-ray polarization depends on which particle acceleration process occurs in the jet. Statistical results of multiple X-ray and optical polarization measurements for a given HSP blazar can therefore determine which of the above-mentioned electron acceleration processes operates. The specific predictions are: (a) Single-zone model (reconnection): similar X-ray and optical polarization; (b) simple shock compression: the smaller X-ray volume causes higher median X-ray than optical polarization and greater fluctuations (Fig. 2-6, red); (c) Shock compression + diffusive particle acceleration: even smaller X-ray volume causes even higher median X-ray than optical polarization and greater fluctuations (Fig. 2-6, black).

LSP and ISP. Leptonic against hadronic X-ray emission. While the radio through optical/UV non-thermal emission from blazars is well understood to be synchrotron radiation from relativistic electrons in the jet, the origin of the high energy emission (down to X-rays in ISP and LSP) is still under debate. In leptonic models, the high energy emission results from Compton scattering of various soft radiation fields by the same population of electrons producing the synchrotron radiation (see below). Hadronic models require also the acceleration of protons to ultra-relativistic energies ($E_p \geq 10^{17}$eV) to dominate the high-energy radiation output via proton synchrotron radiation and synchrotron emission of secondary particles resulting from photo-pion interactions and subsequent electromagnetic cascades.

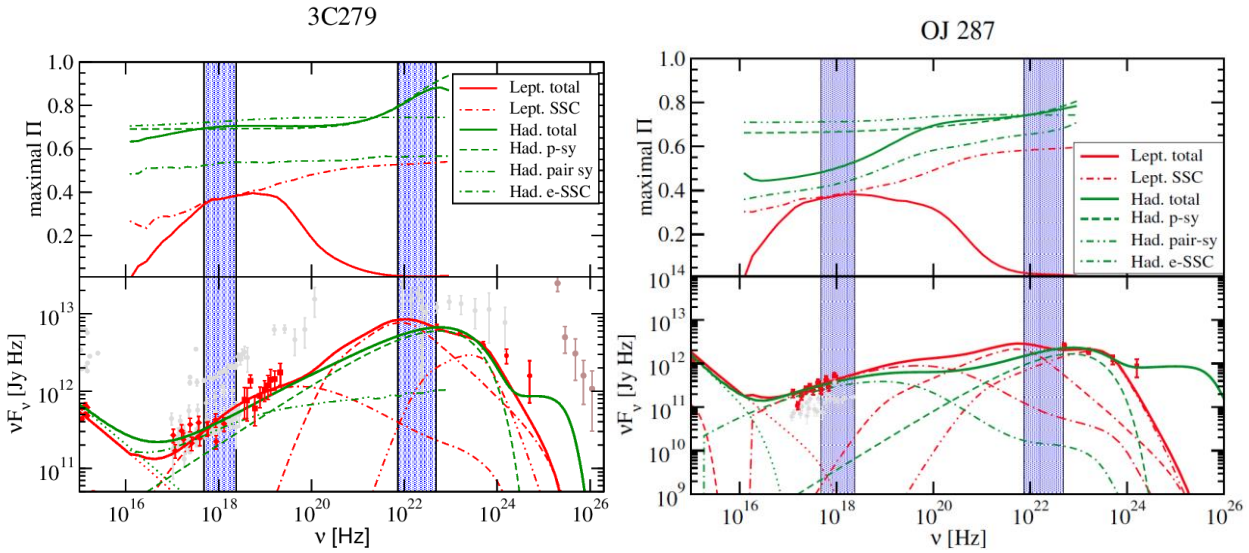

Figure 2-7 Frequency-dependent polarization of 3C279 and OJ 287 in the case of a leptonic (red) and a hadronic (green) single-zone model. Lower panels: Fits to the UV *– γ-ray Spectral Energy Distribution with both models. Upper panels: Maximum percentage of polarization (assuming a perfectly ordered B-field) as a function of frequency. These predictions can be re-scaled to a realistic B-field configuration using the observed optical polarization. X-ray polarization from both 3C279 and OJ 287 can be detected by XIPE under the assumption of a similar polarization degree as in the optical range (i.e. hadronic emission models, see text). From [289].*

Leptonic and hadronic models have different implications on the origin and acceleration of ultra-high-energy cosmic rays and possibly the origin of the TeV-PeV IceCube neutrinos, e.g. [201]. The two scenarios also predict different total jet energetics and mechanisms for jet launching and acceleration. Finally, they imply different modes of particle acceleration requiring large magnetic fields and extremely efficient acceleration for hadronic processes. SED fitting alone is unable to distinguish between the two models, and the cleanest signature of hadronic processes, i.e. the identification of blazars with the sources of TeV-PeV neutrinos, remains unfeasible in the foreseeable future. On the other hand, [289] showed that, for ISP and LSP blazars, hadronic high-energy emission is expected to exhibit a polarization degree that is comparable to the (optical) synchrotron radiation, while a lower polarization degree is expected in the case of leptonic models (e.g. Fig. 2-7). Highly polarized (>30%) X-ray emission with polarization angle changes similar to those seen in the optical, would unambiguously and for the first time identify a hadronic origin of the high-energy emission.

LSP and ISP. Leptonic emission: SSC versus EC X-rays. For LSP sources, in the case of a leptonic origin of the high-energy emission, the high-energy radiation is a combination of synchrotron-self-Compton (SSC) and external-Compton (EC) emission, the latter caused by scattering of seed photons originating from outside the jet, such as the broad-line emission or the IR radiation of a dusty torus. The SSC radiation is expected to exhibit about 1/2 of the polarization degree as the original (synchrotron) seed photon population that can be measured in the optical, yielding a maximum of ~15% polarization degree, with a polarization angle identical to the synchrotron radiation [42], [165]. Conversely, in the EC emission case the polarization angle relates to jet axis rather than to the magnetic field [18]. This provides a simple, but powerful, tool to make for the first time unambiguous measurements of the relative relevance of SSC emission against EC in the X-ray spectra of leptonic jets in blazars.

Jets physics in non-blazar radio-loud AGN. Contrary to blazars, in non-blazar radio-loud AGN the jet is directed away from the line-of-sight and can be, for the closest and brightest candidates, directly imaged in X-rays on arcmin scales. The imaging capabilities of *XIPE* will bring crucial clues concerning the physical properties of the jet. Indeed, the expected polarization signature strongly depends on the emission process at the origin of the jet X-ray emission. If it is synchrotron emission, as in the case of low-power radio galaxies such as Centaurus A and M87, the baseline model is that the polarization should be similar to the radio-optical, provided the emitting regions at the different ranges are co-spatial. Any deviations from this model would imply a complex magnetic topology and stratification of the outflows with high-energy (X-ray emitting) particles distributed in different regions and experiencing different magnetic fields than lower-energy (radio and optical emitting) particles (e.g. [283]). For X-rays produced by inverse-Compton scattering (EC or SSC), the expected polarization depends mainly on the seed photon field. For SSC the incoming photon field is polarized giving rise to polarized X-rays (e.g. [128]). Observations of bright, radio-loud AGN jets will allow us to discriminate SSC from EC processes (e.g. [39]). Furthermore, simulations show that *XIPE* will even offer

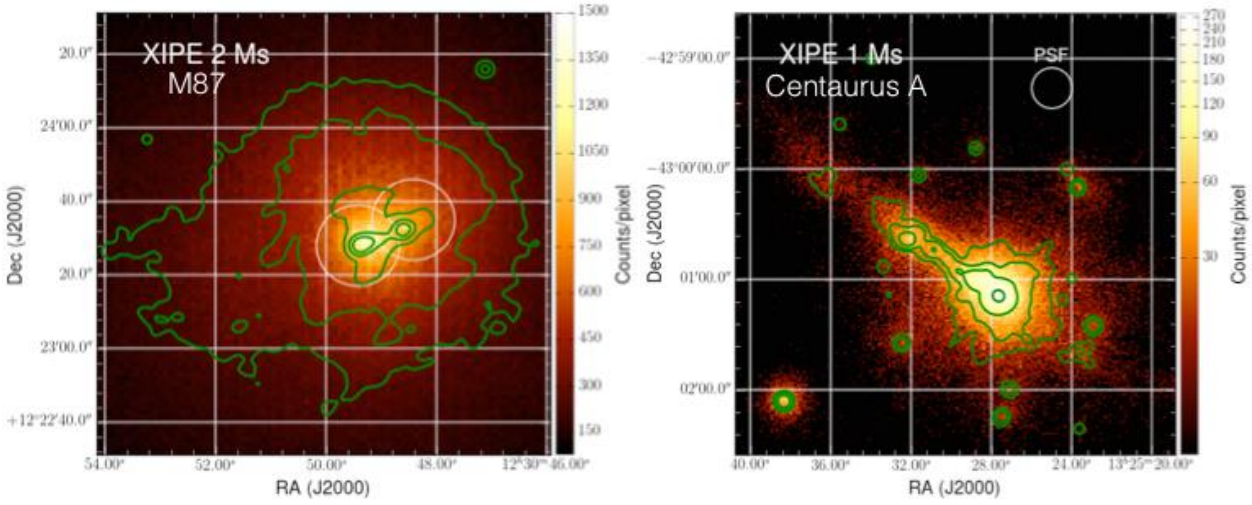

Figure 2-8 Simulation of a 2 Ms (left) and 1 Ms (right) XIPE observation of M87 and Centaurus A, respectively. The green contours correspond to the Chandra image and the white circles to the XIPE PSF. Assuming a jet X-ray polarization of 20% and a polarization angle parallel to the jet axis, the errors on the measured polarization degree and angle are expected to be of 25% and 10°, respectively, in most parts of the jet.

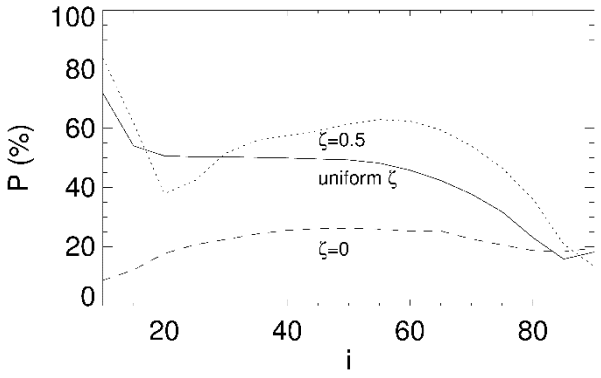

Figure 2-9 Monte Carlo simulations of the X-ray polarization arising from photons scattered by energetic electrons in black hole jets at relativistic bulk speeds, including Comptonization of disc photons as well as scattering of the intrinsically polarized synchrotron photons emitted within the jet (Synchrotron-Self-Compton, SSC). Shown here is the expected polarization degree P of SSC X-ray photons as a function of the jet inclination angle i. The solid line refers to the case of a uniform seed photon field throughout the jet (uniform ζ), whereas the dashed and dotted lines are for seed photons emitted at the jet base (ζ=0) and along the jet (ζ=0.5), respectively. Regardless of the model parameters, a minimum polarization degree of 10 per cent is expected, in stark contrast to the few per cent level expected from disc Comptonization. (adapted from [165]). A 100 ksec XIPE exposure will detect polarization degrees of the order of 1% or less for a handful of nearby Galactic microquasars, including the prototypical high mass black hole X-ray binary in Cygnus X-1.

the possibility to perform for the very first time spatially-resolved polarimetry along the jet for sources like M87 or Centaurus A within a reasonable exposure time of 1-2 Ms (Fig. 2-8).

2.1.4 Micro-quasars

XIPE will be able to discriminate jet emission in micro-quasars/X-ray binaries during different spectral states and thereby constrain the relative importance of X-ray power dissipated by the accretion and ejection flows. Furthermore, XIPE will investigate systematic differences in X-ray polarization between black hole and neutron star systems and follow jet precession in SS443.

Owing to the nearly ubiquitous presence of relativistic radio jets in the so-called hard state of Galactic X-ray binaries, all such sources can be thought of as "micro-quasars" or "μ-quasars" [179], [76]. *XIPE* will be able to solve the long-standing puzzle about the physical nature of their hard X-ray emission. Scenarios with Comptonization of thermal/quasi-thermal disc photons in a hot electron-positron corona compete with synchrotron models of a relativistic jet (see Section 2.3.2 on X-ray binaries for a complementary discussion on the nature of the non-thermal emission in X-ray binaries). Comptonization models predict polarization fractions up to ~10%. Synchrotron emission from the base of a magnetized jet, which in turn can "subsume" the role of the corona [154] are expected to yield polarization fractions well exceeding 10-20% per cent (e.g., [42], [165]; see Fig. 2-9). Hence, high sensitivity X-ray polarization measurements will break this degeneracy.

The high mass black hole X-ray binary and micro-quasar system Cygnus X-1 may provide one of the best examples for what *XIPE* can accomplish for Galactic jet sources. Repeated, multi-wavelength campaigns undertaken over the course of the last two decades, and making use of coordinated campaigns from the radio all the way to the gamma-ray band, have gathered a plethora of high-quality spectral data covering different accretion modes of the system. Yet, in spite of such massive data acquisition and modelling efforts, the contribution of the relativistic jets to the X-ray portion of the spectrum remains a matter of contentious debate. It was shown early on that, jet models provide as good of a description to the broadband radio-X-ray spectrum of Cygnus X-1 as single-component corona models [154].

The recent claim of high level polarization (exceeding 75% between 370 and 850 keV) in the gamma-ray spectrum of Cygnus X-1, as measured by the IBIS and SPI instruments aboard *INTEGRAL* [133], [116] would suggest that the γ-ray emission originates from the same relativistic jet that is resolved at GHz frequencies. [222] argue that the multi-wavelength flux and polarization spectrum of Cygnus X-1 in the hard state are broadly consistent with a simple phenomenological model including a strongly polarized synchrotron jet, a virtually unpolarized, Comptonizing corona, plus a moderately polarized interstellar dust component, where the X-ray polarization signature arises from optically thin synchrotron emission at the jet base.

Nevertheless, in the absence of high-confidence, energy-dependent, polarimetric measurements, the nature of the X-ray emission in this and other systems remains controversial [288], [144], [91]. Thanks to their nearby distance and relatively high luminosity there is a handful of Galactic sources for which an MDP lower than

1% can be reached in less than 1 day of observation. As also discussed in Section 2.3.2, a 180 ksec *XIPE* observation of Cygnus X-1 will yield a per-cent level measurement of the energy-dependent polarized flux. This will at once: i) discriminate between inverse Compton vs. synchrotron emission, and, ii), in the former case, discriminate between spherical vs. wedge coronal geometries. A similar experiment can be carried out for several other Galactic micro-quasars (such as GRS1915+105, GX339-4, Cygnus X-3, Circinus X-1, Sco X-1, SS433) with medium (1-2 day) exposures, thereby providing us with a robust estimate of the relative energetic importance of the accretion flow with respect to the relativistic outflow. It is worth stressing that the integrated, radiative power from the radio jets of micro-quasars is typically dwarfed by the integrated X-ray power emitted by the disk/corona system. However, if the X-ray emission originated from the base of the jet itself, this would require a paradigm shift, implying that the relativistic outflow dominates the power output.

With a carefully planned observational campaign (~100 ks pointings taken in different states after internal and/or external triggers), it will also be possible to chart polarization changes associated with different spectral states. Aside from testing the jet contribution to the X-rays in the hard state, this will yield polarization constraints on the X-ray power law that persists during the soft state, when the compact, relativistic jets are suppressed. While quasi-thermal Comptonization has long been thought to be at the origin of such a component, the possibility remains that a highly relativistic "spine" jet may survive during the soft state, giving rise to high polarization fractions.

Finally, the list of targets includes dynamically confirmed black holes (e.g., Cygnus X-1 and GRS1915+105) as well as known and/or likely neutron star systems (such as Cir X-1 and SS433), so as to investigate any systematic difference between different classes of accretors. The micro-quasar SS443, in particular, features spectacular, large-scale, bi-conical jets. Optical and X-ray emission lines arising from the jets are seen to shift in energy as the jets precesses around their axis with an opening angle of approximately 25° [173]. An exposure of 1 Msec would cover ~10 per cent of the jets' precession period (160 days), enabling us to disentangle the polarization signature from the core vs. the jets by measuring phase-dependent changes.

2.1.5 Gamma Ray Bursts

XIPE may detect, for the first time, the 2-8 keV polarization of bright GRBs and thereby allow us to study particle acceleration, emission physics and magnetic fields in the expanding jets of GRBs during the late-time flares, plateau or re-brightening phases.

Gamma Ray Bursts (GRB) are the instantaneously most luminous explosions in the Universe and are thought to be produced by the birth of stellar-mass black holes during the death throes of massive stars or the merger of compact objects such as black holes and neutron stars.

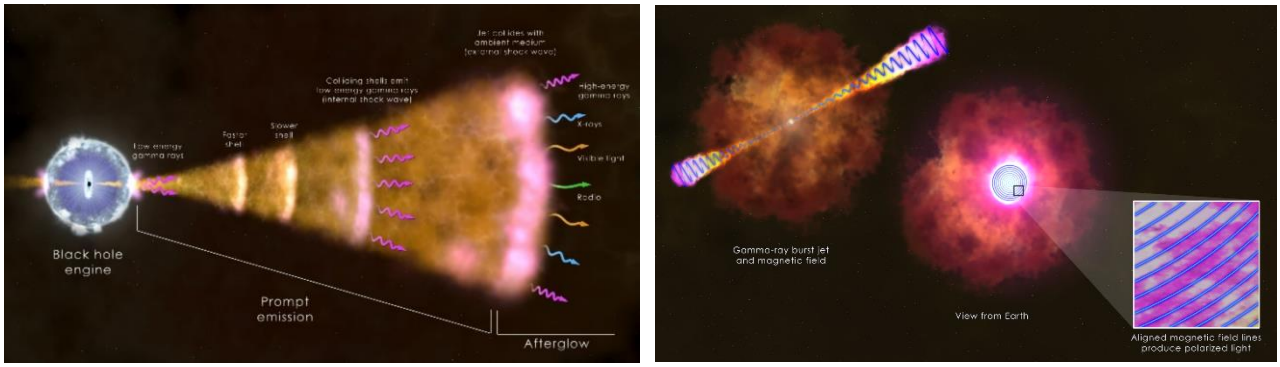

Figure 2-10 Left: artist's impression of GRB expanding ejecta and radiation. All inference of jet structure to date has come from interpretation of light curves. Right: artist's impression of GRB jet magnetic field, which will produce polarized light when pointing towards Earth. XIPE offers a uniquely powerful probe of spatially unresolved jets.

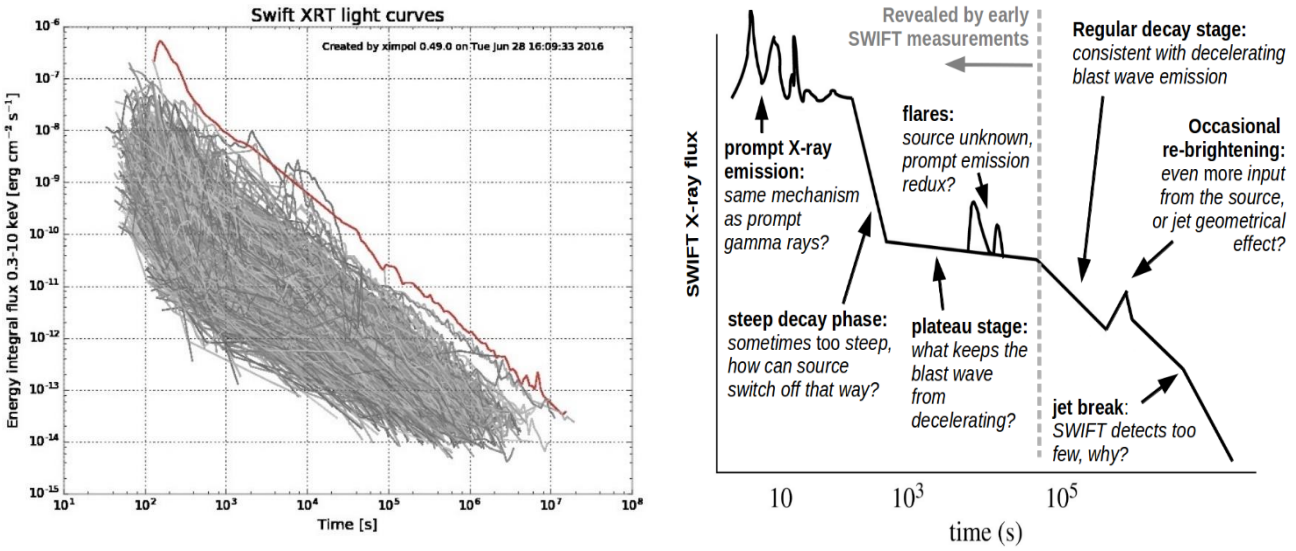

Figure 2-11 Left: All Swift X-ray light curves for GRBs observed for duration of 6 hours or more post burst (Negro, priv. comm). Monster GRB130427A is shown in red. Right: schematic of canonical X-ray light curve revealed by Swift & to be probed by XIPE (van Eerten, priv. comm). Optical/γ-ray light curves display only a subset of these features.

In the process, highly collimated high-speed jets of plasma are ejected that travel outwards at speeds close to that of light and produce bright gamma ray flashes detectable at Earth when the jet points towards us. Long-lived afterglow emission is produced at longer wavelengths - from X-ray to radio - as the expanding ejecta propagate outwards through the circumburst medium (Fig. 2-10).

The mechanisms that produce the prompt radiation, the energetics of the explosions and – most importantly – the nature, origin and role of magnetic fields remain largely unknown. With high Lorentz factors, strong gravity and magnetic fields, GRBs are ideal extreme-physics laboratories. Detectable to the edges of the observable Universe (most distant, spectroscopically confirmed, GRB at z=8.3 [223], [250], they act as beacons for cosmology and, ultimately, probes of space-time itself [257]. However, as distant stellar sources, it is not possible to make spatially resolved images of their jets. Instead, polarization opens a uniquely powerful new observational window to probe magnetic fields properties, jet physics and geometry – never done before in X-rays (Fig. 2-10).

Real-time, autonomous discovery and rapid follow-up of GRBs with NASA's *Swift* satellite [89] has provided an unprecedented collection of well-sampled X-ray afterglow light curves - measured from the first seconds after the high-energy burst up to weeks after (Fig. 2-11). They show structure indicative of complex shock physics, long-lived central engines and blast-wave energetics over a wide range of X-ray flux densities (10^{-14} - 10^{-6} erg cm^{-2} s^{-1} at 0.15-5 keV), but the underlying origin is still unknown. If late-time flares, plateaux and re-brightenings originate from the central engine, we expect the degree of X-ray polarization to be high and

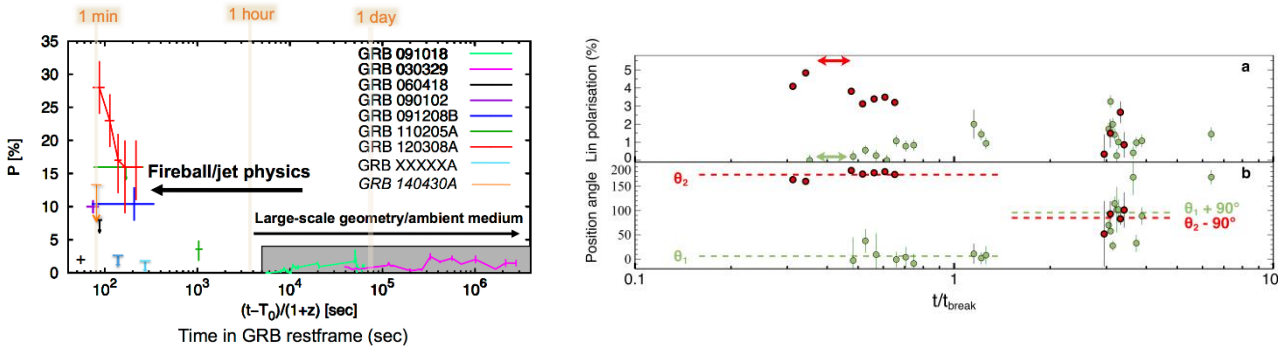

Figure 2-12 Left: recent detections of polarized optical afterglows (P%~30%) soon after the GRB hold promise for direct XIPE detections of ordered magnetic fields in GRB jets [186]. Right: detection of sudden change in polarization position angle of 900 in later-time optical measurements GRB121024A (red) & GRB091018A (green) show XIPE will probe unique signature of jet geometry [278].

detectable with *XIPE* – allowing the first direct determination of particle acceleration and emission mechanisms. It is worth remarking that detection of prompt γ-ray flares with polarization degrees as high as 80% ([55] and references therein) and early optical afterglows with reverse shock polarizations up to 30% have been claimed (Fig. 2-12). Bright, reverse-shock optical flashes and hence the opportunity to measure their polarization are rare; the reason is unclear, but likely due to magnetization properties of the flow before and after the reverse shock. The X-ray polarization will probe this magnetized flow directly, at higher energy density and for a statistically significant sample.

In the *XIPE* era, the Chinese-French satellite SVOM [52] will replace *Swift* to provide GRB discoveries, notifications and well-sampled early X-ray light curves. In the most favourable cases, *XIPE* will be able to repoint within 8 hours in response to external triggers; with a 50-ksec exposure, *XIPE* will provide detection or constraints down to MDP <5 % for a very bright GRB like 130427A. In addition, MDP of few tens % for a sizeable fraction of GRBs will be easily achievable (Fig. 2-13). Even with these relatively high MDPs, *XIPE* has the potentiality of directly probing magnetic fields in soft X-ray emitting plasmas of GRBs; it will revolutionise GRB theories, distinguishing between synchrotron radiation and inverse Compton processes, hadronic or leptonic plasmas, baryonic or Poynting-flux-dominated jets across GRB central engine life-cycles.

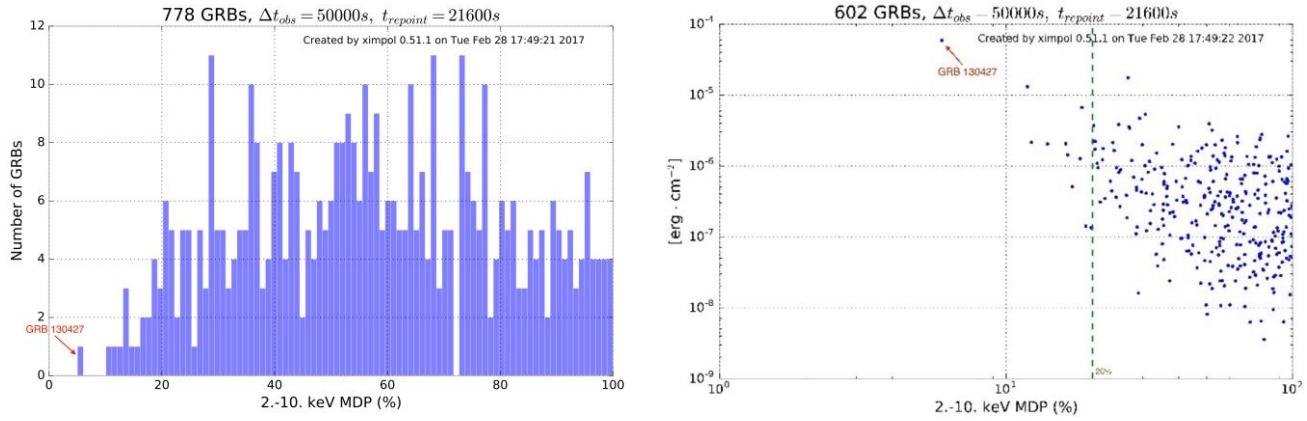

Figure 2-13 Left: MDP for 50-ksec XIPE exposure starting 6 hours post burst. Left: histogram of Swift GRBs from Fig. 2-11 showing MDP<5% for bright GRBs like 130427A; MDP<20% (40%) for 20 (100) GRBs respectively. Right: as function of integrated prompt γ-ray flux over first 600 sec since burst allowing target selection optimisation. Brighter GRBs are XIPE first-choice targets, allowing the polarization across the prompt-afterglow transition to be probed.

2.1.6 Tidal Disruption Events

XIPE will shed light on the origin and site of the X-ray emission in TDEs. It will discriminate between different emission models for non-thermal TDEs, and between the two interpretations of X-ray QPOs.

Tidal Disruption Events (TDEs) are associated to a sudden increase of the accretion rate when a large mass of gas, for instance a star, falls into the tidal sphere of influence of a black hole and is torn apart and accreted. While TDEs can reach the luminosity of a quasar, they are rare (10^{-5}–10^{-4} yr^{-1} per galaxy) and only last for several months or years at most. TDEs display both thermal and non-thermal emission from relativistic and non-relativistic matter [124] that extends from the radio up to hard X-rays.

The emission of TDEs is dominated by an accretion disc (10^{44}–10^{46} erg s^{-1}) peaking in the far-UV/soft X-rays [141]. However, the *Swift* Burst Alert Telescope (BAT) discovered three TDE candidates in the hard X-ray band [27], [32], [44], [30]. A multi-frequency follow-up from radio to γ-rays revealed a new class of non-thermal TDEs. Their emission was associated to a relativistic jet [286], [287], [23], [23] being responsible for the hardness of the X-ray spectrum and to increasing radio emission [137] that was detected a few days after the trigger. Finally, [7] and [264] discover the first radio outflow associated with a thermal TDE, suggesting that jets may be a common feature of TDEs.

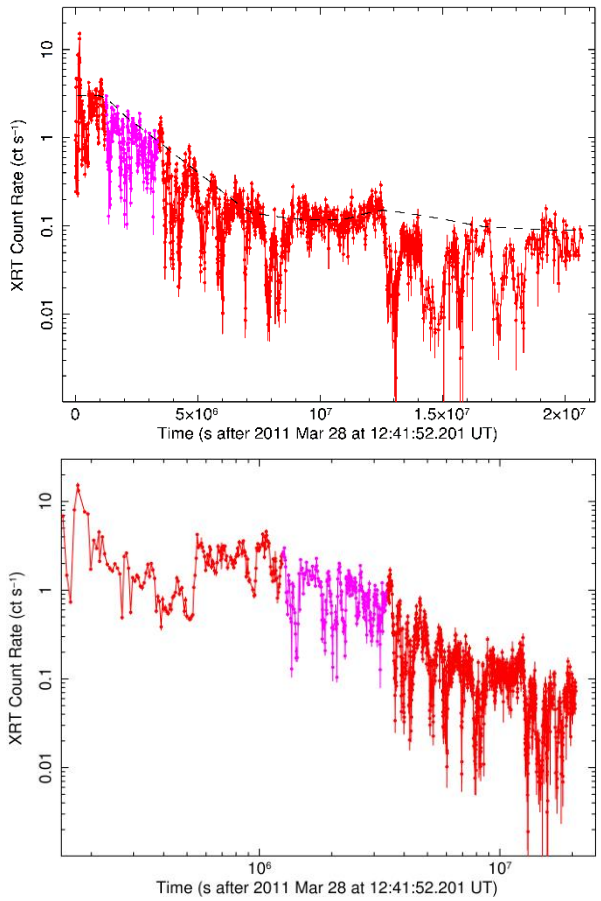

Figure 2-14 QPO signature in Swift/XRT light curves in linear (top panel) and logarithmic (bottom panel) scale. Adapted from [225].

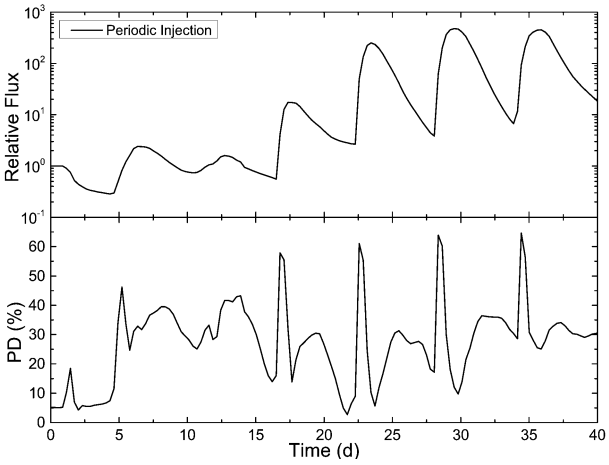

Figure 2-15 Top: relative flux change along the X-ray light curve, assuming synchrotron emission, as predicted in the periodic injection model. Bottom: the same for the polarization degree (PD) variation. The polarization angle (PA) does not vary in this model [292] in contrast to what is predicted for the precessing jet scenario.

The discovery of non-thermal TDEs has raised several questions: what is the jet production efficiency in these events? What is the role of the transient accretion disk and of the spin of the BH in the mechanisms of jet launching? These are general questions, transversal to different classes of astrophysical sources. Non thermal-TDEs, from otherwise in-active galaxies, provide us with important new insight into the mechanisms of jet formation, evolution, and shut-down, on the short time scales of years, and in an otherwise quiescent environment, without any past activity.

Given their brightness (peak luminosity ~ 10^{47} -10^{48} erg s^{-1}) non-thermal TDEs are good targets for *XIPE*. The *XIPE* polarimetric capabilities provide a new and unique diagnostic to understand the properties of the transient jet. Broadly speaking, many of the arguments and objectives discussed for blazars (see Section 2.1.4) apply also here. Observing a transient jet will allow us to track the variable polarization signatures and to determine how the magnetic energy converts to radiation. The spectral energy distribution (SED) of the best studied event, Sw J1644+57, is heavily debated and it is not clear if X-rays are produced by synchrotron [32] or inverse Compton (IC) processes [27]. Its connection with the radio emission is therefore uncertain and there are some arguments based on the timescales of radio and X-ray variability that suggest different sites in the jet where the emission is produced (the radio emission originates farther away from the central black hole). More specific to TDEs are quasi periodic oscillations (QPOs) observed in X-rays. It was found [225] that the dips in the light curve of Sw J1644+57 (Fig. 2-14) were not random but occurred preferentially at time intervals of a few 10^5 s and their higher order multiples. Several models have been proposed to explain the QPOs; in general, they can be classified in two categories: periodic injections or jet precessions. 3D simulations of periodic injections of magnetized plasma show that in this case the polarization degree would be modulated together with the light curve, while the polarization angle would stay constant [292]. On the other hand, in the periodic precession model both degree and angle are modulated.

Although the emission decreases on longer time scales with respect to other transients, such as GRBs, it is important to re-point promptly. The reaction time of 6-12 hours for *XIPE* is reasonable in this context. The capability to detect polarization degrees of a few percent strongly depends on the phase of the TDE evolution observed by *XIPE*, which in turn depends on the delay of the external trigger. The triggers of non-thermal TDEs are expected to come mainly from future radio surveys [263], [59], [171]. The Square Kilometer Array (SKA) will be operative in the 2020s and will provide a deep survey of 2/3 of the sky [210]. A huge number of events will be triggered per day and a proper

multi-wavelength follow-up involving VLBI and optical telescopes (for the transient localization within the host galaxy) is foreseen for a first rough identification [60], [196]. We expect ~ 100 events per year triggered by SKA.

The best X-ray counterparts of radio candidates for *XIPE* are those with F(2-8 keV)$\geq 10^{-10}$ erg cm^{-2} s^{-1} at the beginning of the follow-up. We expect (even if with large uncertainties), a few of such events per year. This threshold in brightness will allow us to perform polarimetric measurements at different epochs of the TDE emission, at least up to 2 weeks since the beginning of the observation. In this way, it will be possible to trace the evolution of the magnetic field and to investigate the processes shaping the X-ray light curve (overall trend plus dips) and the change in the Spectral Energy Distribution [32]. The evolution in polarization degree (with MDP in the range 4-10%) and angle (a few degrees) could be constrained by recurrent observations, each with a 50 ks integration time.

Finally, when evidence of relativistic reverberation [118] is provided by X-ray spectroscopic data, as in *Swift* J1644+57, *XIPE* observations will put interesting constraints on the geometry of the Comptonizing material during the super-Eddington phase of the newly formed accretion disc, to be compared with the sub-Eddington accretion flows of standard radio quiet AGN (section 2.3.2).

2.1.7 Active Stars

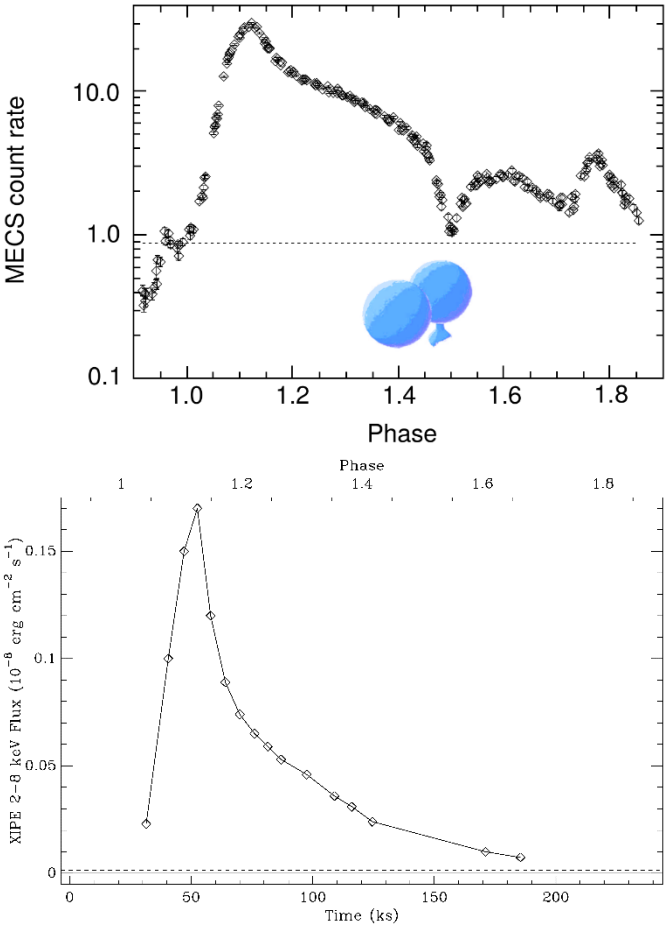

Figure 2-16 A super-hot giant flare on Algol observed by BeppoSAX on 30 August 1997. Top: the flare light curve versus binary phase; the inset shows the binary star configuration at phase 1.45 before the eclipse of the flare on Algol B [228]. Bottom: flare flux versus time from [74] converted to the XIPE energy band.

XIPE may provide the first ever observation of an active star by an X-ray polarimeter and, if the star produces a strong flare, measure the prompt polarization and localize the flare on the stellar disk.

Two sources of polarization in stellar flares are potentially observable in the *XIPE* spectral band: the accelerated electrons, producing the impulsive phase of the flare; and the reprocessing of the flare emission (impulsive and gradual phase) by the stellar photosphere. The continuum emission from non-thermal electrons during stellar flares can only be observed unambiguously in the X-ray band above ~15 keV as in the soft X-ray band the continuum emission is dominated by thermal emission [194]. The thermal emission of the flare can be reprocessed by the stellar photosphere, which produces (unpolarized) fluorescent line emission (e.g., Kα from neutral iron; e.g., [63], [253], [67]) and a polarized scattering contribution to the observed emission that strongly depends on the geometry.

Based on observed properties of the incident hot (T ~100 MK) flare emission, we assessed the reprocessing by the stellar photosphere conducting radiative transfer simulations. We simulated the photosphere with an optically-thick sphere and put the isolated flare emission at a typical height of 0.1 stellar radii (e.g., [63], [253], [67]). The ratio of scattered flux to flare flux increases when the flare moves from the star limb to the star centre. The polarization fraction varies in the opposite way with a maximum value of 0.25% for a flare located close to the star limb (corresponding to a viewing angle of ~77°).

Bright flares from active stars are obviously unpredictable. Since *XIPE* has slew capability of ~6 hours, we cannot take profit of other facilities (e.g., *Swift*/BAT) to detect the flare impulsive phase and trigger a target-of-opportunity observation. Therefore, *XIPE* observations of flares from active stars are challenging. Nevertheless, we include the active star Algol in the observation program.

Algol (β Per) is a triple star, including a close binary component (B8V+K2IV) with an orbital period of ~2.9 days that is the prototype of short-period eclipsing binaries with an early-type primary, emitting no X-rays, and a (near) main-sequence late-type secondary, active in X-rays. Remarkably, a super-hot (~140 MK) giant flare was observed on the limb of the secondary component with *BeppoSAX* [228], [74], Fig. 2-16, top). Another flare was caught by *XMM-Newton* [229], [284]. The duration of the giant flare was 150 ks with an average flux of 0.048×10^{-8} erg cm^{-2} s^{-1} in the 2-8 keV energy (bottom panel of Fig. 2-16), which corresponds to a *XIPE* baseline MDP (2-8 keV) of 2.3%.

Our modelling shows that *XIPE* would not detect the polarization of the scattered flaring flux in Algol. Nonetheless, it would be able to measure the polarization from accelerated electrons during the impulsive phase of a bright flare if the non-thermal flux and the intrinsic polarization are large enough, which can be achieved when the flare is close to the limb (see [125] for a review of the X-ray polarization during solar flares). Moreover, any dip in the flare light curve during the secondary eclipse will independently constrain the location of the flaring region on the disk of Algol B. Algol B would not be a high priority source in the observation program of *XIPE*. Still we consider it worth to be explored as no active star has ever been observed with an X-ray polarimeter. If there is discovery space for active stars with *XIPE,* Algol B would be a promising candidate.

2.1.8 Clusters of Galaxies

Bright clusters, e.g. Perseus, will serve as convenient unpolarized, extended calibration targets for XIPE.

Clusters of galaxies are the largest reservoirs of hot gas in the Universe. The X-ray emission is dominated by thermal bremsstrahlung and line emission, and is therefore expected to be largely unpolarized. However, some polarization may arise due to the mechanism of resonant scattering ([227], [48], [293]). Polarization arises only in the resonant lines of heavy elements, in particular the 6.7 keV line of He-like iron, because the ICM has a significant optical depth in these lines and there is anisotropy in the radiation field. The best target to search for this signal would be the Perseus Cluster, the X-ray brightest cluster in the sky Estimates show that the 6.7 keV emission can be polarized up to 5-10 per cent. However, due to the limited spectral resolution of *XIPE*, this polarized signal will be strongly diluted by the unpolarized emission in the neighboring part of the spectrum, so that the net polarization will not exceed 0.5% in the 6-8 keV energy band. Thus, *XIPE* will not be able to detect the polarization in the 6.7 keV line even with 10-20 Ms of exposure. Another possible polarization mechanism is thermal bremsstrahlung emission due to electron pressure anisotropy ([122]). Computations have shown that the resulting polarization is even weaker, ~0.1%, than for resonant scattering. Thus, *XIPE* will not be able to detect this kind of polarization either.

The abovementioned polarization degrees are of the order of, or even less than, the systematic uncertainties expected for *XIPE*. So, for all practical purposes, Cluster of Galaxies can be considered perfectly unpolarized sources and therefore be used for calibration purposes. Moreover, and for the same reason, they can be observed to search for Axion-like particles (see Sec. 2.4.4).

2.2 Highly magnetized compact objects

Strong or even extreme magnetic fields are present in a variety of compact sources. If the field is ordered, polarized synchrotron emission may be produced. Moreover, strong ***B***-fields frequently channel matter along field lines thereby creating largely aspherical X-ray emission and scattering geometries. Thus X-ray polarimetry will give us new insights into the accretion processes onto magnetized objects: with *XIPE,* it will be possible to probe the origin and the structure of the emission from magnetized white dwarfs and neutron stars in binary systems. Fundamental parameters of the accreting objects such as the mass, magnetic field topology, mass accretion rate and binary inclination, can then be constrained. Understanding X-ray

polarization emerging from accreting millisecond pulsars can also provide strong constraints on the equation of state of ultra-dense matter. In addition to this, since in strong magnetic fields (>10^6 G) the plasma opacity differs between the ordinary and extraordinary polarization mode, a significant linear polarization is expected in the X-ray band. Therefore, X-ray polarimetry can probe the physics of extreme objects such as magnetars. Last but not least, *XIPE* will test vacuum birefringence (a QED effect yet to be verified) in highly magnetized neutron stars (see sec. 2.4.1 for more details).

2.2.1 Magnetic Cataclysmic Variables

XIPE will allow us to break degeneracies in the accretion structure parameters in moderate-to-low magnetic field strength WD, by adding the spin-dependent polarization degree and angle to spectra and pulse shapes.

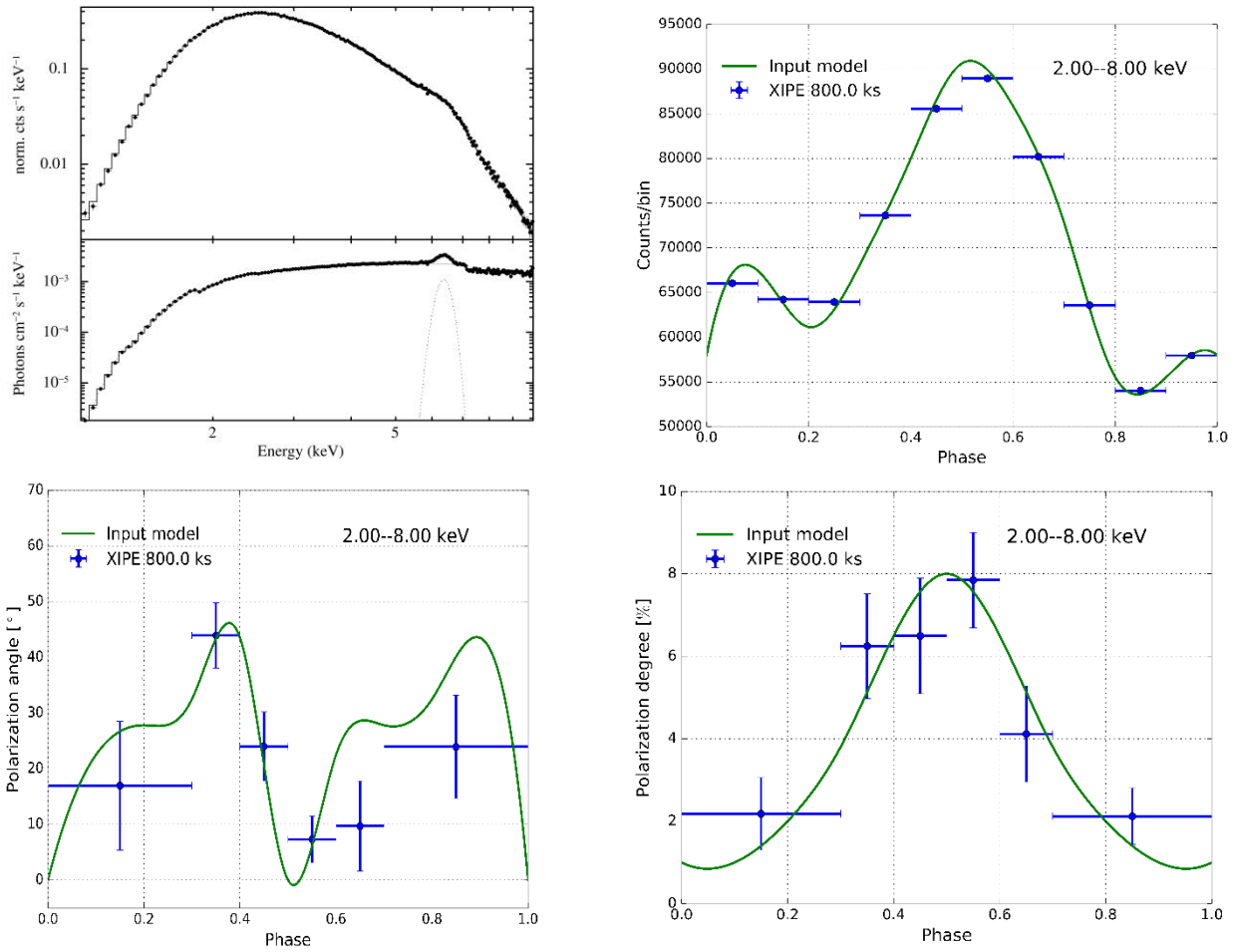

Figure 2-17 XIPE simulation for a bright hard X-ray mCVs, such as GK Per (P_{spin}=351.3 s) in a dwarf nova outburst ($F_{2\text{-}8keV}=1.1\times10^{-10}$ erg cm^{-2} s^{-1}). The figure shows XIPE's capability to detect phase-resolved emission and polarization from an 800 ks observation. The binary inclination is 60° [181]. A high specific mass accretion rate of 10 g cm^{-2} s^{-1} *is assumed in outburst [269]. The expected polarization degree is adopted from McNamara et al. (2008a). Top left: XIPE X-ray spectrum across 2-8 keV for a spectral model derived from an XMM-Newton observation of the outburst spectrum: bremsstrahlung (kT=16 keV), broad Gaussian line at 6.4 keV (EQW=170 eV), total (N_H= 4.9×10^{22} cm^{-2}) and 70%-partial (N_H=3.4×10^{23} cm^{-2}) cold absorption [269]. Top right: The XIPE 2-8 keV spin pulsation using as input model the XMM-Newton EPIC-pn spin light curve and spectral model above; Bottom: polarization angle (left) and percentage (right) variability during the spin period. Blue points are detections above 2*σ.

Cataclysmic Variables (CVs) contain a white dwarf (WD) accreting from a Roche-lobe filling, low-mass star. They are the most abundant type of Galactic low-mass X-ray binaries (see [270], for a review). In recent years, new discoveries in the radio, hard X-ray and high-energy γ-ray domain have shown how incomplete our knowledge of the accretion and emission properties in these systems still is. X-ray polarimetry can shed new

light on the physical conditions and geometry of accretion flows because linear polarization emerges from scattering in aspherical matter flows, such as accretion columns and discs, or during the ejection of matter in nova outbursts.

It is still not entirely understood how the accretion flow is shaped by the intense magnetic field of a WD and how matter settles onto its polar caps in magnetic CVs (mCVs, $\boldsymbol{B}_{WD} \sim 10^6$-$10^8$ G). In systems with strong magnetic field ($\boldsymbol{B}_{WD} > 10$ MG), such as polars, the WD rotation is orbitally locked, which prevents the formation of an accretion disc. Therefore, matter is channelled directly onto the magnetic poles. For a weaker field ($\boldsymbol{B}_{WD} < 5$-10 MG), such as the one in intermediate polars, the WD rotates asynchronously. Then, a magnetically truncated disc can form and matter is transferred onto the WD poles through a curtain-shaped flow [220]. The gas in the accretion column/curtain is heated up to tens of keV in a stand-off shock below which it cools via optically thin bremsstrahlung in X-rays and cyclotron radiation in the optical/nIR bands [130], [282]. A certain fraction of X-rays is absorbed and reprocessed in the polar regions of the WD.

The reprocessed spectrum shows a prominent neutral Fe Kα line at 6.4 keV [68], [102]. The relative proportion of bremsstrahlung to cyclotron radiation strongly depends on the magnetic field strength of the WD, with cyclotron cooling being dominant in strong field systems [281], [80]. The moderate-to-low field mCVs are bremsstrahlung-dominated and represent ideal targets for *XIPE*. Testing models for the accretion structure is going to provide constraints on fundamental system parameters and the emission mechanism.

The optically thin radiation from the post-shock region and the optically thick blackbody emission from the heated WD are not polarized. However, in systems accreting at high specific mass rates, the accretion column may have a high Thomson optical depth, thus making Compton scattering an important process. Pioneering work on X-ray polarization in mCVs assumed a uniform column and predicted a polarization degree up to 4-6% [159]. More recent simulations include a stratified post-shock flow, with the key parameters being the WD mass and radius, the specific mass accretion rate and the ratio of cyclotron to bremsstrahlung cooling [167]. For systems accreting at high rates and seen through extended columns at perpendicular orientation, the predicted polarization can reach values of 7-8%. The polarization position angle depends on the binary inclination and the magnetic colatitude.

The joint analysis of spin pulse profiles, X-ray spectra, and spin phase-dependent polarization degree and angle will eventually fully determine the geometry of the accretion flow. For intermediate polars, where an arc-shaped column likely occurs, the expected X-ray polarization should be even larger [167].

Bright systems such as the intermediate polars, GK Per (during a dwarf nova outburst) and EX Hya, and the prototype polar AM Her (in its high state) are key targets for *XIPE* to perform phase resolved studies. In particular, GK Per is an old nova (Nova Per 1901) with an impressive nova shell remnant [15], [248]. It is thus

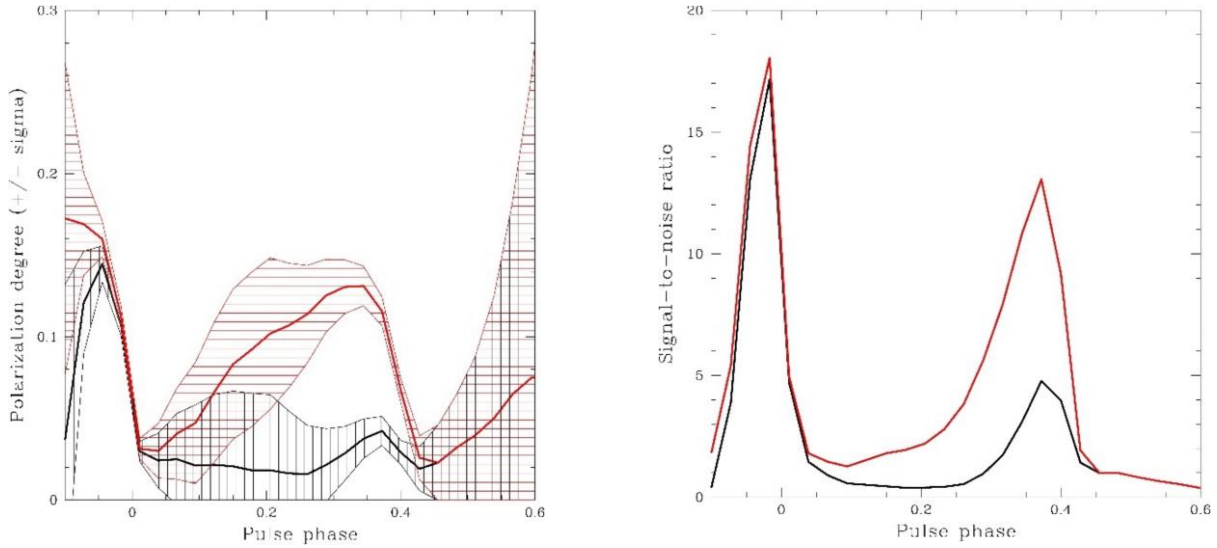

Figure 2-18 Left panel: Polarization degree of the pulsed signal, and the associated 1σ uncertainty strip; red curves: both CO and CX are assumed to have the same polarization degree and polarization angle as the optical pulsed signal in the corresponding phase bin; black curves: CO is the same as before, but CX is assumed to have zero polarization. Right panel: corresponding signal-to-noise ratio of the curves presented in the top panels.

an interesting target to search for polarized emission in its surrounding nebula. EX Hya is an eclipsing system making polarization measures extremely promising. The prototype of polars, AM Her - to be observed in its high state - can provide a key comparison with the results obtained from optical observations [56]. A *XIPE* simulation following [167] for a system like GK Per in outburst [269] is shown in Fig. 2-17, where an 800 ks long observation can allow us to detect polarized X-ray variability at the 351.3 s WD spin period. The simulation assumes a high specific mass accretion rate (10 g cm^{-2} s^{-1}), a ratio of column height to radius H/r=10, M_{WD} = 0.5 M_{Sun}, a magnetic colatitude of β=30° and a binary inclination of i=60°.

2.2.2 Rotation powered pulsars

XIPE will perform phase-resolved polarimetry of the pulsed X-ray emission from the Crab and several other pulsars. This will provide relevant information on the topology of the magnetic field, and allow us to disentangle different components of the pulsed X-ray emission and thereby to put new constraints on the pulsar's emission geometry.

Rotation powered pulsars (RPP) are very promising targets for X-ray polarimetry because their X-ray emission is expected to be highly polarized, similar to what observed in other spectral bands. Polarization data are important to model the geometry of the magnetic field and to locate the acceleration and emission sites of high-energy electrons.

The Crab pulsar. For Crab-like pulsars, and for the Crab pulsar itself, the OPTIMA instrument [238] is providing very precise measurements of linear polarization in the optical band. *XIPE* can verify whether the X-ray polarization shows the same characteristics as in the optical, and therefore whether the emission site is the same or not. This requires accurate phase-resolved polarimetry in particular in those phase intervals where the polarization degree is expected to change rapidly, such as the main peak (P1, the maximum is assumed as phase zero) or the secondary peak (P2, see [238]). Another interesting problem refers to the different energy spectra at the two peaks, usually illustrated by the P2/P1 ratio increasing with photon energy from the optical band to low-energy γ-rays. Until today, there is no clear explanation for this behaviour.

In the scenario presented in [160] the pulsed X-ray emission is due to the superposition of two components with different phase distributions and energy spectra, and therefore with likely different site of origin. The first component, C_O, has the same pulse profile as in the optical. The second component, C_X, is set to have the highest relative intensity of hard X-ray to low energy γ-ray emission. Furthermore, the sum, C_O+C_X, must reproduce the observed pulse profile. It turns out that C_X increases monotonically up to phase 0.4 before having a sharp cut-off. Furthermore, C_O+C_X reproduces the observed pulse profile in the range of 1 keV to a few MeV only by multiplying C_X by an energy dependent factor. The net linear polarization is given by the C_O polarization, i.e. the observed optical polarization, plus the polarization of C_X, to be measured with *XIPE*.

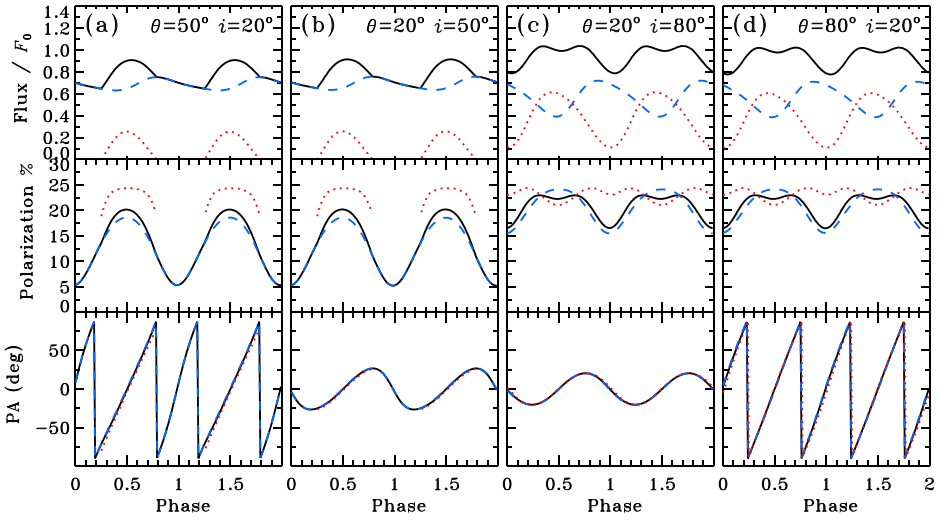

Figure 2-19 The pulse profile and spin-dependence of the polarization degree and angle. The black solid line denotes the contribution of two antipodal spots, while the dashed and dotted lines correspond to the contribution of each spot separately. The pulse profile and polarization degree are degenerate to exchanging i and θ, while the polarization angle shows a dramatically different behaviour allowing both angles to be measured (adapted from [267]).

Any polarization model must take into account that the pulsar is embedded in a PWN emitting highly polarized X-rays as well. From *BeppoSAX* and *NuSTAR* data we estimate the nebular to pulsar flux ratio equal to 11.4. Considering that the nebula will be partially resolved by *XIPE*, only a fraction of its emission will contribute to the polarization measured in the pixel containing the pulsar. Introducing a solid angle scale factor of about 1/4 of the total nebular flux, the resulting nebular to pulsar ratio in the pixel is 2.86. The off-pulse signal, which must be added to the pulsed signal to simulate the full *XIPE* observation, is assumed to have P=19% at a position angle of 156°, as given in [274]. The normalizations of the pulsed and non-pulsed components are defined in a 1 keV window around 3 keV: for *XIPE*, they are equal to 10.5 and 30.0 counts per second, respectively. We then simulated a total exposure of 100 ksec. In Fig. 2-18, right panel, we present the signal-to-noise ratio of the polarization degree and, in the left panel, the polarization degree with the 1σ uncertainty strip as a function of pulse phase; red curves are for a polarized C_X, black curves for a zero-polarization C_X. We can conclude that the proposed exposure is comfortably sufficient to measure a polarization similar to the optical one. More important, based on its polarization properties, it will be possible to distinguish C_X from C_O in the framework of the two-component model.

Other pulsars to be observed with XIPE. The sensitivity of *XIPE* allows us to reach a 10% MDP in a 1 Ms observation down to a flux limit of 2×10^{-12} erg cm^{-2} s^{-1}. Thereby, a purely non-thermal X-ray spectrum with photon index Γ=2 and hydrogen column density $N_H=10^{21}$ cm^{-2} is assumed. Most pulsars with a non-thermal X-ray flux above 2×10^{-12} erg cm^{-2} s^{-1} are embedded in bright PWNe, which narrows down the selection to about 20 sources where the PWN flux, integrated over a region of 30 arcsec, is less than 0.1 of the pulsar flux. The list includes well known pulsars, such as PSR B1509-58 (151 ms). We exclude the LMC pulsar PSR B0540-69 (50 ms), because with *XIPE*'s angular resolution its X-ray emission is dominated by the bright PWN. Other pulsars, e.g. PSR B1055-52 and PSR B0656+14, are ideal cases for clean polarization measurements as they are not associated to PWNe. We can never rule out that a faint PWN is more strongly polarized than a bright pulsar, but since all of our targets are also X-ray pulsars, we may always disentangle the pulse from the non-pulse polarization by phase-resolved polarimetry.

2.2.3 Accreting millisecond pulsars

XIPE will unambiguously constrain the observer's inclination with respect to the rotation axis and the hot spot in AMPs. These measurements are crucial for the determination of the equation of state of neutron stars from time-resolved spectroscopy. For bright sources, the energy dependence of the polarization will also constrain the angular displacement between the accretion shock and the thermal emission region.

Accreting millisecond pulsars (AMPs) contain weakly magnetized neutron stars (with $B=10^8$-10^9 G), spun up to ms periods by accreting matter from a low-mass companion ([279], [200]). More than a dozen sources, with spin periods ranging from 1.67 to 5.49 ms, are known today. All of them are transients going into outburst every few years. In the neutron star vicinity, accreting matter follows the magnetic field lines hitting the surface close to the magnetic poles. AMP spectra consist of a blackbody component, originating from a hot spot on the star surface with typical temperatures of about 1 keV, and a hard power-law component, probably due to Comptonization in a radiative shock surface, with a temperature of 30–60 keV and Thomson optical depths <1–2 [206]. Rotation of the hotspot causes a modulation of the observed flux with phase because of the changing projected emission area and of Doppler boosting. The information about the emission pattern, the rotational velocity and the neutron star compactness are recorded into the pulse profiles. Therefore, their analysis can, in principle, recover the neutron star mass and radius and thus constrain the neutron star equation of state [207], [140], [211], [175]. Degeneracy between parameters, however, has not allowed to get strong constraints on M and R from existing data [207], [134], [136], [135]. Polarization measurements will be crucial in breaking this degeneracy.

Radiation scattered in the shock is expected to be linearly polarized up to 20%, depending on the pulse phase, the photon energy and the geometry of the system [267].

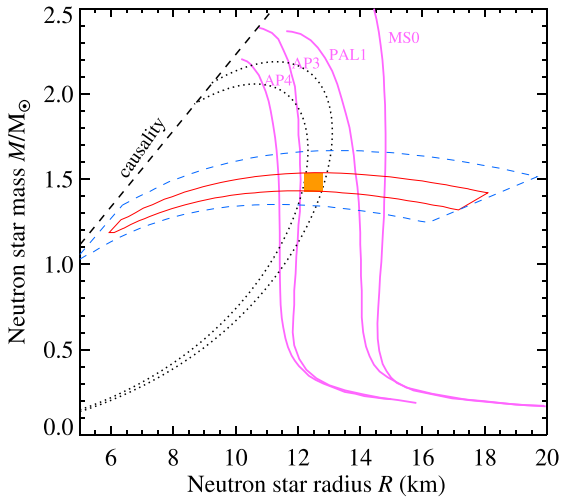

Figure 2-20 Constraints on M and R from the pulse profiles of AMP SAX J1808.4-3658 coming from RXTE data (blue dashed contour, see [207]. With XIPE measurements of the inclinations i and θ from the phase dependent polarization angle the constraints significantly improve (red solid contour). The spectral evolution during post-bust cooling stages of the photosphere can help to further constrain M and R (dotted curves). The pink curves correspond to models for different EOS of cold dense matter.

Both the observed polarization degree and angle change with the rotational phase (Fig. 2-19) following variations of the angle at which the spot is observed and its projection angle onto the sky. Once the rapid rotation and gravitational light bending are taken into account [77], [78], [267], the phase-dependence of the polarization angle allows us to constrain both, *i* (the observer's inclination) and *θ* (the inclination of the hot spot).

In a 1 Ms observation of bright AMPs, like SAX J1808.4-3654 or XTE J1751-305, *XIPE* will reach a MDP of 2% in 10 phase and 3 energy bins and to measure polarization angles with a 2° accuracy (for *P*=10%). This will allow us to determine the main geometrical parameters such as *i* and *θ* (Fig. 2-19) with an accuracy of about 5°, breaking the degeneracy between the parameters and significantly improving the constraints on *M* and *R*. The energy dependence of *P* will enable us to have an independent measure of the electron and seed photon temperatures in the shock and to test the Comptonization model for the hard component. The energy dependence of Ψ can constrain the displacement of the shock from the blackbody-emitting region. For weaker AMPs, a 1 Ms exposure will not determine the energy dependence of the polarization, but the geometrical parameters can still be measured with nearly the same accuracy.

X-ray bursts and their spectral evolution during the photospheric cooling tail (observed e.g. with NICER and Athena) from the same AMPs will give additional, independent *M-R* constraints (e.g. [245], [209], [190]). Combined with the polarimetric measurements, this will put even stronger constraints on the equation of state of cold dense matter (see dotted black curves in Fig. 2-20 and the resulting *M-R* error box).

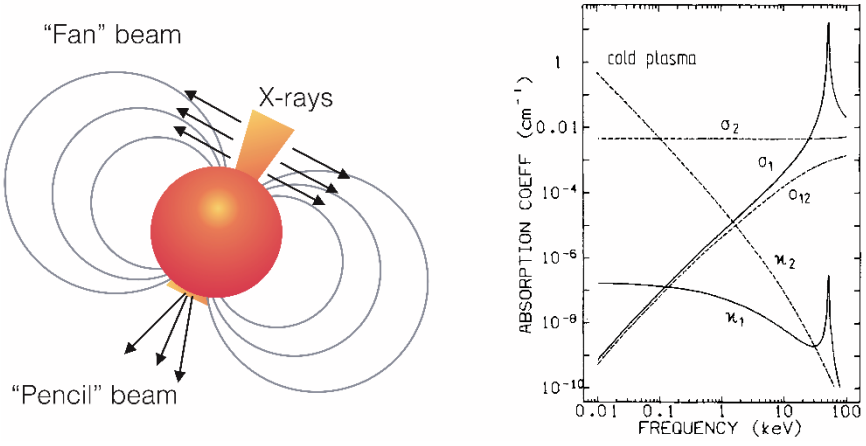

Figure 2-21 X-ray pulsars are expected to exhibit a change of the intrinsic beam pattern accompanied with a change in polarization phase dependence for low ("pencil" beam) and high ("fan" beam) luminosities. Scattering and absorption opacities are significantly different for ordinary (dashed) and extraordinary (solid) modes below the electron's cyclotron energy and exhibit resonant features at cyclotron energy as illustrated in right panel (figure from [265],[265]).

2.2.4 Accreting X-ray pulsars

XIPE will break important model degeneracies from spectral-timing analysis alone, in particular discriminating between the two accretion scenarios involving a "fan beam" or a "pencil beam", and provide an independent tracer of the magnetic field geometry in XRPs.

Accreting X-ray pulsars (XRPs) are among the brightest X-ray sources and represent prime targets for X-ray polarimetry. In these systems, the strong magnetic field channels matter supplied by the binary companion onto the polar caps of the neutron star. Close to the neutron star surface, the accretion flow stops either by Coulomb interaction or by the pressure of the emerging radiation. The accreting plasma couples to magnetic fields of B~$10^{12\text{-}12}$ G and therefore the emerging X-rays are expected to have strong polarization. *XIPE* will be able to detect it in tens

of X-ray pulsars. The analysis of the observed polarization signature will not only help us to solve several long standing questions regarding the astrophysics of XRPs - it will also probe some yet unexplored aspects of fundamental physics such as vacuum birefringence (see Sec. 2.4.1).

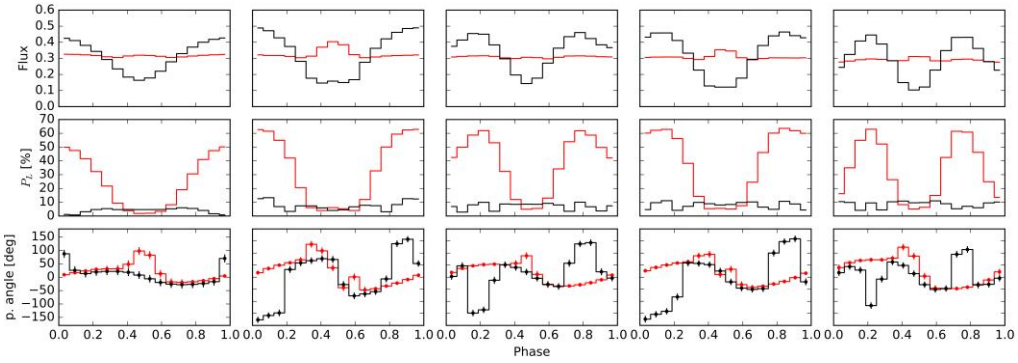

Figure 2-22 Intensity (top row), polarization percentage (middle row) and angle (bottom row) as a function of pulse phase for a "fan" (red) and a "pencil" (black) beam scenario. From left to right we assume different orientations of the neutron star and line of sight with respect to the observer (according to the original work by [170] for the angles i1/i2 of 50/20, 45/45, 75/45, 60/45, 80/60). The error bars in lower plot illustrate the expected uncertainty in the polarization angle assuming a 160 ks XIPE observation of a bright pulsar similar to Vela X-1. XIPE would allow us to discriminate unambiguously between the two beam patterns.

Radiative transfer through strongly magnetised plasma is usually treated separately for the ordinary (O) and the extraordinary (X) modes respectively defined by a parallel or perpendicular orientation of the electric field vector with respect to the external magnetic field *B*. For photon energies below the electron cyclotron energy $h\nu<E_{cyc}=h(eB/m_ec)\sim12\ B_{12}$ [keV] the opacity of the X mode κ_E is drastically smaller than for the O mode κ_O ([103]). Radiative transfer through such birefringent plasma implies a high degree of linear polarization. Magnetic fields of accreting pulsars typically exceed 10^{12} G and, therefore, strong polarization is expected for the *XIPE* energy band. Polarization degree and angle depend on the integrated opacities along the line of sight and thus on the photon energy and the orientation of the neutron star with respect to observer.

Analysing the variation of the polarization properties with energy and pulse phase allows us to probe the structure of the emission region. The scattering and absorption cross sections exhibit resonant peaks around the cyclotron energy. When observing the corresponding features in the energy-dependent polarization we can measure the magnetic field strength in the line forming region. While E_{cyc} is expected to lie above *XIPE*'s energy range for most pulsars, there is at least one exception, the bursting pulsar GRO J1744-28. Moreover, for a number of sources magnetic field estimates are lacking or are unreliable so that polarimetric observations could be crucial.

Despite several decades of studying, the configuration of the emission region in XRPs remains uncertain. Generally, it is believed that in low luminosity objects accreting matter impinges the surface of the neutron star close to the polar areas where the energy is released more or less isotropically. At higher luminosities (above $L_x\sim10^{37}$ erg/s) radiative pressure overcomes gravitational drag by the neutron star and the emission region extends farther out to form the so-called accretion column [16]. The beam pattern in these two cases is usually visualised as either "pencil" (low luminosities) and/or "fan" (high luminosities) patterns as illustrated in Fig. 2-21. The transition luminosity between the two modes depends on fundamental properties of the neutron star such as the magnetic field, mass and radius. A robust determination of the emission geometry in X-ray pulsars would allow us to estimate them and, ultimately, provide constrains on the equation of state of supra nuclear matter.

Nonetheless, reconstruction of the intrinsic beam patterns of X-ray pulsars based on the observed pulse profile alone is currently strongly model dependent ([127], [127]). On the other hand, the sweep in the polarization angle with pulse phase and the corresponding change in polarization percentage have opposite trends (from negative to positive near the pulse peak for a fan beam and reversely for a pencil beam, see Fig. 2-22). This effect is easily detectable, and can break model degeneracies in the assumed emission geometry. Apart from this, the sweep in the polarization angle can also act as a tracer of the ***B***-field geometry in XRPs, which remains a subject of long-standing debate. Any rapid change of the polarization angle may be an indication of a non-dipolar magnetic field. This is an essential step to understand the formation mechanisms of spectra and pulse profiles in XRPs and *XIPE*'s contribution would be indispensable here. Indeed, taking into account the strong

fluxes and polarization expected in X-ray pulsars, the high sensitivity of *XIPE* is especially suitable for studying in detail the pulse phase variability of the polarization properties. Already for moderate exposure times, such a study is possible for tens of persistent and transient sources (Fig. 2-22).

2.2.5 Magnetars

XIPE will uncover the magnetar geometry (inclination of the line of sight and of the magnetic axis with respect to the spin axis). This will give crucial, quantitative information on the magnetosphere of magnetars (magnetic twist, currents) and on the mechanism that triggers their powerful outbursts. Furthermore, X-ray polarimetry with XIPE is a unique tool to test the magnetar scenario itself against other accretion models. XIPE polarization measurements will also be fundamental in guiding the modelling of short burst emission, which is a complex theoretical challenge, presently still largely undeveloped.

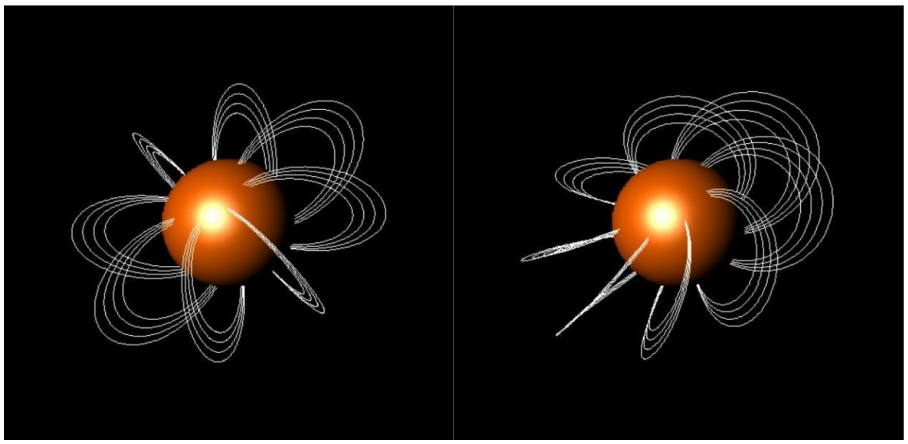

Figure 2-23 A dipolar field (left) and a globally twisted dipole (right); from Turolla, Zane & Watts (2015).

X-ray polarimetry offers a unique opportunity to unveil the intimate nature of ultra-magnetized neutron stars, or magnetars, observationally associated with the Soft γ-repeaters and the Anomalous X-ray Pulsars (SGRs and AXPs). X-ray timing and spectral observations already allowed us to gather insight in their physical properties. There is a vast consensus that the persistent emission of magnetars requires thermal photons produced by the cooling star surface to be reprocessed inside matter flowing along the closed field lines of a "twisted" ***B***-field (the so-called Resonant Cyclotron Scattering, RCS, scenario, [255], [259]). The appearance of a toroidal component is associated to the transfer of internal magnetic helicity to the external field, as the star crust deforms in response to the huge magnetic stresses. A reservoir of internal helicity is responsible for the activity of magnetars discriminating them from other neutron star classes having a comparable *B*-field but no SGR-like behaviour. Putting the RCS scenario to an ultimate test is bound to answering the more fundamental question of how magnetars do form and how they are related to other Galactic populations of isolated neutron stars.

Current spectral modelling is often based on a "globally twisted" field (see Fig. 2-23) and the theoretical predictions are in general agreement with the observations of SGRs/AXPs across the 0.5-10 keV band. Still, a number of key issues are unresolved. (1) Spectral measurements alone cannot provide the basic geometrical angles (inclination of the line-of-sight, χ, and of the magnetic axis, ξ, with respect to the spin axis), which are fundamental in assessing the geometry of the emitting region. (2) Spectral fitting is largely degenerate and fails to constrain unambiguously the model parameters, thus hindering us from a precise characterization of the magnetospheric properties (charge velocity, amount of twist). (3) There are strong indications that the twist is limited to a bundle of field lines (the current-carrying or *j*-bundle). Again, spectral analysis is not sensitive enough to the magnetic field topology and cannot tell us what the real magnetic configuration is.

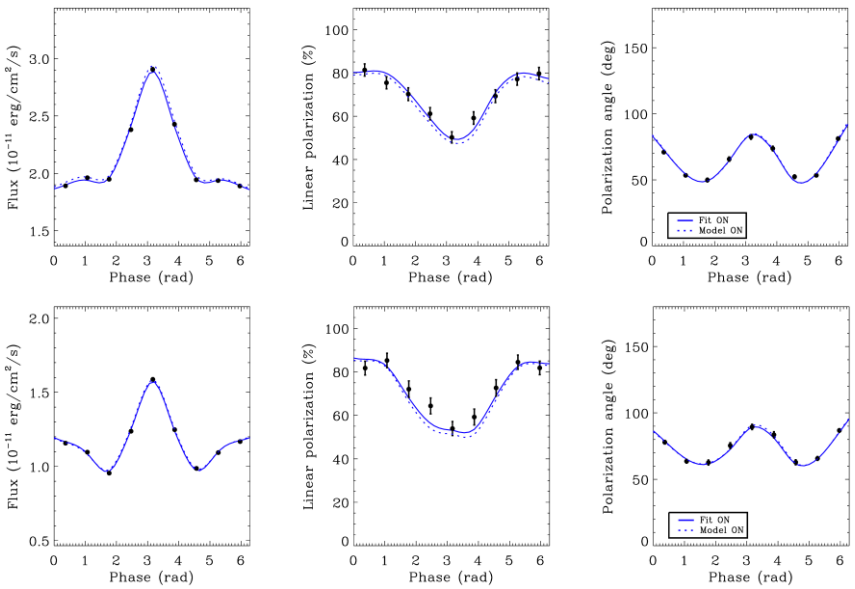

Figure 2-24 From left to right: light curve, polarization fraction and polarization angle for AXP 1RXS J1708 (upper panels) and SGR 1806-20 (lower panels). Seed thermal photons are assumed 100% polarized in the extraordinary mode. The data points (filled circles with error bars) were generated according to the model shown with the dashed line. The full line shows the simultaneous best-fit.

X-ray polarimetry will address all these issues. Fig. 2-24 shows the light curves, polarization percentage and polarization angle for two sources, AXP 1RXS J170849.0-400910 and SGR 1806-20, as measured by *XIPE* with an exposure time of 250 and 350 ks, respectively. simulated data were fitted using an archive of theoretical models obtained with the code of [251] (see also [192]) for different values of the twist angle $\Delta\phi$, the bulk electron velocity β and the two angles χ and ξ. *XIPE* can recover the model input parameters with high precision, including the viewing angles, and disentangle the magnetic twist/charge velocity, where spectroscopy alone fails.

Furthermore, *XIPE* can probe the topology of the magnetic field, discriminating between a globally twisted field and other non-potential magnetic configurations. Figure 2-25 shows a comparison of simulated *XIPE* data for two different theoretical models again based on the method by [251].

The first model (solid line) was calculated with a globally twisted dipole field, the second one (dashed line) assuming a self-consistent, force-free magnetostatic equilibrium [266] with B_p=2×10^{15} G, kT_{surf}=0.74 keV, β=0.6 and F_{unabs}=1.8×10^{-11} erg cm^{-2} s^{-1} in the 2-10 keV band. The simulated *XIPE* data were then generated assuming $\Delta\phi_{N\text{-}S}$=0.3 rad, β=0.2 and an exposure time of 250 ks. The spectra in the two cases are nearly undistinguishable, while the polarization degree is smaller by about 20% in the global twist model, well within *XIPE* capabilities to discriminate.

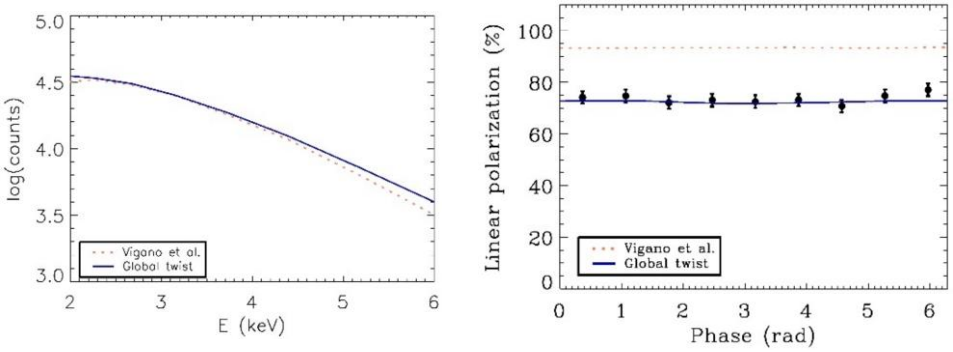

Figure 2-25 Left: phase-averaged X-ray spectrum (counts are in arbitrary units) for the two magnetic configurations discussed in the text. Right: XIPE simulated polarization fraction according to the globally twisted field in the 2-6 keV range, as compared with the two models. Here χ=40° and ξ=0°.

X-ray polarization measurements with *XIPE* can test the RCS model (and hence the magnetar scenario itself) against the alternative accretion scenario [258]. Fig. 2-26 shows the polarization percentage, as a function of rotational phase, for two photon energies, 1.6 keV (left panel) and 3.8 keV (right panel). The simulations are based on the RCS model (with the same parameters as in the case of 1RXS J1708) and the accretion column model by [170]; in both cases χ=75° and ξ=45°. Phase- and energy-resolved polarization measurements will make it possible to put competing scenarios to a definite test.

The emission of short (~0.1-10 s), intense (L_X~10^{39}-10^{43} erg s^{-1}) X-ray bursts is a hallmark of magnetars. The strongest events, known as intermediate flares (IFs), are emitted erratically during periods of intense activity, like in the so-called "burst forest" of SGR 1900+14 in 2006 [111]. The IF spectrum is thermal, with two

blackbody components at kT~5-9 keV, and believed to originate from a cooling, magnetically confined pair fireball which was produced by a sudden injection of energy into the magnetosphere [254]. No detailed model for the burst's radiation properties exists. It was suggested that the two components come from the photospheres of the X and O modes [111]. Therefore, X-ray polarimetry is the key method to understand the physics governing the burst emission.

The bursting phase may last a few days; if a trigger instrument is available during *XIPE*'s lifetime, it may repoint to observe suitable X-ray bursts. Simulations show that *XIPE* will successfully measure the polarization fraction and angle in a bright, single IF down to P=20%. Much lower MDPs can be reached by summing together the data of different flares if their polarization angles are found to be consistent.

It is important to point out that the above calculations were performed including the QED effect already mentioned. The discussion on how X-ray polarimetry can provide the ultimate test to this effect is deferred to sec. 2.4.1.

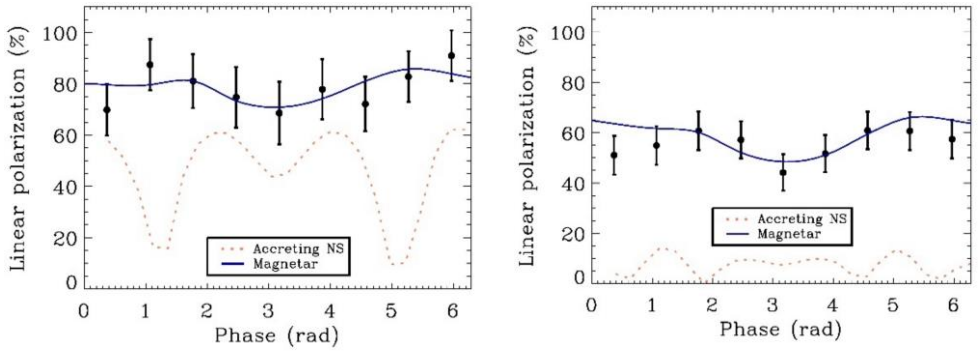

Figure 2-26 Polarization fraction vs. phase as computed for the RCS magnetar model (blue line) and the accreting column model (orange, dashed line). Left: E=1.68 keV. Right: E=3.8 keV.

2.3 Scattering-induced polarization

X-ray scattering by free or bound electrons gives rise to polarization. The spatially-averaged polarization depends on the geometry, and it is null only if both the emitting region and the radiation field are perfectly spherical. Many X-ray sources are believed to be strongly aspherical and scattering-induced polarization provides an important diagnostic of their (spatially unresolved) internal structure.

In general, such X-ray polarization is due to (multiple) scattering events between radiatively coupled media, for instance black hole coronae and their underlying accretion disk in X-ray binaries or active galactic nuclei. The non-thermal X-ray emission in these objects is believed to emerge from Comptonization of soft photons in the very hot plasma of the corona. For many years the nature and structure of the corona has been a matter of controversy, as parameter degeneracy does not allow us to unambiguously determine the coronal geometry from X-ray spectral data alone. Modelling of the radiative coupling and scattering in the corona allows us to relate the observed X-ray polarization to the coronal geometry and viewing angle.

In Active Galactic Nuclei, scattering processes can serve to test the geometry of outflows on larger scales. X-ray polarimetry of the molecular clouds in the Galactic Centre is going to provide the ultimate test if the Supermassive Black Hole in Sgr A* was active a few hundred years ago.

2.3.1 X-ray binaries

XIPE can discriminate between different geometries of the hot corona in X-ray binaries and disentangle a possible jet component. Furthermore, phase-resolved polarimetry would probe the nature of low frequency QPOs and test the Lense-Thirring precession model.

For X-ray binaries, the main goals of *XIPE* are to determine the geometry of the corona, to constrain the contribution of synchrotron jet emission, and to test models for the observed quasi-periodic oscillations.

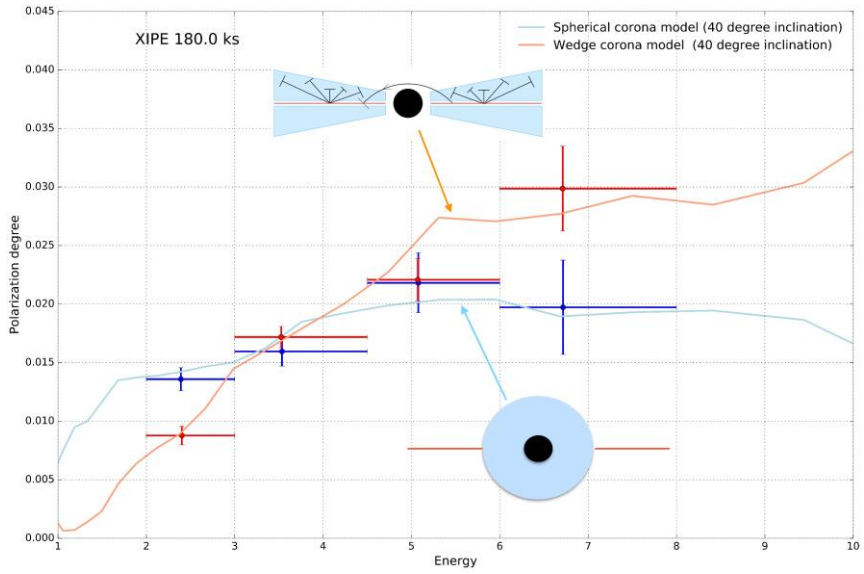

Figure 2-27 Predictions for the XIPE polarization spectrum expected from a wedge corona (red) and a spherical corona at the centre of a truncated disc (blue). The high energy emission is due to Comptonization of soft X-ray disk photons by hot thermal electrons in the hot corona (kT_e=80 keV, τ=1.7), the parameters were fixed to approximate the spectrum of Cyg X-1 in the hard state. The model also includes a reflection component from the outer disc as well as all the relevant special and general relativistic effects. The Monte-Carlo code used is equivalent to the one used by [232] but also includes the Klein-Nishina effects, [128]). The crosses show simulated XIPE data for a 180 ks observation of Cyg X-1.

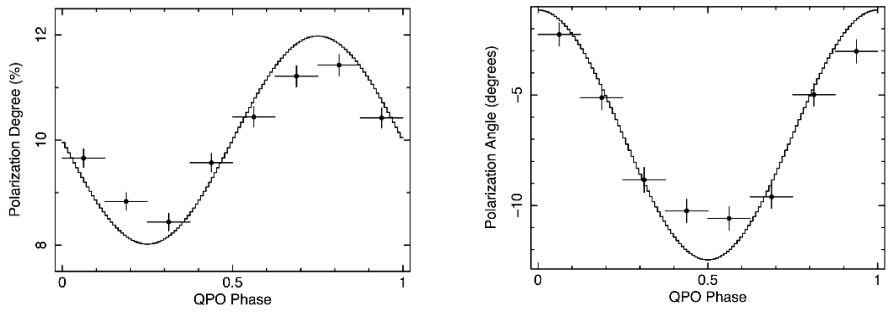

Figure 2-28 Simulations of the expected modulated polarization in GRS 1915+105 (200 cps and a 1 Hz QPO with a 10% fractional rms amplitude). The broadband noise is generated according to a Lorentzian power spectrum and the simulated light curve is then multiplied by the QPO oscillations predicted by the LT precession model. The amplitude and relative phase of the flux, polarization degree and polarization angle as a function of QPO phase are chosen to match the calculations from [110]. The quasi periodic nature of the oscillation is also taken into account. A filtering method is then used to phase fold the simulation data. Full curves: model, Crosses: simulated 52 ks XIPE observation of GRS 1915+105.

Probing the nature of the X-ray emission. The primary X-ray spectrum of X-ray binaries is supposed to be produced in a hot corona surrounding the compact object and Comptonizing soft photons from the accretion disc. The polarization level and its dependence on X-ray photon energy encode decisive constraints on any coronal model ([231]). The two scenarios of a spherically compact or a wedge geometry have a very similar X-ray spectrum and a weak polarization level (a few percent at most). Nonetheless, for the wedge corona the polarization degree in the *XIPE* band is nearly independent of photon energy, while in the case of a spherical corona, a significant increase in polarization fraction is expected. We show in Fig. 2-27 that *XIPE* is sensitive to the different geometries (e.g., using 180 ks exposure on Cyg X-1). Besides the geometry of the corona, polarization will provide complementary information on (i) the source of the seed photons for the Comptonization, i.e. disc emission vs synchrotron (as in advection dominated accretion flows), (ii) the electron energy distribution in coronae: thermal vs non-thermal and their Thomson depth, (iii) the dynamics of the corona, i.e. outflowing/base-of-jet vs static/accreting. It is often argued that rather than a Comptonizing corona, synchrotron emission from the compact relativistic jets may dominate the non-thermal X-rays of black hole binaries. The synchrotron emission from jets is expected to produce significantly more polarization (10% or more) than Comptonization in the corona. Any measurement at such polarization level by *XIPE* would prove that the X-rays come from the jet rather than the accretion flow (see Sect. 2.1.3).

Probing the nature of QPOs. Low Frequency Quasi-Periodic Oscillations (LFQPOs) in the range of ~0.1-10 Hz are regularly observed in X-ray binaries. There is no consensus on the origin of LFQPOs. A popular model associates the oscillations to the Lense-Thirring (LT) precession of a hot accretion flow [109]. The hot flow mostly resembles a geometry with a truncated disc and an inner hot corona as described in the previous

subsection. LT precession is a frame dragging effect caused by the misalignment of the angular momentum of an orbiting particle and the BH spin. It leads to systematic precession of the orbit. Numerical simulations have shown that in the case of a hot, geometrically thick accretion flow, this effect leads to global precession of the hot flow [85]. The hot flow precesses like a solid body, and the net precession frequency is a weighted average of the LT precession frequencies between the inner and the outer radius of the hot accretion flow. Due to the much longer viscous time scale, global LT precession does not affect the outer thin disc. A mixture of relativistic Doppler beaming, gravitational light bending and Compton anisotropy modulates the emission of the precessing hot flow. The model predicts the right range of observed LFQPO frequencies. Their amplitude depends on the details of the geometry and the viewing angle of the observer. The rms is usually larger at high inclinations and can reach 10 percent. Interestingly, the model also predicts a modulation of the polarization fraction and angle (see [110]). Detecting such a modulation with *XIPE* will allow us to test of the LT precession model and provide new, independent constraints on the geometry of the corona and inclination angles. Fig. 2-28 shows that *XIPE* would allow us to recover the polarization modulation using the phase folding method [262].

2.3.2 Radio-quiet Active Galactic Nuclei

XIPE can constrain the geometry of the hot corona in radio-quiet AGN, measure the orientation of the dusty torus, and investigate variations in the morphology of the circumnuclear material.

X-ray polarimetry will bring new and unique information on the environment of radio-quiet Active Galactic Nuclei: from the very close neighbourhood of the supermassive black hole (hot corona, accretion disk), to the diffuse regions at pc scales (dusty torus, scattering outflows).

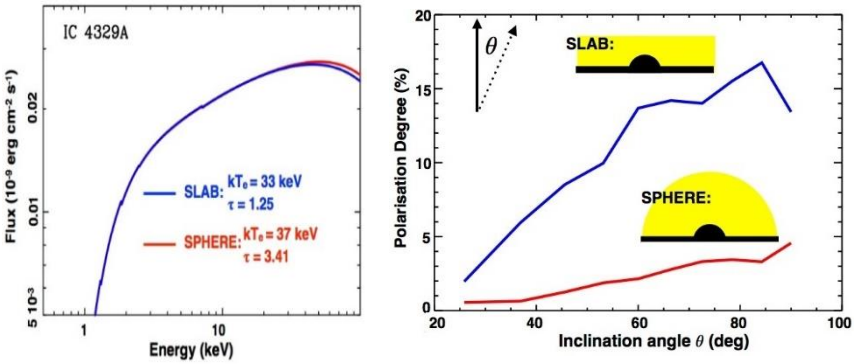

Figure 2-29 Best-fit models applied to the Seyfert-1 galaxy IC4329A. Two different disc-corona geometries are assumed: SLAB in blue, SPHERE in red. The best-fit values of the corona temperature kT_e and the vertical/radial optical depth τ are indicated on the figure ([29]). Left: the two geometries give a very similar spectrum. Right: polarization degree (integrated over 2-8 keV) as a function of the inclination angle for both geometries. The polarization degree is always larger for the slab. An MDP of ~2% would be sufficient to discriminate the two geometries from each other.

The neighbourhood of the supermassive black hole: hot corona and underlying accretion disk. The coronal emission of AGN is supposedly produced like in X-ray binaries (see previous section), the main difference being that the accretion disk emits at optical/UV instead of X-ray temperatures. Producing hard X-ray photons thus requires more subsequent Compton up-scattering than for XRBs. The coronal emission is expected to be polarized, with the polarization percentage depending mainly on the geometry and optical depth of the corona [128]. Figure 2-29 compares the expected polarization degree from a slab-like vs. a sphere-like geometry. Although the two geometries can produce a similar spectral shape (but with different coronal temperature and/or optical depth), the polarization is always stronger for a slab-like geometry and will allow us to discriminate between the two scenarios, breaking the degeneracies. With a total time investment of ~2 Ms, *XIPE* can measure the polarization degree of a representative sample of 6 bright, unobscured (e.g. free of obscuring and scattering environment) Seyfert galaxies (i.e. IC 4329A, MCG-8+11+11, GRS 1734-292, NGC 2110, NGC 5506 and MCG 5-23-16). Together with broad band X-ray spectroscopic measurements of the corona's physical parameters, polarization measurements with *XIPE* will provide a full characterization of the inner accretion flow structure.

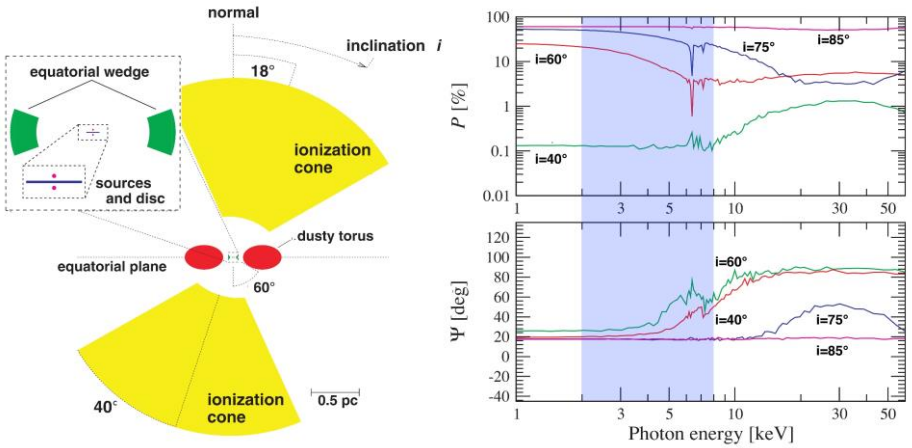

Figure 2-30 Left: Sketch of the possible geometry of the circumnuclear matter in NGC 1068. Right: expected polarization degree P and angle Ψ (measured from the direction perpendicular to the torus axis) as a function of photon energy for different inclination angles i ([94]). A misalignment between the ionization cone and the torus axis would translate into a measurable polarization angle Ψ. The grey area corresponds to the XIPE energy range.

The pc-scale environment: dusty torus, polar scattering region. On pc-scales, different reflecting regions are also present. The so-called "dusty torus" is required in AGN unification models to explain obscured vs. unobscured source properties (e.g. [13]). Despite the name, the actual morphology of the 'torus' is largely unknown, and X-ray polarimetric observations will be crucial to study this issue, as well as to determine its orientation and relation with the optical ionization cones (IR interferometric measurements indeed suggest a misalignment, [213]). The integrated 2–8 keV polarization should vary from a few percent at low inclinations (unobscured objects) up to tens of percent at larger viewing angles (obscured objects, see e.g., [94] and Fig. 2-15). Such X-ray polarization measurements will be easily reachable for bright sources. A 3 Ms observing plan (with a few hundreds of ks per object) of the 4 brightest obscured AGN (Circinus, NGC 7582, Mkn 3 and NGC 1068) will reach a MDP of 5% for each object. X-ray polarimetry will also help constraining the level of fragmentation. A clumpy torus as postulated by [191] would best explain the recently observed hard X-ray variability in NGC 1068 ([149]).

Polarization is also sensitive to morphological changes, like the ones expected from a receding torus or cloud eclipses ([148], [150]). Variations of the polarization degree by a few percent and significant variation (>10°) of the polarization angle are expected during the successive covering and uncovering of the inner part of the accretion flow by eclipsing clouds ([148]). An MDP of a few percent will allow us to study these effects by monitoring (on a timescale of months/years) a dedicated sample of AGN known to show eclipses (see Table 2 in [219] and Table 3 in [155]).

2.3.3 Sgr A* and molecular clouds in the Milky Way

XIPE will measure the polarization of the reprocessed radiation in the molecular clouds around Sgr A and verify if it is due to irradiation by X-ray emission from a past active phase of the supermassive black hole. In this case, XIPE observations would allow us to construct a 3D map of the molecular clouds around Sgr A*.*

A special application of scattering-induced polarization around a SMBH can be found for the Galactic Center. At a distance of ~ 8 kpc from Earth, the object known as Sgr A* is the closest known SMBH, with a mass ~4 million times the solar one. Sgr A* is extremely X-ray dim with a quiescent level of ~10^{-11} the Eddington luminosity. However, it was found by [246], [126], [218] that several prominent molecular clouds within ~100 pc from Sgr A* are hard X-ray sources, their spectra being characteristic of X-ray reflection by cold gas illuminated by an external source (X-ray Reflection Nebulae, XRNe, Fig. 2-31).

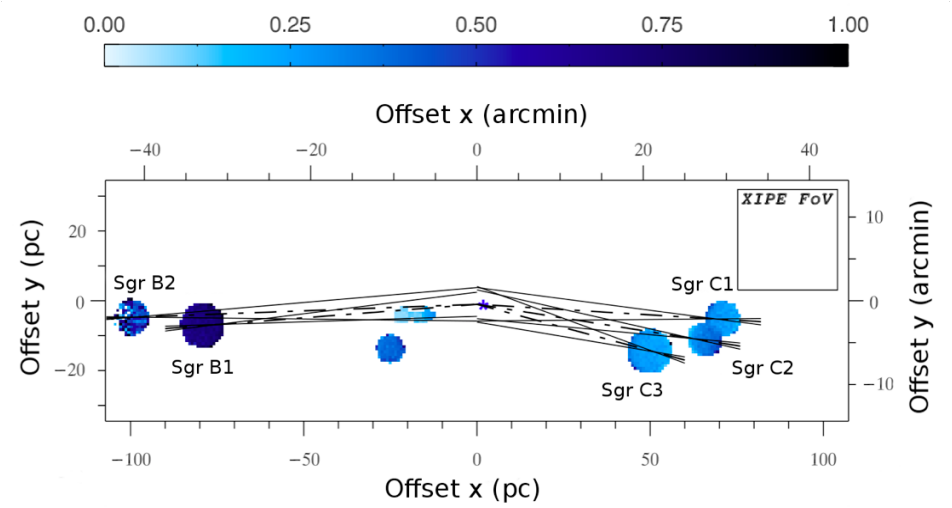

Figure 2-31 Simulated polarization map of the Galactic Centre [9]. The polarization fraction is colour-coded: white colour indicates no polarization and dark-blue is for maximum polarization (100%). The XIPE field of view (FoV) is shown on the top-right corner and the spatial resolution of the map corresponds to the pixel resolution of XIPE. A blue star indicates the position of Sgr A. Black segments are representative of the estimated polarization position angle (dashed line) and its associated error (solid line).*

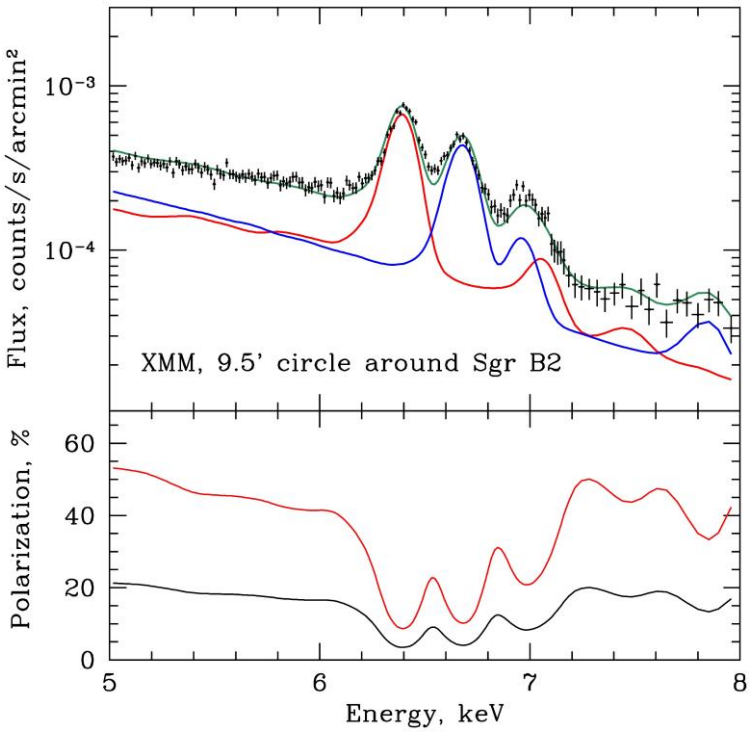

Figure 2-32 Top: spectrum extracted from a circle around the Sgr B2 clouds (XMM-Newton data). The red and blue lines show the decomposition of the spectrum into XRN and hot plasma components [4]. Bottom: expected polarization of the pure XRN component as a function of energy for scattering angles of 90° and 135° [8].

Established XRNs are the Sgr B and Sgr C complexes as well as a number of clouds known as the "Bridge". The lack of sufficiently bright, persistent irradiating sources nearby led to the hypothesis that the observed XRN emission is the "echo" of an outburst of Sgr A* that happened a few hundred years ago, when its luminosity was $10^{39\text{-}40}$ erg/s. What we see today would then be the reflected radiation delayed by the light travel time across the ~100 pc region. If true, this means that in the recent past our Galactic Centre hosted a low-luminosity AGN and we can reconstruct the history of its energy release using the XRNs ([47]).

Alternative irradiation scenarios do exist: X-ray transients that power different molecular complexes [153] or the interaction of low energy cosmic ray electrons with the molecular gas [260]. The former mechanism cannot be excluded, but it requires a population of sufficiently powerful transients to be located close to each molecular complex. As for the latter hypothesis, the XRN fluxes vary on time scales of 5-10 years [187], [203] excluding the possibility that cosmic ray electrons are responsible for the bulk of the emission. Still, both alternative mechanisms could contribute to some extent to the observed XRN signal.

X-ray imaging polarimetric measurements would fundamentally improve our understanding of XRNs. The reflected emission from a compact illuminated source must be polarized [49], [147], providing direct evidence that it comes from an XRN. Additional constraints would come from the energy-dependence of the polarization degree (Fig. 2-32). Finally, the direction of the polarization has to be perpendicular to the projected line from the molecular cloud to the illuminating source. Therefore, the observation of one XRN with *XIPE* would be sufficient to verify if Sgr A* can be the illuminating source. Observing two different XRNs would even locate the coordinates of the illuminating

source in a model-independent way (Fig. 2-31). The polarization percentage is a strong function of the scattering angle, implying that, additionally, *XIPE* can find the position of a given XRN on the line-of-sight (Fig. 2-32). It is thus possible to reconstruct the 3D distribution of the molecular gas in the Galactic Centre region – an insightful mapping that is very difficult to obtain by other means. Notice that this will also be useful to reconstruct the light-curve of the past flare of SGR A*.

The reflected fluxes from Sgr B, Sgr C and the "Bridge" imply that a 1 Msec exposure of any of these regions would yield a clear measurement and an error on the position angle below 2 degrees [147]. The flux of each XRN varies on time scales of several years. The actual observing program will be updated accordingly. Simulations show that it is highly unlikely that all currently bright XRNs will have faded away on times scales shorter than 100 years ([47]).

2.3.4 Ultra-luminous X-ray sources

XIPE can observe the brightest ULXs providing valuable information on the geometry of super-Eddington accretion flows in X-ray binaries, and crucial information to understand the nature of pulsating ULXs.

Ultra-luminous X-ray sources (ULXs) are non-nuclear accreting compact objects in nearby galaxies. Their apparent luminosities exceed the Eddington limit of Galactic stellar mass black holes (3×10^{39} erg s^{-1} for a 20 solar mass black hole). A natural explanation is that they may harbour black holes with masses in between stellar mass black holes in binary systems and supermassive black holes in the centre of galaxies. Extreme ULXs like ESO 243-49 HLX-1 and M82 X-1 may be good candidates in this respect [73], [199]. However, X-ray observations with *XMM-Newton* favour the interpretation that most ULXs are likely powered by supercritical accretion onto stellar mass black holes [92].

X-ray polarimetry may play an important role in understanding the nature of ULXs and the poorly known physics of super-Eddington accretion. Massive outflows are expected for supercritical accretion and the emergent X-ray emission may be more or less collimated and/or strongly Comptonized in the wind. Models suggest that the spectral-timing properties of ULXs are related to their accretion rate and the viewing angle [247], [172]. 3-D MHD simulations by [114] also suggest that the polarization degree and angle are a function of the viewing angle. Therefore, X-ray polarimetry constitutes a new channel to constrain the ULX models and an efficient probe of the accretion geometry in the supercritical regime. Due to their large distances from Earth ULXs are much fainter than Galactic accreting black holes. For the brightest ULXs *XIPE* could observe a MDP of 5%-10% assuming a 1 Ms exposure.

Surprisingly, the transient ULX M82 X-2 with a peak luminosity over 10^{40} erg s^{-1} was found to be an accreting pulsar [14]. Recently, two more ultra-luminous accreting pulsars were discovered in NGC 7793 ([112]; [86]) and NGC 5907 ([112]). How a pulsar can exceed its Eddington limit by such a large factor (~10^2) is mysterious. Models range from magnetars ([188]) to low-B nascent millisecond pulsars ([121]). The ULX pulsars are interesting targets for *XIPE*, as high degree of polarization is expected from highly magnetized systems. X-ray polarimetry may help distinguish whether these sources are magnetars or low-B neutron stars. M82 X-2 is not an ideal choice because it resides in a crowded region in the center of the starburst galaxy M82. The ULX pulsars in NGC 7793 and NGC 5907 are the brightest sources, respectively, in their host galaxies and can be observed with *XIPE*. They are transient sources, with a flux of roughly 10^{-12} erg cm^{-2} s^{-1} in 2-8 keV at the peak, corresponding to an MDP of about 10% with an exposure of 1 Ms.

2.4 Fundamental Physics

Cosmic sources and the Universe as a whole are natural laboratories to study effects of Fundamental Physics that are extremely difficult or altogether impossible to test on Earth. X-ray polarimetry is particularly valuable in this respect as distinctive signatures on the polarization are expected from radiation transfer through strong magnetic and/or gravitational fields.

It is one of the most exciting goals of *XIPE* to test vacuum birefringence, a QED effect in extreme magnetic fields that was predicted 80 years ago, but never unambiguously verified. While producing no effect in the

flux modulation, vacuum birefringence should induce characteristic signatures in the phase modulation of the X-ray polarization of magnetars (and possibly also in sources with less extreme magnetic field).

The polarization properties of radiation emerging from the vicinity of a black hole event horizon depends on the gravitational theory assumed. In principle, X-ray polarization could thus test General Relativity (GR). Still, the polarimetric differences between competing theories are too small to be of any practical use ([108]). On the other hand, once GR is assumed, the energy-dependent polarization percentage and rotation of the polarization angle with photon energy in Black Hole X-ray Binaries in the soft state provides a new, independent tool to measure the black hole spin. A time-dependent rotation of the polarization angle may also be used to measure the spin in supermassive black hole of AGN, though the required exposure time may be prohibitively long, and certainly help solving the long-standing debate on the true origin of the broad feature around 6 keV (relativistically distorted iron line vs. complex absorption).

On a more speculative side, energy-dependent rotations of the polarization angle from distant sources may occur by a vacuum birefringence that is related to a Lorentz Invariance Violation (LIV) as predicted by some Quantum Gravity theories. *XIPE* will search for these effects by observing blazars at different distances and, in case of a negative result, put tight upper limits on the LIV.

Axion-like particles (ALPs), one of the dark matter candidates, are expected to interact with photons in an external magnetic field, significantly modifying their polarization properties, either reducing the polarization degree of a background blazar or introducing polarization in an otherwise unpolarized source. A polarization degree of even a few percent in a Galaxy Cluster would be an exciting indication of the presence of ALPs.

2.4.1 Quantum electrodynamics

XIPE can unambiguously test the QED birefringence expected in the extreme magnetic field of magnetars and X-ray pulsars, verifying the effect predicted eighty years ago but yet to be unambiguously confirmed.

One of the first predictions of quantum electrodynamics - even before it was properly formulated - was vacuum birefringence in strong magnetic fields [99], [276], a prediction that remained robust when QED was formulated more carefully [231]. In a weak magnetic field ($B \ll B_{QED}=4.4\times10^{13}$ G), the difference in the refraction index between photons whose electric field is parallel or perpendicular to the magnetic field (O− and X−mode, respectively) simply is ([104]):

$$\Delta n = \frac{\alpha}{4\pi}\frac{2}{15}\left(\frac{B}{4.4\times10^{13}\ \mathrm{G}}\right)^2 .$$

while for $B \gg B_{QED}$ the dependence of Δn on B is linear. For terrestrial fields this is vanishingly small and has not yet been measured in the eighty years since the prediction. On the other hand, astrophysically this effect can be important for neutron stars and white dwarfs [105]. For these objects, although the difference in refraction index is still much smaller than unity, the combination $\Delta n(l/\lambda)$, where l is the length over which the refraction index changes and λ is the wavelength of the light, may be very large. This means that the polarization states of the light evolve adiabatically, so light originally polarized in the X−mode will remain in the X−mode even if the direction of the field changes. From the point of view of the observer, the direction of the polarization will follow the direction of the magnetic field as the light propagates through it.

Magnetized neutron stars naturally produce polarized X-ray radiation and, furthermore, the field strengths are sufficiently strong and the length scales sufficiently large for vacuum birefringence to decouple the polarization states with dramatic effects on the observed polarization. The recently observed optical polarization in the isolated neutron star RX J1856.5-3754 [174] is consistent with vacuum birefringence, but other models are not yet ruled out.

Although black holes themselves do not harbour magnetic fields, recent calculations indicate that the vacuum polarization may be important for the propagation of radiation near black hole accretion disks if magnetic fields provide the bulk of the viscosity [35].

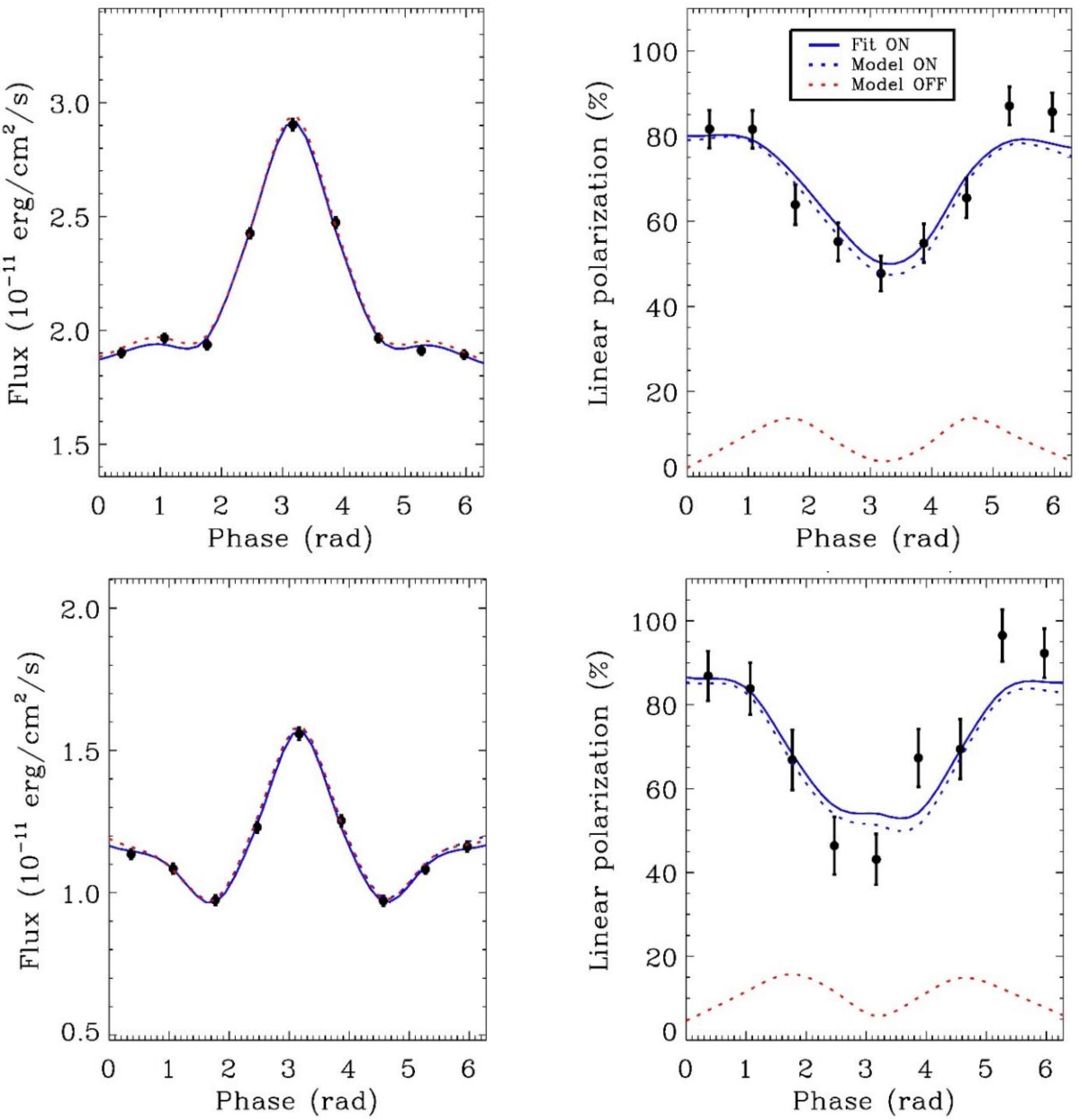

Figure 2-33 From left to right: light curve and polarization fraction for AXP 1RXS J1708 (upper panels) and SGR 1806-20 (lower panels). Thermal surface photons are assumed to be 100% polarized in the extraordinary mode. The data points (filled circles with error bars) were generated according to the model shown with the dashed blue line. The full line shows the simultaneous best fit, while the dashed red lines correspond to the same models but without QED effects. The geometrical angles are χ=90° and ξ=60°.

The QED effect is strongest in magnetars, whose *B*-fields range from 10^{14} to 10^{15} G, and it is for these objects that the calculations are most comprehensive. Vacuum birefringence increases the expected linear X-ray polarization at the surface of a neutron star from about 5-20% to nearly 100% ([107]).

Radiation coming from the surface of an ultra-magnetized neutron star is expected to be strongly polarized because of the much reduced opacity for X−mode photons (e.g. [96]; but see [22]). Photons will then resonantly scatter on magnetospheric charges and this can change the polarization state (mode switching), and finally reach infinity (see e.g. [259]; see Sect. 2.2.5). As radiation propagates outwards, the strong magnetic field forces the direction of the wave electric field to instantaneously adapt, over a length scale $\ell_A = \lambda/\Delta n \leq 1$ cm at X-ray energies near the surface, to the direction of the local magnetic field, so that the photon keeps its linear polarization, either X or O (mode locking or adiabatic propagation). This is a pure QED effect and it will take place until the length scale $\ell_B \approx r/6$ over which the *B*-field evolves is larger than ℓ_A. The adiabatic region extends

up to the polarization-limiting radius, $r_A \sim 30\ (B_p/10^{13}\ G)^{2/5}\ (E/1\ keV)^{1/5}\ R_{NS}$, after which the electric field direction freezes ([105], [106]; see also [251]).

The existence of the adiabatic region is crucial for the observed polarization properties of highly magnetic neutron stars. In order to compute the polarization fraction and angle of the detected radiation, the Stokes parameters of the single photons, each of which is referred to the magnetic field direction at decoupling (i.e. at $\sim r_A$), must be rotated to bring them to a common frame (the instrument frame). This rotation strongly depolarizes radiation, more so for the smaller values of r_A. Would the adiabatic region have vanishing depth (r_A coincident with the star radius R_{NS}), fully polarized radiation at the surface would appear at most 20% polarized at the observer on Earth. This is, therefore, the maximum polarization expected in the absence of QED effects. On the other hand, if r_A is some tens of stellar radii, as expected in magnetars, the effects of rotation are much less dramatic and radiation is received with almost its original polarization degree ([252], [107]).

Resonant Compton scattering typically occurs within ~ 10 R_{NS}, well inside the adiabatic region, so that the photon polarization state between scatterings does not change, decoupling scattering and QED effects [79], [251]. The wave equation, then, needs to be solved only outside the scattering region, typically from just below r_A to infinity. Results of Monte-Carlo runs for the lightcurve and the polarization degree are shown in Fig. 2-33 for two bright persistent magnetar sources, AXP 1RXS J1708 and SGR 1806-20, together with the simulated *XIPE* response for an integration time 100 ks each. The same Monte-Carlo simulations were then run without accounting for vacuum polarization effects, and also shown in Fig. 2-33 for comparison. While the flux is the same, the polarization degree dramatically changes. The "QED-off" results for the polarization degree cannot be reconciled with the data for any combination of the model parameters, proving that an observation with *XIPE* can indeed disambiguate the two possibilities and provide the first evidence for vacuum polarization effects in a strong magnetic field. QED effects can also be probed in 4U 0142+61, where the contribution of resonant Compton scattering is less important in the *XIPE* band, but the results for QED are equally dramatic [36].

Vacuum birefringence also modifies the scattering and absorption cross sections, which exhibit resonant features close to the so-called vacuum resonance energy ([265], [168]). As a result, strong variations of the polarization degree and angle at corresponding energies are expected. The resonant energy E_v depends on the magnetic field strength and the plasma density $E_v \sim 13 n_{e,22}^{1/2}/B_{12}$ (here $n_{e,22}$ is the plasma density in units of 10^{22} cm^{-3}). For magnetars, the low plasma density and high magnetic field imply that this energy is below the *XIPE* band, while for X-ray pulsars it is expected to lie within the *XIPE* band for most sources (Ghosh 2013). Polarimetric observations of X-ray pulsars will thus also allow us to test the vacuum birefringence. We note that while QED effects are stronger in magnetars, X-ray pulsars are typically much brighter sources and, therefore, easier targets to observe. Once the importance of QED effects is confirmed, an estimate of the radius of the neutron star may in principle be obtained [37], but the effect is probably too subtle to be accessible with *XIPE* in reasonable exposure times.

2.4.2 Strong gravity

XIPE can provide independent constraints on the black hole spin in Galactic black hole X-ray binaries and discriminate between complex absorption and relativistic reflection models in Active Galactic Nuclei.

Galactic Black Hole X-ray Binaries. Stellar mass black holes are the most promising sources to probe strong gravity effects and to put constraints on the angular momentum (spin) of black holes with *XIPE*. They provide us with large X-ray count rates and the cleanest method to measure the spin when in the so-called high/soft state. In this state, the dominant spectral component across the 2-8 keV band is thermal emission from the accretion disc. Strong gravity effects rotate the polarization angle of the disc radiation progressing along a geodesic towards the observer. The rotation angle depends on the location of the emitting point on the disk. When integrating the emission across the disk azimuth, a net rotation remains. The closer to the black hole the emitting point is, the larger the net rotation. Since the emission is locally thermal and since the temperature decreases with the disk radius, eventually a rotation of the polarization angle (along with variations in polarization degree) with energy should be observed ([241], [50], [163], [61], [62], [230], [231]). Such

measurements can be taken with *XIPE* and compared with the black hole spin estimated from fitting the thermal disc spectrum, X-ray reflection or quasi-periodic oscillations.

The latter three methods are not related to the polarization method and do not always mutually agree with each other. Thus, X-ray polarimetry with *XIPE* will add new, independent constraints on the black hole spin and help us to understand the final stages of the gravitational collapse of very massive stars.

Figure 2-34 shows simulations (based on [61]) for a 110 ks exposure of the black hole X-ray binary GRS1915+105 in the high/soft state, assuming different spin values, a=0 (zero spin), a=0.9 and a=0.998 (maximum spin). The energy dependence of the polarization degree and angle are different in the three cases, clearly indicating that *XIPE* will discriminate between them. In particular, simulations show that the spin value can be recovered with a statistical error Δ of about 0.1, 0.01 and 0.001 for a=0, 0.9 and 0.998. The relativistic effects are more pronounced, and the intrinsic polarization higher, for high inclination angles, making GRS1915+105 (70 degrees inclination, [180]) the ideal source. However, other less inclined sources can still be profitably explored with reasonable exposure times (a few days). Additionally, about 6 transient BH binaries are expected during 3 years of *XIPE* operation, which may be other good candidates to search for General Relativity effects.

Active Galactic Nuclei. In AGN, the disc thermal emission is outside the working band of *XIPE*. However, thermal photons are Comptonized and scattered in the hot disk corona, whose precise geometrical shape is unknown and will be studied with *XIPE* (see Section 2.3.2). Part of the X-ray corona emission hits the accretion disc, where it is reprocessed and partly reflected towards the observer. There is increasing evidence that the X-ray emitting corona is very compact ([217], [66]), with a mean height varying with time (e.g., [177], [70], [198]). The polarization degree and angle of the reflected radiation must vary accordingly ([62]), in a way that depends on the spin of the black hole. The effect is likely to be small, however, and its search will be a by-product of AGN observations performed for, e.g., coronal studies (see Sec. 2.3.2).

The reprocessed emission may also bear imprints of General Relativity effects, such as the broadening of the iron line in the *XIPE* energy band. Such a broad iron line was reported for the first time in MCG-6-30-15 ([249]) and then confirmed by several other measurements with different X-ray satellites (see, e.g., [280], [69], [178], [152]). However, other authors argued that the spectral shape of the broad iron K line in this and other sources could also be modelled as a non-relativistic feature arising from partial covering ([176]). X-ray polarimetry may help to resolve this debate because the partial absorption in a clumpy outflow intercepting the line of sight generally induces low polarization and always produces a polarization degree and position angle that are constant across the iron line band. On the contrary, in the reflection case the polarization is large, the polarization degree changes with the energy, and the position angle varies systematically across the iron line ([151]). Simulations show that in the case of MCG-6-30-15 and NGC 1365, two of the most debated sources,

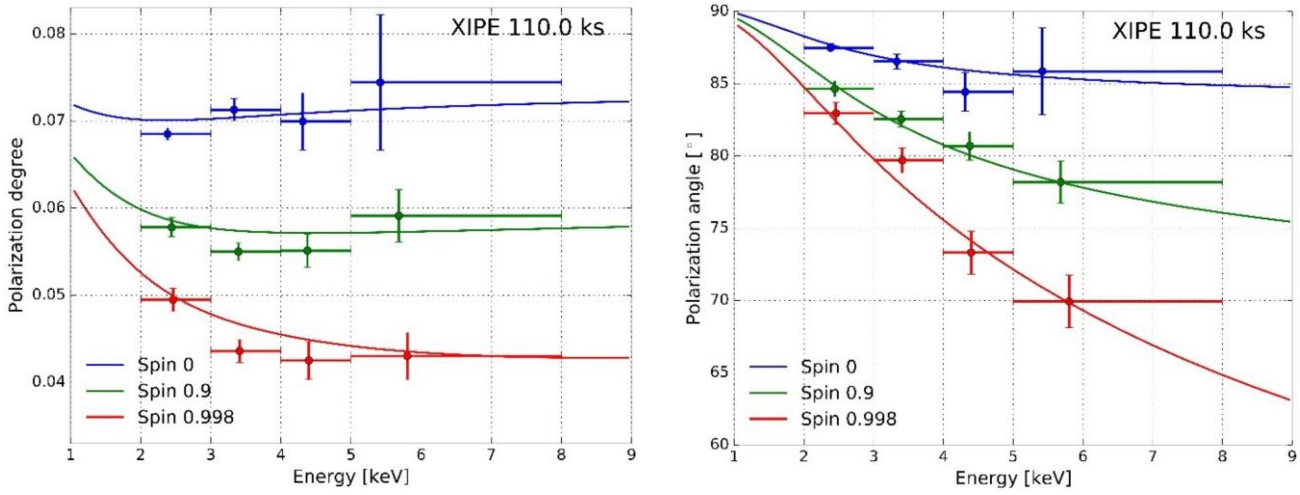

Figure 2-34 Simulated 110 ks XIPE observation of GRS 1915+105 in the soft state for 3 angular momenta of the black hole: the Schwarzschild case (a=0), a moderate black hole spin (blue, a=0.9) and the extreme Kerr case (red, a=0.998). The figure shows the polarization degree (left) and the polarization position angle (right) as a function of photon energy.

in the rather conservative assumption of 2% intrinsic polarization, *XIPE* is able to distinguish between the two models with the large, but still affordable, exposure time of a few Ms.

2.4.3 Quantum Gravity

XIPE can put tight constraints on effects, like vacuum birefringence, expected in some Quantum Gravity theories by searching for rotation of the polarization angle from distant blazars.

One of the most ambitious efforts of modern physics is to develop a theory that unifies gravity with the other fundamental forces within a single theoretical framework. Different approaches to Quantum Gravity (QG) are being pursued such as Loop QG, String, and non-commutative space-times. A common feature of most of the approaches (but not all, e.g. [221]) is that deviations from known physics, specifically Lorentz Invariance Violation (LIV), are predicted near the Planck scale (energies of 10^{28} eV or lengths of 10^{-35} m), far beyond what is currently achievable in the laboratory [9]. Thus, efforts to find good observational tests have turned towards astrophysical measurements where tiny effects at accessible energies can be translated into observable effects when accumulated over (literally) astronomical distances (for a review see [164] and [138]). One such effect is vacuum birefringence, i.e. a dependence of photon propagation in vacuum on polarization [87].

There are two ways, in which *XIPE* could play a crucial role: (1) detection of a net polarization integrated over the whole energy band from astrophysical sources at very large distance; (2) study of the rotation of polarization angle as a function of energy over cosmic distances. In the first case, by integrating over the 2-8 keV band, LIV would generate fluctuations in the polarization cancelling each other, so that the net signal would be zero. Therefore, any detection of polarization from a cosmic source at distance $d(z)$ implies the lack of vacuum birefringence and therefore a constraint on LIV. A strong advantage of this option is that a detection of polarization is enough - no modelling of the cosmic source is required. However, non-detection could result from a lack of intrinsic polarization at a level detectable with *XIPE* rather than birefringence, so it is important to use high redshift sources for which *XIPE* can establish the polarization degree of their low redshift counterparts. The scale of the constraint is given by the dimensionless parameter ξ, which is inversely proportional to the difference of the squares of the photon energies (fixed by the *XIPE* bandpass) and the source distance. The best constraints will come from the most distant source for which *XIPE* can achieve polarization detection. A blazar in outburst with a 2-8 keV flux in excess of 5×10^{-12} erg cm^{-2} s^{-1} will require an exposure of about 500 ks to reach an MDP of 7%. There are a few sources known to reach such fluxes. The BL Lac AO 0235+164 is one of the highest redshift blazars where the X-ray band is dominated by synchrotron radiation and thus likely to be significantly polarized [82]. Its redshift of z=0.94 would lead to a constraint of $\xi<10^{-12}$. At higher redshifts, it is possible to find only quasars, but in those sources the X-ray band is dominated by external Compton processes, making it difficult to assess the level of intrinsic polarization; a question that the study with *XIPE* of nearby quasars will help address. A detection of X-ray polarization from the quasar PKS 2126-158 (z=3.268; MDP=5% with a 500 ks exposure time) would allow us to set a tight constraint of $\xi<10^{-13}$. The *INTEGRAL* polarization detection of GRB 140206A placed a limit of 10^{-14} [95], but this was performed with instruments neither designed nor calibrated for X-ray polarimetry.

The second case, the study of the rotation of the polarization angle may allow for more sensitive constraints. However, even a positive result will require careful analysis of the astrophysical processes to determine the angle at the source (based on theoretical modelling and/or observations at longer wavelengths) and to rule out all possible astrophysical explanations of the rotation. The fact that *XIPE* observes X-rays offers the advantage that the measurement is not affected by Faraday rotation, as it is the case for radio observations. A 500 ks exposure of a source with 2-8 keV flux of 5×10^{-11} erg cm^{-2} s^{-1} and 10% polarization, will allow us to measure the angle with an error of about 1.8°, which in turn translates into an improvement on the upper limit of ξ by a factor ~5. *XIPE* could also measure the intra-band rotation, so overcoming the difficulties outlined above, but at the expense of very long exposures (a few Ms) on bright sources.

2.4.4 Axion-like Particles

XIPE can perform sensitive searches for Axion-like Particles by searching for polarization signatures in Clusters of Galaxies.

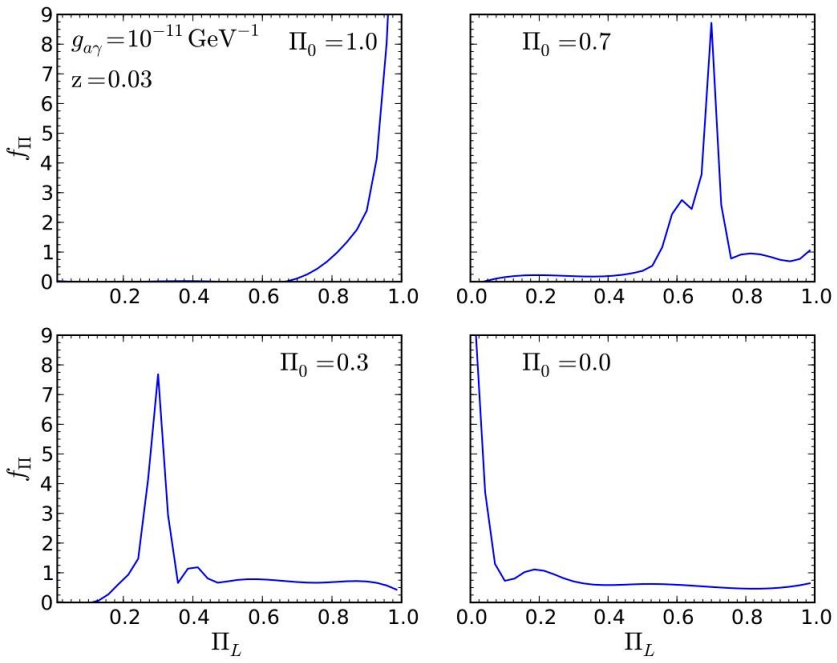

Figure 2.35 Expected probability density function f_π for the final linear polarization after propagation in the extragalactic magnetic field considering a sample of sources at z = 0.03 with initial polarization of 100%, 70%, 30%, 0.0%.

A generic prediction of many extensions of the Standard Model for elementary particles is the existence of axion-like particles (ALPs) (for a review, see [113]. They are extremely light pseudo-scalar bosons which couple only to the photon through the term $g_{a\gamma}$ a $\boldsymbol{E}\cdot\boldsymbol{B}$ in the Lagrangian, where a is the ALP field, $\boldsymbol{E}$ is the electric field of the propagating photon and $\boldsymbol{B}$ the external background magnetic field. ALP mass m and $g_{a\gamma}$ are unrelated parameters. Outside the Galaxy, $\boldsymbol{B}$ is poorly known but it is usually supposed to have a domain-like structure, with coherence length 1-10 Mpc, strength up to 1 nG in all domains but random orientation in every domain [212]. In such a situation, two relevant physical phenomena can take place. Because of the above photon-ALP coupling term, only photons polarized inside the plane defined by B and the photon momentum mix with ALPs, whereas those with polarization perpendicular to that plane do not. So, such a term acts like a polarizer [145]. X-ray photons emitted by a background polarized source propagate in the domain-like random B network before reaching us. Because of such a randomness, the initial linear polarization is expected to get smeared out [17]. The probability density function f_Π is evaluated for all possible linear polarizations, assuming $g_{a\gamma}=10^{-11}$ GeV^{-1} and m=10^{-14} eV. The results are shown in Fig. 2-35 for a sample of source at z=0.03 and four possible initial linear polarizations P_0=100%, 70%, 30%, 0. Once *XIPE* has defined the polarization properties of e.g. blazars in the local Universe, by observing more distance objects one can check whether the polarization is modified along the trajectory towards the observer.

An even more compelling test is suggested by Fig. 2-35, which shows that on the right of the peak there is a nearly constant long tail, which is the polarization imprinted by the magnetic domain closest to us. So, even by looking at a fully unpolarized source one may detect a linear polarization degree. Galaxy Clusters are the best candidates. The X-ray emission can be totally explained with thermal bremsstrahlung. The presence of a non-thermal component is seriously constrained by *Swift*/BAT [7] and NUSTAR [88]. The polarization expected from anisotropies in the collective motion of electrons amounts to only ~0.1% [122], lower than the systematic uncertainties of *XIPE* (see sec. 2.1.8). Another source of polarization may be the resonant scattering of photons in lines [227], which is also expected to be very low and in any case can be easily removed with the spectral sensitivity of *XIPE*. The imaging capability of *XIPE* can be used to remove regions of radio halos as well as any other suspicious part, such as AGNs or regions in the process of merging. Therefore, for all practical purposes Cluster of Galaxies are expected to be intrinsically unpolarized, and the detection of a polarization of even a few % in a Galaxy Cluster would point to something that cannot be explained in terms of the cluster plasma itself. With an observation of 10^5 s of Abell 2199 (z=0.031) and Abell 496 (z=0.036), *XIPE* can reach a MDP of 4.9% and 5.2% respectively. For a single cluster a long pointing of 10^6 s can be foreseen, in order to arrive to a MDP<1.5%.

3 Scientific requirements

The scientific cases presented in Section 2 require polarimetry of source emission in the X-ray energy range; moreover, the measurement of polarization has to be spectrally, temporally and angularly resolved. In this section, required sensitivity and scientific performances are derived from the scientific objectives described above, in order to exceed the expectations from theoretical models. This will allow *XIPE* to meet its scientific objectives with an adequate safety margin. The main *XIPE* scientific requirements are presented in Table 3-1 and discussed below.

Table 3-1 Summary of XIPE main scientific requirements.

Characteristic	Requirement (Goal)	Note	Science driver
Polarimetric sensitivity	<10%	In the 2-8 keV energy range, for a flux of $2x10^{-11}$ erg s^{-1} cm^{-2} for an observation of 100 ks	Detect polarization for *XIPE* targets
Mirror effective area	>1100 cm^2	At 3 keV	Apportioning of Polarimetric Sensitivity requirement
High-energy mirror effective area	>600 cm^2 (>800 cm^2)	At 7 keV	Apportioning of Polarimetric Sensitivity requirement
Focal plane detector efficiency	>10%	At 3 keV	Apportioning of Polarimetric Sensitivity requirement
Focal plane detector modulation factor	>30%	At 3 keV	Apportioning of Polarimetric Sensitivity requirement
Spurious polarization	<0.5%		Detect polarization as low as 1%
Energy range	2-8 keV (1.5-12 keV)		Trade-off among *XIPE* scientific objectives
Energy resolution	<25%	At 5.9 keV	Detect polarization variation with energy
Energy resolution for point sources	<20%	At 5.9 keV	Detect polarization variation with energy
Angular resolution	<30 arcsec <20 arcsec	At 3 keV, HEW	Resolve main structures of *XIPE* extended targets
Field of View	>10 arcmin	Diameter	Observe most of *XIPE* targets with a single pointing
Timing resolution	8 μs		Fold light curves of millisecond pulsars
Time synchronization with UTC	4 μs		Compare *XIPE* observations with those of other observatories
Reaction to target-of-opportunity request	<12 h	From trigger of the SOC; during normal working hours	Observation of transient sources
Mission lifetime	3 years (5 years)		Carry out *XIPE* observation plan.
Observation duration	5 ks – 4 Ms		Achieve a sufficient sensitivity to perform spatially, spectrally and time-resolved observations
Number of targets per years	>150	Not including monitoring observations (if necessary)	Carry out *XIPE* observing plan

Number of monitoring observation per year	>350	If necessary	Observe periodically key variable sources if no external trigger is available
Forbidden direction	None		Not prevent observation of any potential target
Field of Regard	50% of the sky		Carry out *XIPE* observing plan
Stability on degree of polarization measurements	<5% (<2%)		Compare observations at different epochs
Angle of polarization knowledge	5 arcmin	With respect to celestial reference frame	Comparison with other observatories
Background	$\leq 8\text{x}10^{-4}$ ct s^{-1} cm^{-2} keV^{-1} $detector^{-1}$	Assuming 3 detectors	1/3 of the counting rate of the faintest *XIPE* target
Maximum flux (without grey filter)	2 Crabs	Corresponds to $4\text{x}10^{-8}$ erg s^{-1} cm^{-2}. With a dead time <10%	Observation of bright targets
Dead time	<300 μs		Observation of bright targets
Pointing accuracy	3 arcmin	Diameter distance, 2 σ	Maintain the target in the center of the field of view to limit vignetting
Misalignment of telescope(s)	<7%	Observation time loss due to vignetting	Limit the vignetting
Astrometric accuracy	10 arcsec	Diameter, at 2 σ	Locate unknown sources

3.1 Measurement of linear polarization in X-rays

In the X-ray energy band, linear polarization is usually measured by means of the azimuthal response of the instrument, which is called *modulation curve*. For photoelectric polarimeters as those on-board *XIPE*, the modulation curve is practically the histogram of the photoelectron directions of emission, measured on the plane orthogonal to the direction of incidence. If the radiation is polarised, the modulation curve shows a cosine square modulation, whose amplitude is proportional to the degree of polarization and whose phase is related, and coincides for photoelectric polarimeters, with the angle of polarization. The amplitude of the cosine square modulation obtained in case of completely polarised photons is called *modulation factor* μ; usually, it has to be measured or derived by accurate Monte Carlo simulations as it is never 100% for real instrument and most often changes with energy.

The measurement of polarization can be extracted from the modulation curve with different approaches which are, however, substantially equivalent. The "classical" one, which is described in the following, is to fit the modulation curve with a cosine square function *M(φ)* with free amplitude and phase:

$$M(\varphi) = A + B\cos^2(\varphi - \varphi_0)\,,$$

where $a = B/(B + 2A)$ is the measured cosine square amplitude. The polarization *P* is derived by normalising the measured amplitude for the value corresponding to completely polarized photons, expressed through the modulation factor:

$$P = \frac{1}{\mu}\frac{B}{B + 2A} = \frac{a}{\mu}$$

The angle of polarization coincides with φ_0 in the instrument frame of reference, and then it can be referred to sky coordinates by means of the knowledge of the pointing direction.

3.1.1 Minimum Detectable Polarization

Sensitivity of polarimetric observations is limited mainly by the statistical fluctuations in the instrumental azimuthal response. Other limiting factors are the presence of spurious systematic modulations, which may mimic the presence of a cosine square variation in the modulation curve, or the background of the observation. However, as it will be discussed in the following, none of these contributions has a practical impact on the *XIPE* sensitivity.

In case of photoelectric polarimeters, the modulation curve is the histogram of the photoelectron direction of emission. Although such distribution is – statistically speaking – flat when the incident radiation is not polarized, the number of events emitted in each azimuthal bin is Poisson-distributed and a fit with a cosine square function always returns a certain amplitude and hence polarization value. The polarization signal which can be attributed to statistical fluctuations, at a certain confidence level C.L., is called Minimum Detectable Polarization (MDP) and it is calculated as ([271]):

$$MDP = \frac{2\sqrt{-\ln(1-C.L.)}}{\mu\, R_S}\sqrt{\frac{R_S + R_B}{T}} = \frac{4.29}{\mu\, R_S}\sqrt{\frac{R_S + R_B}{T}}\ (at\ 99\%\ C.L.),$$

where R_S and R_B are the source and background counting rate, respectively, and T is the observing time.

MDP is usually calculated at the 99% confidence level. This implies that if the polarization detected in a specific measurement is higher than the corresponding MDP of that measurement, then there is less than 1% probability that the detected signal is caused by statistical fluctuations. On the contrary, if the detected polarization is lower than the MDP, there is more than 1% probability that the signal is random, and therefore the measurement is not significant at that confidence level. A lower MDP corresponds to a better sensitivity.

It is worth noting that the equation expressing the MDP highlights the fact that X-ray polarimetry requires a huge number of photons, with respect to spectroscopy or imaging, to achieve a sufficient sensitivity. For example, even in the best-case-scenario of source-dominated measurements (R_B=0), it would take 2x10^6 counts for an instrument with μ=0.3 to achieve a MDP of 1%, which is adequate to discern the expected signal from many cosmic sources.

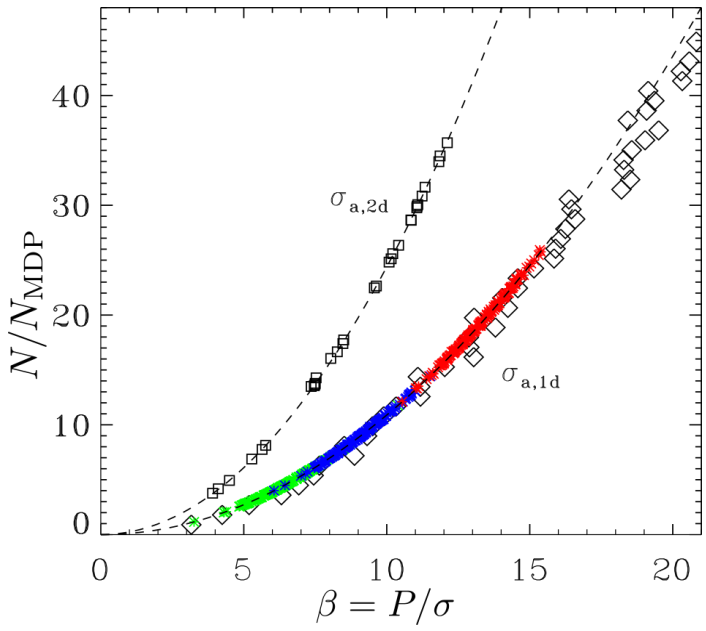

Figure 3-1 Number of counts needed, in units of N_{MDP}, to achieve a certain signal to noise β.

3.1.2 Significance

If the background is negligible, as it is for most *XIPE* observations (see Section 3.2.8), the formula above allows to relate the number of counts collected, *N*, to the MDP:

$$MDP = \frac{4.29}{\mu}\frac{1}{\sqrt{N}},$$

where $N=R_S T$. It follows that the number of counts N_{MDP} which has to be collected to reach a MDP equal to a certain assumed polarization *P* is:

$$N_{MDP} = \left(\frac{4.29}{\mu P}\right)^2.$$

The N_{MDP} value can be related to the number of counts needed to achieve a certain Signal to Noise (*S/N*, or β) of the measurements, defined, as is customary, as the ratio between the measured polarization and its error σ. In Figure 3-1, the number of counts required to reach a certain value of β is reported as a function of β.

The two curves refer either to the measurements of the degree of polarization ($\sigma_{a,1d}$) only, or of both the degree and the angle of polarization ($\sigma_{a,2d}$). If both the degree and the angle of polarization are measured, a measurement with P=MDP ($N/N_{MDP}=1$) corresponds to a S/N of 2.02 in *P*; instead, if only the polarization measurement is interesting, a measurement with *P=MDP* (*$N/N_{MDP}=1$*) has a *S/N* of 3.03 in this parameter (see [244] for more details). The two curves in Figure 3-1 are well represented by the following relations:

1 parameter case: $\frac{N}{N_{MDP}} = \beta_{1d}^2 \frac{2}{4.29^2}$

2 parameters case: $\frac{N}{N_{MDP}} = \beta_{2d}^2 \frac{1}{4.1}$

At the 99% C.L., $N_{MDP} = \left(\frac{4.29}{\mu P}\right)^2$ and the relation among the signal to noise, the polarization and the collected counts *N* is:

1 parameter case: $\beta_{1d} = \sqrt{\frac{N}{2}}\mu P$

2 parameters case: $\beta_{2d} = 0.472\sqrt{N}\mu P$

The uncertainty on the polarization angle is given by $\sigma = 28°.5/\beta_{2d}$.

3.2 Requirements

3.2.1 Polarimetric sensitivity

Polarimetric sensitivity requirement for *XIPE* is expressed through the MDP: The Minimum Detectable Polarization at the 99% confidence level shall be lower than 10% for a reference source with flux $2\text{x}10^{-11}$ erg s^{-1} cm^{-2} in the 2-8 keV energy range and power law spectrum with index 2 (i.e., 1 mCrab), assuming an observation lasting 10^5 seconds. This is completed with a requirement on the possible contribution of instrumental spurious signal, which shall be lower than 0.5%.

The expected polarization from theoretical models is reported for several representative sources belonging to different classes in Table 3-3. In the same table, the *XIPE* sensitivity for any specific observation, derived by the requirement specified above, is also reported, together with the Current Best Estimate (CBE) sensitivity. The table shows that *XIPE* polarimetric sensitivity requirement allows for solid margins to achieve mission objectives, and that the expected signal is much higher than the possible contribution of spurious instrumental effects.

Polarimetric sensitivity requirement breakdown

For a fixed reference source spectrum, the MDP depends on (see Section 3.1): (i) the modulation factor, (ii) the number of collected counts and (iii) the background counting rate. *XIPE* measurements will be largely

source-dominated (by orders of magnitude) for the reference source specified above (see also Section 3.2.8); as a consequence, it is safe to assume that the sensitivity requirement translates into requirements on the modulation factor and the number of collected counts. The former is a specific characteristic of the technique used for measuring the polarization, and of its practical implementation; the number of collected counts, given a source flux and an observing time, depends, instead, on the quantum efficiency of the detector and on its collecting area.

An apportioning of the polarimetric sensitivity requirement in its fundamental contributions is reported in Table 3-2. As all of these quantities depend on the energy, a reference energy of 3 keV, which is representative of the required energy range (see Section 3.2.2), is chosen. *XIPE* takes advantage of grazing incidence mirrors to achieve a sufficient collecting area, whereas the requirements on the focal plane detector prescribe the use of state-of-the-art photoelectric polarimeters to achieve a good quantum efficiency and modulation factor in the energy range of interest.

Although the collecting area at 3 keV is representative of the *XIPE* polarimetric sensitivity for many targets, some sources, e.g. molecular clouds in the Galactic center or NGC1068, are strongly absorbed at this energy and the study of the (polarized) scattered radiation requires having a sufficient sensitivity at higher energy. This drives the *XIPE* requirement on the high energy collecting area, which is 600 cm^2 with a goal of 800 cm^2 at 7 keV, assuming a detector efficiency of 1% at this energy.

3.2.2 Energy range and spectral capabilities

The large number of different scientific objectives of the *XIPE* mission can be pursued with polarimetric observations in the X-ray energy range; notwithstanding, any specific goal can be better (or more easily) achieved in slightly different energy bands. In Table 3-4 the feasibility of the different *XIPE* scientific objectives is compared in different X-ray energy intervals, roughly corresponding to polarimeters based on different techniques. It is evident from the table that the "classical" X-ray energy range between about 1 and 10 keV is the best trade-off for achieving all the *XIPE* scientific goals, and that photoelectric polarimeters are required in this energy range. This sets the *XIPE* requirement on the energy range, which is 2-8 keV with a goal of 1.5-12 keV. In many cases, e.g., the identification of acceleration regions in SNRs, a peculiar dependence on energy of both the degree or the angle of polarization is expected. To take advantage of these observables, *XIPE* observations shall have to be resolved in at least 3 independent energy bands. Expressing this requirement in an easily and measurable way, the spectral resolution of *XIPE* shall be better than 25% at 5.9 keV.

It is worth mentioning that the spectral resolution requirement is at least partially related to the sensitivity requirement, because the number of energy bins in which a certain observation can be split depends also on the capability to collect in each bin a sufficient number of photons to detect the expected signal. However, for intermediate-bright, point-like sources (e.g., galactic binaries and some extended sources like the Crab PWN and the brightest SNRs), *XIPE* will be able to collect sufficient statistics to spectrally resolve the observation in more bins, and therefore an additional requirement is set, that is, that the energy resolution shall be better than 20% at 5.9 keV for point-like sources. This will be beneficial, e.g., for the measurement of black hole spin in galactic X-ray binaries.

Table 3-2 Apportioning of the XIPE sensitivity requirement.

SCI-POL-R-010: MDP<10%		
Contribution	**Value**	**Conditions**
Mirror effective collecting area	>1100 cm^2	At 3 keV
Focal Plane Detector efficiency	>10%	At 3 keV
Focal Plane Detector modulation factor	>30%	At 3 keV
	MDP<10%	Between 2-8 keV, for the reference observation

Table 3-3 Comparison between requirement sensitivity, derived from the XIPE polarimetric sensitivity requirement, and theoretical predictions for a number of representative sources of different classes. XIPE polarimetric sensitivity requirement allows to concisely express the fact XIPE sensitivity will be sufficient to detect the expected signal for many classes of sources, with a solid safety margin. The CBE column reports the Current Best Estimate of XIPE performance. The flux is given in units of 10^{-11} cgs, while T_{exp} is in ks.

Object	$F_{2\text{-}8\ keV}$	T_{exp}	MDP (%)	CBE	Expected Polarization	Science goal
Crab Nebula PWN	1950	20	ΔP<1.3% Δφ <2deg in 13 regions	ΔP<0.8% Δφ <1.3deg in 13 regions	>19% ([273], [268])	Map of the Nebula
Vela PWN PWN	6.0	100	MDP=8.9%	MDP=5.7%	>10% ([268])	Mean polarization
Cas A SNR	116	1000	MDP=4.1%-7.2% in 7 regions	MDP=2.6%-4.6% in 7 regions	>10% in selected regions ([34], [71])	Map of the remnant
Cyg X-1 μQSO	1000	100	MDP=0.44%	MDP=0.28%	<5%@2.6 keV ([275])	Jet, corona
Mrk 421 Blazar	27	100	MDP=2.7%	MDP=1.7%	>10-20% ([208], [43])	Jet
Cen A (jet) Radiogalaxy	4	200	MDP=4.8%	MDP=3.1%	>10-20% ([208], [43])	Jet (spatially resolved)
Am Her MCV	10	1000	MDP=4.4% /10 phase bins	MDP=2.8% /10 phase bins	5-10% ([162])	Accretion column
SAXJ1808 AMP	100	100	MDP=4.4% /10 phase bins	MDP=2.8% /10 phase bins	>5-10% ([267])	Scattering corona
Her X-1 LMXB Pulsator	90	100	MDP=4.7% in 10 phase bins	MDP=3.0% in 10 phase bins	>10% ([170])	Fan vs. Pencil beam
1RXS J1708 Magnetar	4	250	MDP=14% in 10 phase bins	MDP=9% in 10 phase bins	>50% ([251], [261])	Vacuum polarization
GX339-4 (outburst) XRB	500	100	MDP=0.62%	MDP=0.40%	>a few % ([231])	Corona
GX339-4 (quiescence) XRB	4	1000	MDP=2.2%	MDP=1.4%	Unknown	Corona
NGC1068 AGN	0.5	1000	MDP=6.3%	MDP=4.0%	10% ([94])	Torus geometry
IC4329A AGN	10	100	MDP=4.4%	MDP=2.8%	> a few % ([231])	Corona
SGR B complex Molecular cloud	0.3	1000	ΔP<6.3% and Δφ<5°	ΔP<4% and Δφ<3°	>20% ([49], Marin et al. submitted)	Past activity of SgrA*
GRS1915+105	1300	500	ΔP<0.78% and Δφ <1 deg	ΔP<0.50% and Δφ <1 deg	>5% ([61], [230])	BH spin
MCG-6-30-15 AGN	4	1000	MDP=2.2%	MDP=1.4%	5% ([62])	BH spin

3.2.3 Imaging capability

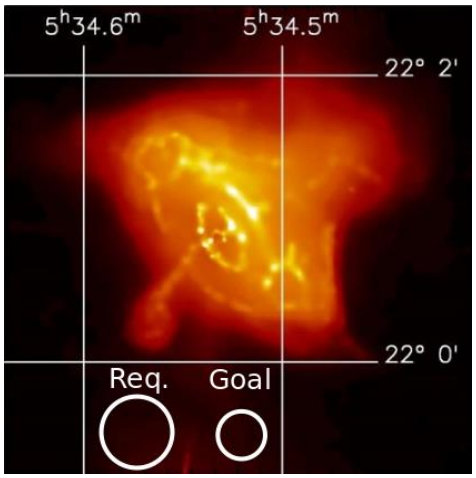

Figure 3-2 Requirement and goal HEW angular resolution of XIPE compared with Crab nebula structures.

Imaging capability has traditionally allowed for a tremendous increase of sensitivity, especially in case of the study of high energy sources. Imaging allows to resolve complex fields and extended sources, and to suppress the background of orders of magnitude, making possible the observation of faint sources. For *XIPE* observations, imaging requirement is driven by the study of extended sources. Current high-resolution measurements show that SNRs, PWNe, extragalactic jets and the Galactic Centre have complex structures, each with different processes going on. Therefore, spatially-resolved observations are required. *XIPE* angular resolution requirement is to achieve a Half-Energy Width (HEW) of 30 arcsec, with a goal of 20 arcsec, which allows to resolve the main structures of extended sources which will be observed by *XIPE*, e.g., the jet in Cen A or main features in the Crab PWN and in SNRs. For SNRs, the polarimetry capability of *XIPE* is substantially "statistically-limited" in the sense described above, so a better angular resolution would be of limited improvement for achieving the *XIPE* scientific objectives.

Another *XIPE* characteristic is driven by the observation of extended sources, that is, its field of view. This shall be larger than 10 arcmin in diameter to observe most of the extended targets (e.g. shell-like SNRs) with a single pointing, including uncertainties in the satellite pointing.

3.2.4 Timing

A number of key *XIPE* targets will be highly variable in time, from millisecond to years-long scales. This has not only an impact on both the time resolution and accuracy with which *XIPE* shall record the arrival of the photons (timing requirement), but also on the observing strategy as it will be discussed in Section 3.2.5.

Timing requirement is driven by the fastest phenomena that *XIPE* shall observe, that are, pulsations from accreting millisecond X-ray pulsars. These sources have periodicities of a few milliseconds, and therefore a (much) better temporal resolution is required to effectively bin and fold their light curves. *XIPE* shall time-tag the arrival of the photon with a resolution of 8 μs, which allows also for an adequate space for unexpected discoveries.

The time-tag in *XIPE* data shall be adequately synchronised with a reference time. *XIPE* targets have usually a remarkable multi-wavelength signature, which can be observed by other observatories both in space and on ground. To allow for a meaningful comparison with data collected by these instruments, *XIPE* time shall be synchronised to Universal Coordinated Time with an uncertainty of 4 μs.

3.2.5 Observation strategy

XIPE observation strategy shall be based on a pre-determined sequence of long staring observations, as most targets have a known position in the sky which can be observed as they become accessible during the year. Notwithstanding, *XIPE* observation strategy shall also take into account that some scientific objectives can be achieved only by observing targets when peculiar physical conditions occur in the source, that is, in specific flux or spectral states. The most straightforward example is the measurement of spin of galactic black hole, which can be derived only by observing the source when the accretion disk extends very close to the compact object, that is, in the soft state. The interesting state in which most of the key XIPE targets have to be observed last from several days to months, and thus do not impose strong constraints on the repointing capabilities.

The spectral state of variable X-ray sources is usually monitored by dedicated instruments; interesting changes are quickly reported to the scientific community to encourage observations with other instruments and multi-wavelength campaigns. It is expected that, when *XIPE* will be in-flight, the occurrence of spectral state relevant for the achievement of the mission scientific objectives will be signalled by other observatories, e.g. the Chinese-French satellite mission SVOM or ground-based optical and radio telescopes, at least for same specific

classes of sources. For this reason, *XIPE* shall implement Target of Opportunity (ToO) observations within 12 hours (goal within 8 hours) from the trigger to the SOC during working hours, interrupting the pre-determined observation planning to be resumed after the ToO.

Table 3-4 Energy ranges in which XIPE scientific objectives can be achieved and comparison with measurement techniques.

Sources	< 1keV	1-10 keV	> 10 keV
Acceleration phenomena			
PWN	**Yes (but large absorption)**	**Yes**	**Yes**
SNR	**No**	**Yes**	**Yes**
Jet (Microquasars)	**Yes (but large absorption)**	**Yes**	**Yes**
Jet (Blazars)	**Yes**	**Yes**	**Yes**
GRBs	**Yes**	**Yes**	**Yes**
TDEs	**Yes**	**Yes (difficult for thermal events)**	**Yes (non-thermal events only)**
Emission in strong magnetic fields			
WD	**Yes (but large absorption)**	**Yes**	**Difficult**
RPP	**Yes (but large absorption)**	**Yes**	**Yes**
AMS	**No**	**Yes**	**Yes**
X-ray pulsator	**Difficult**	**Yes (but no cyclotron lines)**	**Yes**
Magnetar	**Yes (better)**	**Yes**	**No**
Scattering in aspherical geometries			
Corona in XRB & AGNs	**Difficult**	**Yes**	**Yes (difficult)**
X-ray reflection nebulae	**No**	**Yes (but long exposure)**	**Yes**
Fundamental Physics			
QED (magnetar)	**Yes (better)**	**Yes**	**No**
GR (BH)	**No**	**Yes**	**No**
QG (Blazars)	**Difficult**	**Yes**	**Yes**
Axions (Blazars, Clusters)	**Yes**	**Yes**	**Difficult**

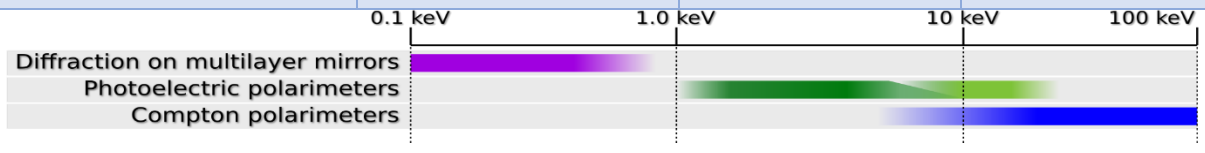

Even in case no external facilities will trigger its observations, *XIPE* shall be able to perform key observations on variable sources to achieve the mission core scientific objectives. This shall be fulfilled by implementing a specific observation strategy on a handful (about a dozen) of the most relevant targets in each class of variable sources. Such targets shall be observed on a regularly basis with *XIPE* for a short time (about 300 s) during the passage from a pre-determined observation and the following. Such monitor observations will be used to check the source spectral state: when an interesting spectral state is detected, a longer observation to measure the polarization is triggered.

3.2.6 Observation plan

Scientific objectives of *XIPE* will be achieved by observing several key sources for each class. The indicative number of targets, for each class, that *XIPE* shall observe to achieve its scientific requirement is reported in Table 3-5; in the same table, there is also the goal number of targets that shall be observed adding the possible extended phase.

Given the *XIPE* sensitivity requirement (see Section 3.2.1), the duration of the nominal mission shall be 3 years, with a possible extended duration of 2 years, to observe the key sources identified in Table 3-5. To collect a sufficient number of photons, the duration of each specific observation will range between 5 ks and 4 Ms, depending not only on the source flux but also on the number of bins (temporal, spectral or spatial) in which the collected data has to be split to achieve a specific scientific objective. The observation scheduling shall be able to accommodate at least 150 scientific targets and at least 350 monitoring observations (if necessary) during 1 year. None forbidden directions should occur to prevent observation of any potential target.

The requirement to observe all sources in the *XIPE* observing plan for a sufficient time drives the requirement on the Field of Regard (FoR), that is the fraction of the sky that shall be visible at any time. To achieve a sufficient flexibility in observation scheduling, *XIPE* shall have a FoR of 50% of the sky; this shall also assure that *XIPE* will have a high probability (50%) to be able to observe a transient event appearing randomly in the sky.

Table 3-5 Summary of the number of sources that XIPE will observe during nominal (required targets) and nominal + extended mission duration (goal targets).

Class	Required key targets	Goal key targets
Accreting millisecond X-ray pulsars	6	10
Blazars	19	31
Cataclysmic Variables	5	8
Galaxy clusters	1	2
Magnetars	5	7
Molecular Clouds	2	3
Pulsar Wind Nebulae & Rotation-powered Pulsars	5	8
Radio galaxies	5	8
Radio-Quiet AGNs	6	10
Supernova Renmants	5	8
X-ray binaries with black hole	7	11
X-ray binaries with neutron star	5	8
X-ray binaries with unknown companion	2	4
X-ray pulsars	8	13
TOTAL	**81**	**131**

3.2.7 Polarimetric response knowledge

An essential observable to achieve the *XIPE* scientific objectives will be the measurement of source polarization at different epochs. To achieve this, *XIPE* response stability to polarization shall be better than 5% of the measured polarization, with a goal of 2%, after applying all the calibration factors. Polarization angle shall be referred to sky coordinates with an uncertainty lower than 5 arcmin, which is 1/3 of the uncertainty on the most significant *XIPE* measurement, to allow for strict comparison with polarization angle measured at different wavelengths.

3.2.8 Background

Background limits the sensitivity to polarization, as discussed in Section 3.1, but it has little practical impact on *XIPE* observations. The majority of *XIPE* targets will be relatively bright X-ray sources, because of the need to collect, in a reasonable observing time, the huge number of counts required to achieve an adequate sensitivity. *XIPE* takes advantage of grazing incidence mirrors to reach a sufficient collecting area, and this has also the benefit of increasing the signal to noise ratio of the measurement to a point which makes the background contribution negligible.

However, there are exceptions, i.e., faint sources which will be *XIPE* targets because the expected polarization is very high. The most important (and potentially rewarding) example are the molecular clouds in the centre of our Galaxy. These sources are diffuse and faint, a few 10^{-12} erg s^{-1} cm^{-2}, so they drive the *XIPE* background requirement, that shall be $\leq 8x10^{-4}$ ct s^{-1} cm^{-2} keV^{-1} $detector^{-1}$ (assuming 3 detectors), which is about 1/3 of the target counting rate. For comparison, the counting rate for the reference source used to specify the *XIPE* polarimetric sensitivity requirement is 0.18 ct s^{-1} $detector^{-1}$.

3.2.9 Maximum flux

XIPE shall be able to observe bright sources, up to two times the flux from the Crab nebula, with a dead time lower than 10%. This requirement stems from the fact that many targets are variable sources, which needs to be observed in their brightest spectral state. This implies that the instrument dead time shall be less than 300 μs. This requirement is at the base of the provision of filters in the Filter and Calibration Wheel. The observation of sources characterized by a flux higher than 2 Crab shall be observable through the usage of a grey filter.

3.2.10 Pointing and alignment requirements

XIPE shall observe extended sources with a single pointing; during observation, the source shall remain in the central part of the field of view of the instrument to limit the loss of collecting area due to vignetting. This implies that the target source shall be centred within the nominal FoV with an accuracy of 3 arcmin at 2 σ, and that the misalignment of the *XIPE* telescope(s) shall be such that the observation time loss, that is, the collecting area loss, is below 7%. Astrometric accuracy shall be of 10 arcsec (diameter, at 2 σ), to locate with sufficient precision the position of unknown variable sources.

4 Payload

XIPE payload comprises of three identical, co-aligned, telescopes, each one composed of a Mirror Unit (MU) and of a corresponding Detector Unit (DU), and one Instrument Control Unit (ICU). The DU is the sensitive part of the payload, hosting the focal plane X-ray polarimeter based on the Gas Pixel Detector (GPD). This design is chosen to achieve the collecting area requirement discussed above with an optimized response in the energy range of interest, while satisfying the mission requirement on, e.g., the spacecraft launcher and total cost. The use of three telescopes (instead of just one) is at the cost of an increase of a factor 3 of the measurement background, which however is not driving the *XIPE* design.

4.1 *Mirror Assembly*

A Mirror Unit consists of (see Figure 4-1):

- A set of nested reflective shells shaped as paraboloids and hyperboloids according to the geometry of a Wolter I X-ray mirror;
- A cylindrical case containing the shells;
- Two end structures (spiders) which support the shells at their front and rear end;
- A rear cover blocking the opening of the innermost shell;
- A mounting flange interfacing with the Mirror Unit holding Structure;
- An optional thermal blanket;
- A thermal baffle.

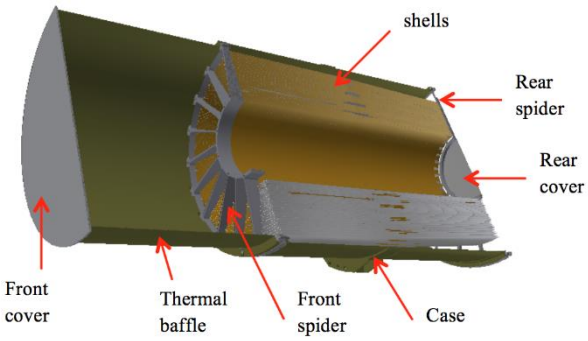

Figure 4-1 Mirror Unit elements.

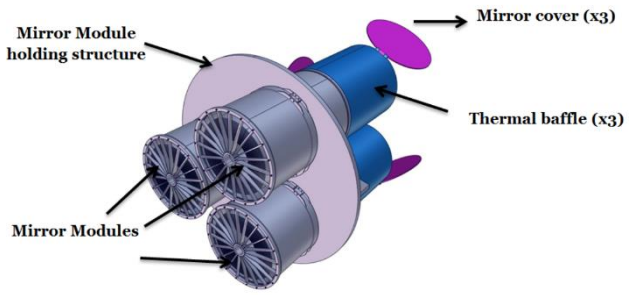

Figure 4-2 Conceptual drawing of the mirror assembly.

These mirror units are based on a very consolidated and proven technology, fully developed in Europe and already used for the mirror units of *BeppoSAX*, JET-X, *Swift*-XRT, *XMM-Newton*, and *eROSITA*. The *XIPE* MUs foresee a two spiders structure for the integration of the shells into the MU. Note that this is different than in the case of *XMM-Newton* or *eROSITA*, whose MUs are with only one spider. However, this is not a new situation. In fact, the first MU with electroformed shell in Nickel have been developed and realised with two spiders. Four MUs with two spiders have been realised for the *BeppoSAX* satellite and five for the JET-X project. In any case a single spider structure could be envisaged also for *XIPE*, reducing the weight. The final decision will be taken during the phase B.

The *XIPE* MUs are made of 30 nested electroformed nickel shells with a length of 60 cm and a diameter ranging from 19 to 40 cm, with a thickness in the range of 0.2 – 0.3 mm. The thickness of each shell is determined on the basis of the thin and light design studied and developed for previous missions and follows the rule (thickness/radius) = 1.7×10^{-3}, down to 0.2 mm thickness. For the smaller shells for which the above rule would have given thinner thickness the thickness is fixed at 0.2 mm. The reflecting surface is made by a 30 nm Ir + 10 nm of amorphous Carbon coating. *XIPE* shells are thinner and have a reflecting coating different than the ones developed for mission that have been completed (gold in

the case of JET-X, as well as of *BeppoSAX* and *XMM-Newton*). Notwithstanding, thinner shells have been already realised for *eROSITA*, while for the Simbol-X and NHXM projects thinner shell with much more complex coating have also been developed. Therefore, the realisation of the MU foreseen for *XIPE* is based on solid technology.

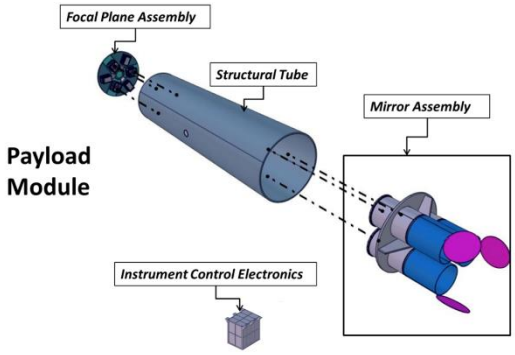

Figure 4-3 Sketch of the Mirror module structure

Thermal baffles radiatively controlling the Mirrors are foreseen to control the temperature and the temperature gradient of each Mirror Unit. Each thermal baffle is mounted on the external ring of one of the two spider structures of a Mirror Unit. In order to minimize contamination, covers are also foreseen. Each mirror cover is in principle, mounted on the front section of a baffle. A thermal blanket can also be mounted in front of each MU in order to facilitate a stable thermal environment. This will be decided during the Phase B of the project. The thermal environment for the mirror modules will guarantee that the Half Energy Width (HEW) is not degraded by more than 10 arcsec. The rate of change of mirror temperature, in any phase, operational or non-operational, must not exceed 10°C per hour with a maximum thermal gradient on the mirror being 1.0°C (longitudinal) and 1.0°C (azimuthal). There is no power requirement from the MUs other than that needed to power the thermal heaters. The three Mirror Units together with any required baffle and cover will be assembled in the Mirror Assembly (MA) mounting structure to form the MA (see figure Figure 4-2). The MA provides also the interface to mount the MA on the Telescope Metering Structure and then on the Service Vehicle Module through the Thrust cylinder.

4.1.1 Optical design

Goal Mirror Unit (4m focal length)		
Item	**Definition**	**Mass (kg)**
1	Shells	37.412
2	Spider 1	4.855
3	Case + flanges	8.703
4	Spider 2	1.817
5	Screws	0.126
6	Rear cover	0.263
Total		**53.176**
Total with DMM		**63.811**

Table 4-1 mass of a Mirror unit components

During the Phase A study, two configurations were investigated, one foreseeing the MU with a 3.5 m focal length and 27 shells and one with a 4 m focal length and 30 shells. The study has shown that 4 m focal length MUs with 30 shells can be accommodated inside the VEGA-C fairing, therefore this is now the baseline configuration. A longer focal length allows us to increase the effective area at higher energies, while the larger number of shells increases the effective area at all energies. The total mass of a single mirror module with these parameters is of ~53.1 kg (63.8 with a 20% margin, see Table 4-1). The optical design is such that the field of view is kept unobstructed up to 10 arcmin diameter. These parameters provide a point spread function with an HEW<20 arcsec on axis with a small degradation off-axis (10% at 5 arcmin off-axis) as proven both by simulations and analytical calculation. We note that these values are also confirmed by fully integrated prototype mirrors ([241]) including the recently made *eROSITA* mirrors ([33]).

In soft X-rays, a simple high-Z coating is sufficient to guarantee high reflectivity, and Iridium (or Platinum) is a viable solution. However, near the atomic energy edges, which falls in the *XIPE* energy range, the reflectivity drops where the photoelectric absorption increases steeply. Fortunately, over-coating with a low-Z layer greatly improves the reflectivity at energies below 5 keV ([197], [54]). We computed the effective area of the *XIPE* telescope in the 0.1-10 X-ray band both by using analytical formulae ([242]) and by using ray-tracing simulations. We assumed an equivalent mirror roughness of 4 Å and a reflective coating of *i)* a 30 nm thick layer of Iridium or *ii)* a 30 nm Ir + 10 nm of amorphous Carbon (Pt+C can also be assumed instead of the Ir+C coating, with a very small decreases of the effective area). The results for the two coatings are shown in Figure 4-4. The Ir+C design enables a much higher response in the vicinities of the target energy of 3 keV. In addition,

this design provides an on-axis effective area of 550 cm^2 per single module at 3 keV. At 5 arcmin off-axis, the effective area at 3 keV is still of ~500 cm^2. The radius at which the collecting area corresponds to 50% of the on-axis value, is about 30 arcmin, which is much larger than that accessible by the focal plane instrument. In all these calculations, a 10% reduction of the effective area is assumed due to the spider obstruction (the dependence of the spider obstruction on the off-axis angle can be neglected).

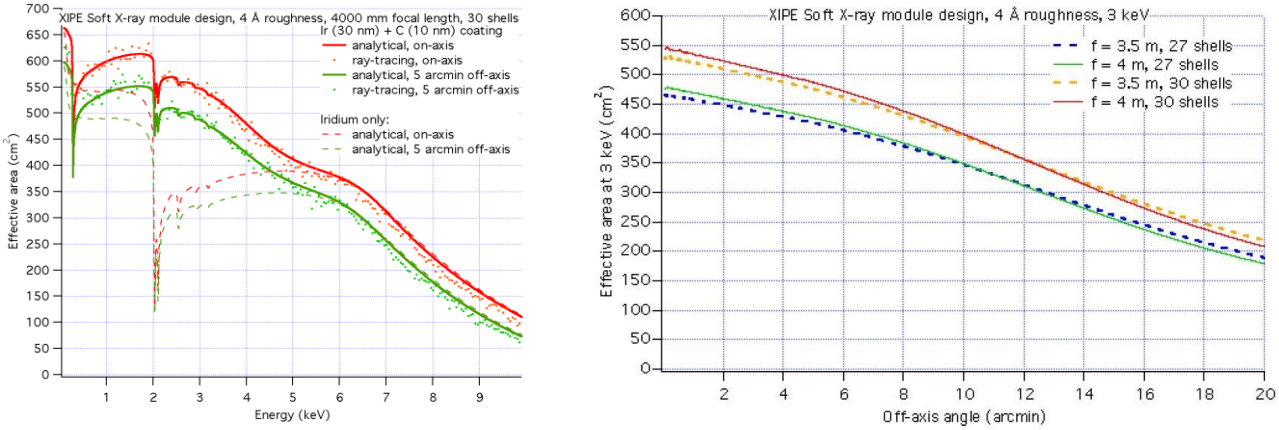

Figure 4-4 Effective area of a single XIPE mirror module, on-axis (red lines) and 5 arcmin off-axis (green lines). The accuracy of the analytical computation is confirmed by the outcomes of the ray-tracing. The computations without the Carbon over-coating are shown as dashed lines, and return a much lower effective area.

4.2 Telescope Structure

One *XIPE* telescope is composed by one Mirror Unit and the corresponding Detector Unit. The three Detector Units are hosted in their enclosure and screwed on the Focal Plane Support Items to make the Focal Plane Assembly (FPA). The Mirror Assembly is placed inside the Service Module requiring the largest off-the-shelf launch adapter. The metering tube in Carbon Fibre provides the correct distance for arriving at a focal length of 4 m. On the opposite side of the metering tube there is the FPA by means of an interface ring in titanium.

4.3 Instrument

The *XIPE* Instrument, named XPOL, is the focal plane part of the payload. It comprises of:

- Detector Units, hosting the Gas Pixel Detector (GPD)
- The Focal Plane Structure, which provides their mechanical interface and hosts thermal control items
- The Instrument Control Unit (ICU), which interfaces the DUs with the spacecraft.

4.3.1 The principle of operation: the photoelectric effect

Polarization from a photon beam is measured by means of the photoelectric effect in gas. Following the photon conversion in the gas, the photoelectrons are ejected in directions that carry a significant memory of the electric field of the photon (see Figure 4-5). When the beam is linearly polarized the electrons are ejected preferentially along the direction of polarization. The differential cross-section of photoelectric effect of s-electrons is ([100]):

$$\frac{\partial\sigma}{\partial\Omega} = r_0^2 \frac{Z^5}{137^4}\left(\frac{mc^2}{h\nu}\right)^{\frac{7}{2}} \frac{4\times\sqrt{2}\times sin^2(\vartheta)cos^2(\varphi)}{(1-\beta\cos(\vartheta))^4}$$

where r_o is the classical electron radius, Z is the atomic number of the target material and β is the electron velocity, as a fraction of the speed of light c.

The photoelectron is slowed down by ionizing collisions with outer electrons of the atoms of the medium. The energy loss increases with decreasing kinetic energy (Bethe law for low energy).

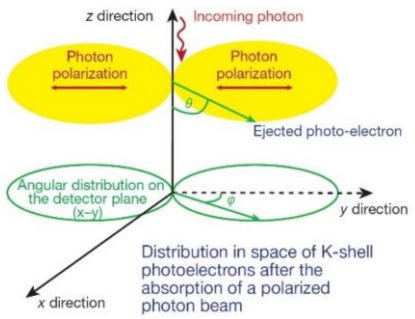

Figure 4-5 Basic physics of photoelectron effect

Electrons are also scattered by charges in the nuclei with no significant energy loss. This follows the screened Rutherford law. Whereas scattering crucially depends on the atomic number, slowing down is only moderately dependent. The first part of the photoelectron path has indeed a lower charge density, but it is closer to the initial direction of the photoelectron and so also closely related to the photon polarization direction. The second part has a higher charge density but it is randomized. The possible Auger electron track does not bring information on polarization. The primary ionizations ("track") are then projected onto the sense plane after diffusion and multiplication. The charge density is proportional to the energy loss, and is therefore related to the electron kinetic energy. The Gas Pixel Detector allows for efficiently exploiting the photoelectric effect with a device that provides, for each collected event, the charge-image of the track and the trigger time.

4.3.2 Implementation: the Gas Pixel Detector

The GPD ([53], [21]) is a proportional counter with a revolutionary readout. It has been developed, and continuously improved in Italy, by INFN of Pisa in collaboration with INAF-IAPS. Schematically (see Figure 4-6 and Figure 4-7), a GPD is made by a gas volume enclosed by a top beryllium window, a Gas Electron Multiplier (GEM) which amplifies the charge of the electron tracks generated in the drift gap and a pixelated charge collection plane which is the top layer of an ASIC CMOS chip.

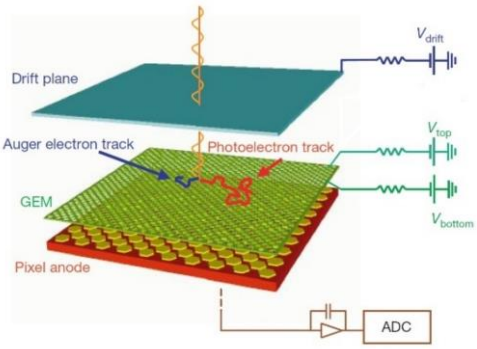

Figure 4-6 The sketch of the GPD

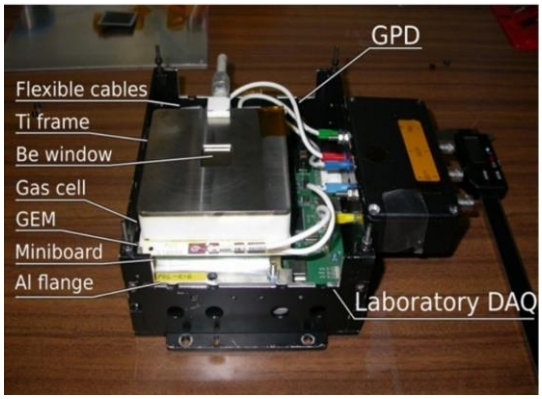

Figure 4-7 the real GPD and the Data Acquisition system

The Beryllium window is glued on a titanium frame and an additional conductive glue provides the electrical contact. The titanium frame, in turn, is glued to a MACOR spacer which provides the 1-cm drift thickness. The MACOR is glued onto the GEM support frame which is glued to the Kiocera package. The Kiocera package hosts the Application Specific Integrated Circuit (ASIC) and provides the electrical connections from the outside space to the internal ASIC.

The drift field is chosen to provide the smallest transverse diffusion during the drift which is about 1800 V/cm. The GEM is a planar insulator (Liquid Crystal Polymer) perforated, by laser etching, with microscopic holes and copper plated on both sides. The electric field in each hole is high enough to multiply the charge of the initial track without affecting its shape. The GEM is produced by SciEnergy (Japan) and it is proved to be more stable at the power-on with respect to the wet etched kapton foil produced at CERN. Indeed, GEM was invented at CERN ([224]) 20 years ago for use in the harsh environment typical of particle accelerator. The GEM by Scienergy was chosen to have an even more robust design for space applications.

The ASIC CMOS has been developed since 2005 employing 0.18 um technology. Thanks to local triggers, common to each cluster of 4 pixels, the ASIC autonomously defines a Region of Interest (RoI) surrounding the collected track and providing its corresponding digital coordinates.

Table 4-2 Characteristics of the Gas Pixel Detector

Beryllium window thickness	50 μm
Drift thickness	1 cm
Mixture	He20%-DME80%
Pressure	1 Atm
Drift voltage	- 2600 V
Top GEM Voltage	- 870 V
Bottom GEM Voltage	- 400 V
GEM thickness	50 μm
GEM hole pitch	50 μm
GEM hole diameter	30 μm
ASIC number of pixels	105600
ASIC pixel pitch	50 μm hexagonal
ASIC full scale linear rnerge	30000 e
ASIC Pixel noise	50 e_{rms}
Pixel readout rate	1-10 MHz
Total power dissipation	0.5 W

An ASIC trigger output signal is used to time-tag the event within 3 μs from photon absorption. The energy of the event is evaluated by the integral of the charge contained in each pixel of the collected track. The impact (conversion) point, which is related to imaging, and the emission direction, which is related to polarization, are evaluated by the algorithm described in Section 4.3.5. The main characteristics of the GPD are shown in Table 4-2. The performance of the GPD have been studied at the calibration facility of INAF-IAPS. Here we produce monochromatic and polarized radiation using Bragg-diffracted (at 45°) lines characteristic of anodes of many different X-ray tubes. We can measure the energy resolution, the position resolution, the modulation factor as a function of energy and the rate. We use a Data Acquisition System developed by the INFN. In the next figures we show some results of this calibration activity on GPD prototypes ([185]).

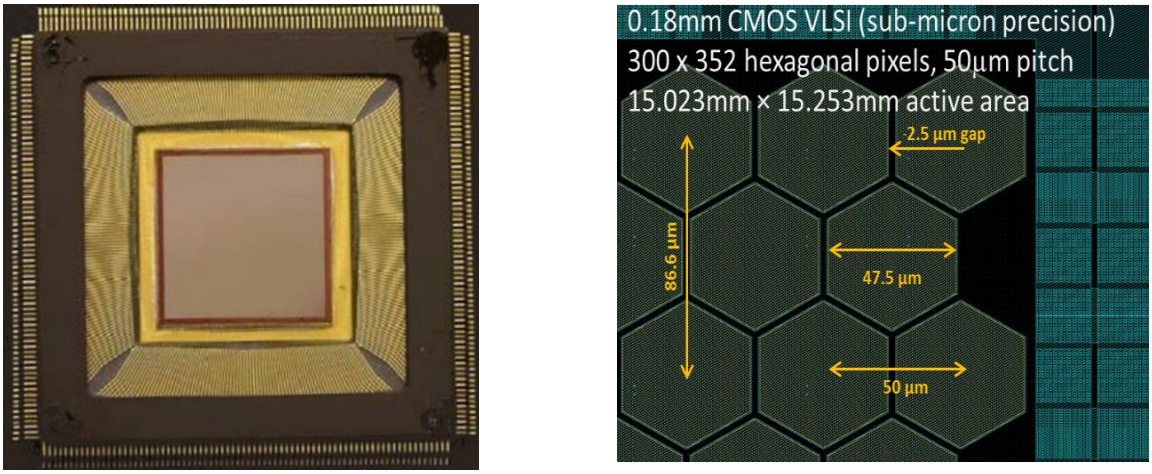

Figure 4-8 (Left) the ASIC CMOS which is the front-end electronics of the GPD. (Right) the pixelated readout plane of the ASIC CMOS

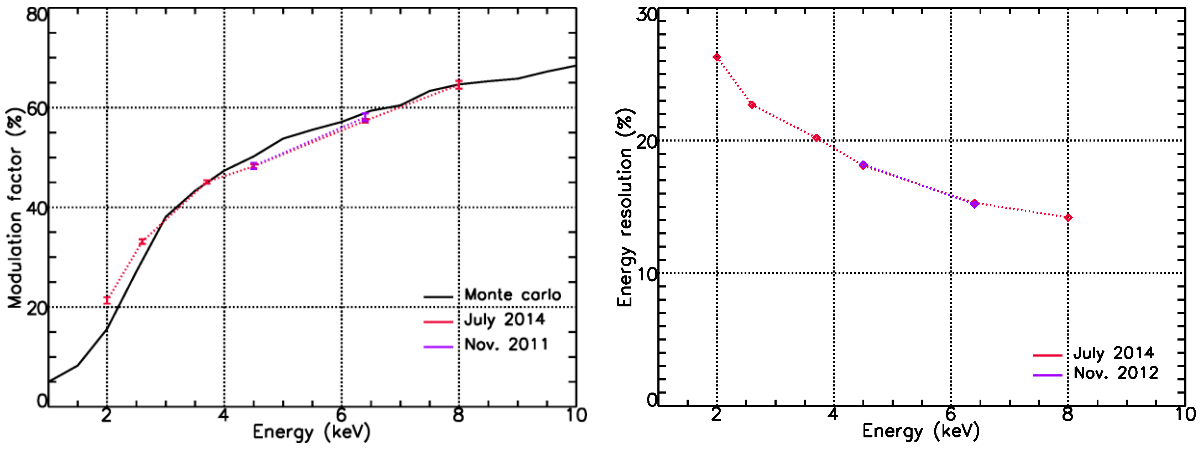

Figure 4-9 (Left) Measured modulation factor (points) vs energy compared with the Monte Carlo expectation (solid black lines). (Right) Energy resolution as a function of energy.

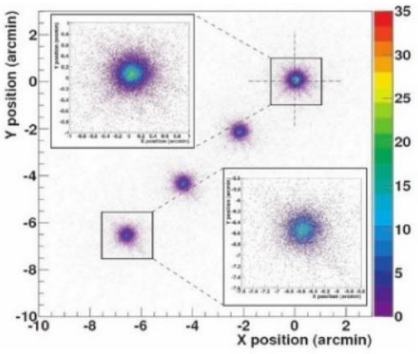

Figure 4-10 Imaging performances on-axis and off-axis measured at PANTER *(Germany).*

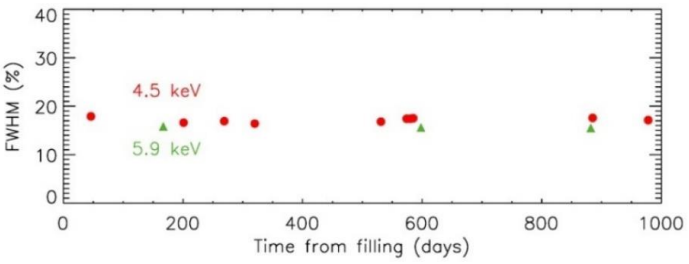

Figure 4-11 Energy resolution during three years of operation.

The measured modulation factor is well within the *XIPE* requirement and increases with energy following Monte Carlo expectation (Figure 4-9 left). The energy resolution (Full Width at Half Maximum, FWHM(E)/E) improves with energy as expected and the requirement at 6 keV is met with wide margins (Figure 4-9 right). The energy resolution was found constant within 3 years of operation (see Figure 4-11).

The imaging capability of the Gas Pixel Detector was studied both in laboratory ([240]) and at the PANTER X-ray test facility ([72]), where the GPD was placed in the focus of a mirror (Figure 4-10), a spare model of JET-X project, with quality equivalent to that of *XIPE* mirrors. The measured Half Energy Width (HEW) on-axis was 22.7'', 23.2'' and 28.9'' at, respectively, 2.98 keV, 4.52 keV and 8.05 keV, well within the requirement of *XIPE*.

4.3.3 The Back End Electronics (BEE).

The BEE (Figure 4-12) is a subassembly of the DU. It takes care of the electrical and data interface with the GPD, hosts the GPD high-voltage power supplies, manages the detector configuration, the data taking and executes the following tasks:

- Communication with the *XIPE* ICU, Telecommand reception and processing, Telemetry and Science data formatting and transmission via SpaceWire link;
- GPD bias, configuration and read out;
- Time-tagging of the event with better than or equal to 8 μs timing resolution;
- Science Data pre-processing (zero-suppression);
- DU housekeeping acquisition;
- Filter and Calibration Wheel control and monitoring (see Section 4.3.8);
- GPD Thermal Control;
- Generation and distribution of all the supply voltage and references needed by the DU.

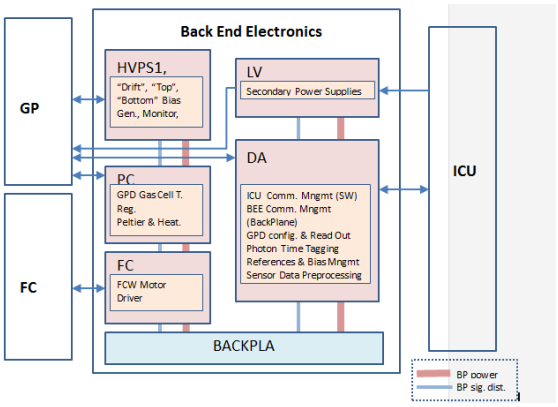

Figure 4-12 BEE scheme.

A single SpaceWire Link between the ICU and the BEE is dedicated to Science data and House Keeping Packets transmission as well as to the BEE Status Control. The maximum science data throughput is 2 Mbps.

4.3.4 The Instrument Control Unit (ICU)

The ICU (Figure 4-13) is located in the Service Module at about 5-meter from the DUs. During phase A study we moved some of the functions located in the ICU at the time of the *XIPE* proposal into the BEE to cope with the long distance in power transfer. The ICU interfaces with the DUs and the Service Module (SVM), and it is in

charge of data processing, instrument controlling and power distribution.

In order to acquire and process the scientific data, the ICU will:

- Manage the individual SpaceWire data interfaces to the three DUs;
- Retrieve science data and housekeeping (HK) data from their Back-End Electronics;
- Store data into the Mass Memory before sending them to on-board data handling for downlink;
- Generate the Quick Look Analysis (QLA) data from the science data;
- Take care of SpaceWire Telemetry interface to the spacecraft;

In order to control the instrument, the ICU will:

- Perform the execution and distribution of commands;
- Manage the Pulse-per-Second (PPS) signal and the 1 MHz clock for the on-board time and synchronization of the Back-End Electronics (BEE);
- Manage the payload operation modes;
- Perform instrument health monitoring;

In order to distribute the power, the ICU will:

- Perform instrument health monitoring;
- Receive the regulated primary power from the SVM;
- Generate required low voltages for the ICU;
- Distribute and switch on/off the regulated primary power to the subsystems;
- Generate HK data about voltage, current, temperature and operational parameters;

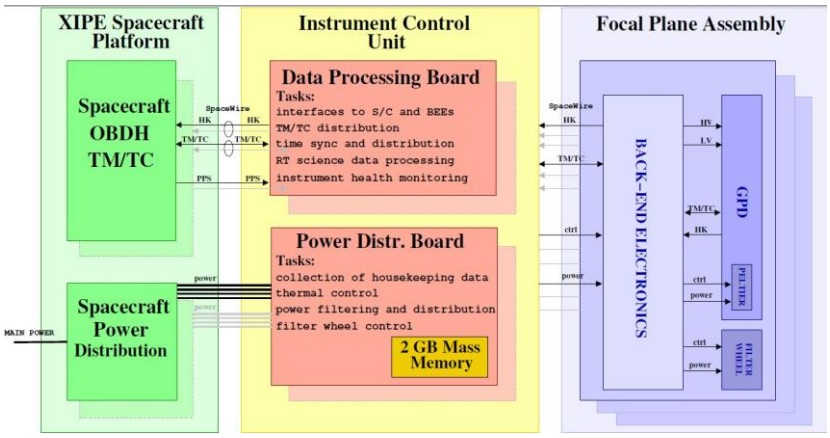

Figure 4-13 ICU Block Functional Diagram.

The ICU is capable of performing the above tasks and is based on the concept, shown in Figure 4-13. The ICU will process a steady maximum counting rate of 2100 cts/s (corresponding to ~2 times the Crab Nebula in 1 – 12 keV) of science data implementing the operative modes defined in Section 7 below. The ICU is designed to be cold redundant.

The ICU performs, during an observation, an on-line evaluation and on-board generation of some scientific calculation of QLA to provide (1) light curves in 5 energy bands and in 9 angular regions for each telescope; (2) Images of the central area of each telescope; (3) modulation curves of the central area in two energy bands for each telescope. This procedure will be performed for each source (main target and monitored source). QLA will be downloaded with priority for an anticipated telemetry rate of 3 kbit/s. Data will be analysed at SDC for checking the scientific status of the planned observations that will allow, for example, triggering a TOO upon observing monitoring sources.

4.3.5 The reconstruction algorithm: determination of the impact point and of the emission direction

An algorithm has been developed ([195]) over many years to determine the impact point (related to imaging) and the emission direction which is related to the polarization. This algorithm takes into account the morphology of the track explained in 4.3.1 (see also Figure 4-14). Indeed, what is important is the initial (less dense) part of the track and not the last (denser) one. We summarized the algorithm in the following 4 steps:

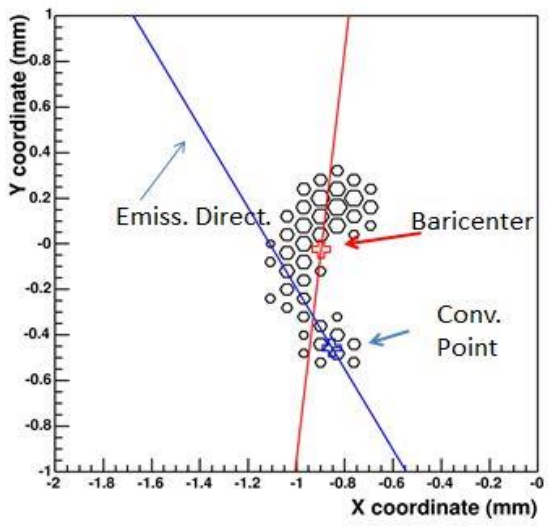

Figure 4-14 A real track with the evaluation of its first two momenta in the I and II step of the algorithm.

1. The barycentre is evaluated (using all the triggered pixels).

2. The principal axis of the track is evaluated maximizing the second moment of charge distribution (red line).

3. The conversion point is reconstructed by using the third moment along the principal axis to select the less dense side and using the above second moment (length) to select a region (between an inner and an outer radius) to determine the conversion point by means of an another barycentre determination.

4. The emission direction is reconstructed by means of the maximization of the second moment with respect to the conversion point but weighting the pixels according to their distance from it.

This algorithm will run in the ICU CPU for generating in real-time the QLA data during *XIPE* observations and on-ground, where improved software will be tested during the observation phase for reaching a better sensitivity.

4.3.6 Optimization of the gas mixture

The 1 bar He-DME (20-80) mixture, superior with respect to pure DME mixture (0.8 atm) was validated by measuring the performances of detectors with these different filling (Figure 4-15 left; [183], [184]).

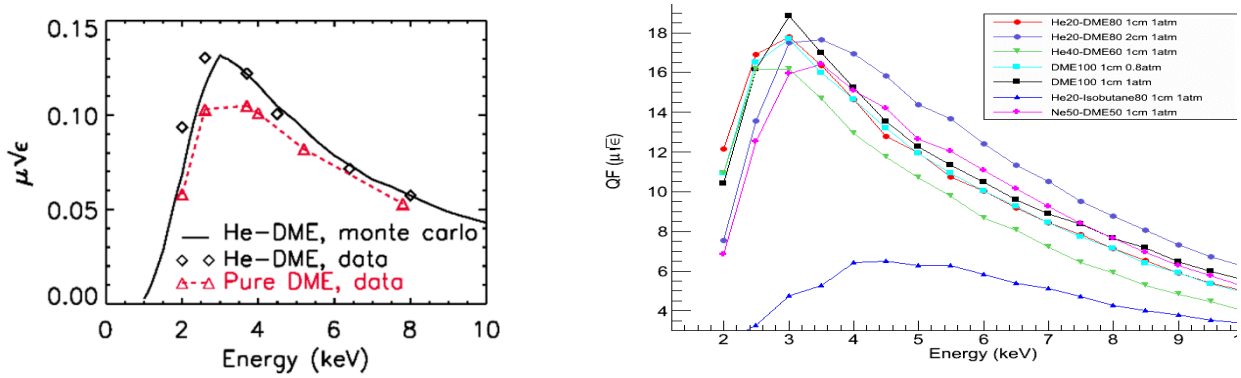

Figure 4-15 (Left). Comparison of the quality factor for two gas mixtures as derived from measurements (Right). Monte Carlo simulation of the quality factor for different gas mixtures. The best low energy application is provided for the Helium DME mixture.

Monte Carlo simulations of GPDs (Figure 4-15 Right) with different gas mixtures also showed that the He-DME 20-80 1-Atm provides the best peak sensitivity except for the pure DME mixture (1 atm) that is however less performant, at lower energies, as expected.

4.3.7 Expected in-orbit background

To evaluate the background rate of *XIPE*, we modelled using GEANT 4 the whole spacecraft and payload including the optics and sun shield, the solar panel and the focal plane assembly. The focal plane is modelled with more details for the items closer to the detector sensitive area. The baseline orbit of the *XIPE* satellite is an Equatorial Low Earth Orbit (LEO) with the altitude below 600 km and the inclination lower than 6°. In this radiation environment, the background sources considered are primary cosmic rays (protons, electrons, positrons and alphas), secondary particles (produced in the Earth atmosphere, protons, electrons, positron), albedo components (gammas and neutrons), and the cosmic X-ray background (CXB). The input spectra are the same as those used for simulations for the *LOFT* and *BeppoSAX* mission ([38]) that have approximately

the same Low Earth Orbit with an altitude of 600 km and an inclination of 5°. Both prompt and delayed emission (the latter resulted to be negligible) have been evaluated.

We also converted the energy release for each background component produced by the GEANT simulator in ion/electrons pairs using our in-house Monte-Carlo software (used for X-rays) for diffusion, multiplication and collection and the same analysis software used for the data. After applying only two kind of background rejection techniques (single cluster and pixel number) we got 7.2×10^{-3} count/s/cm2/keV with secondary positrons and primary protons proving the largest contribution. An additional factor of two in reduction can be reached shielding the back-side of the GPD. The other selection techniques to be implemented (amplitude selection, track topologies, skewness, etc.) are aimed to reach the goal of $8\ 10^{-4}$ count/s/cm^2/keV/detector.

4.3.8 Filter and Calibration Wheel

Figure 4-16 Filter wheel with the DU lid and position sensors.

The Filter and Calibration wheel (FCW; see Figure 4-16 and [285]) is the electro-mechanical system that allows for the in-orbit positioning of the filters and calibration sources in correspondence with the GPD entrance window.

The main driver for the design of the filter wheel is the repeatability of the positioning of polarized calibration source, for measuring the polarization angle with a stability of 3.5 arcmin. A trade study and a production of a bread-board has been performed also for other items, like the compactness, the mechanisms and the encoders, and the result is the present design. The holder wheel consists of an aluminium disc, supported on a spindle with 8 locations for either filters or sources. The wheel is actuated via a worm wheel on the circumference which is driven by a stepper motor. The stepper motor needs 200 steps for one full rotation, so one step of the motor rotates the worm wheel by 1.8 degree. This gives plenty of margin with regard to the positioning of the polarised calibration source. The angular position measurement is provided by a quad photo diode sensor illuminated via a pinhole in the filter wheel with an LED. The advantage of the quad photo diode solution is that it is a non-contact and accurate measurement solution. A bread-board has recently been made with high vacuum compatible radiation-hard stepper motor driving the worm wheel. All dimensions are within the required specification and demonstrating the repeatable positioning it boosted the TRL of the method of driving and sensing very significantly.

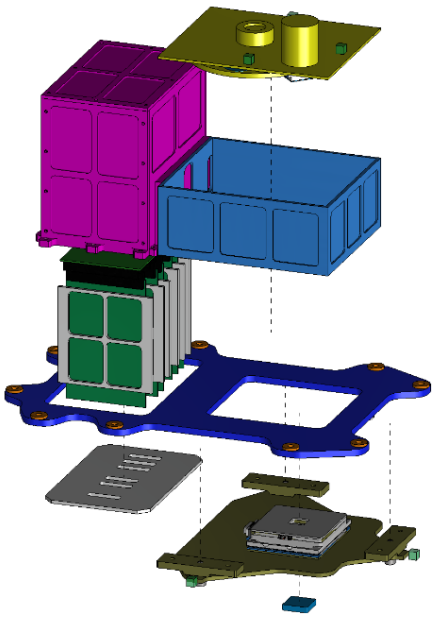

Figure 4-17 Exploded view of the DU.

4.3.9 Detector Unit and Focal Plane Structure

The Detector unit (DU) comprises the GPD, the FCW, the Back End Electronics and their mechanical interfaces and housing. The exploded view is shown in Figure 4-17. The BEE case (magenta) is connected to the GPD housing (blue). The lid of the cover (yellow) hosts the FCW. The alignment of the GPD with respect to the corresponding mirror and the start tracker is performed by means of an "isostatic" mounting on the Focal Plane Structure on three points with three optical cubes. The mechanical interface of the units are plates that act also as thermal interfaces. A Peltier cooler managed by the DU associated electronics will help to maintain the GPD gas cell at the operative temperature range. The FPA structure is supposed to be thermo-regulated to maintain the temperature of all the units within the operative and non-operative ranges.

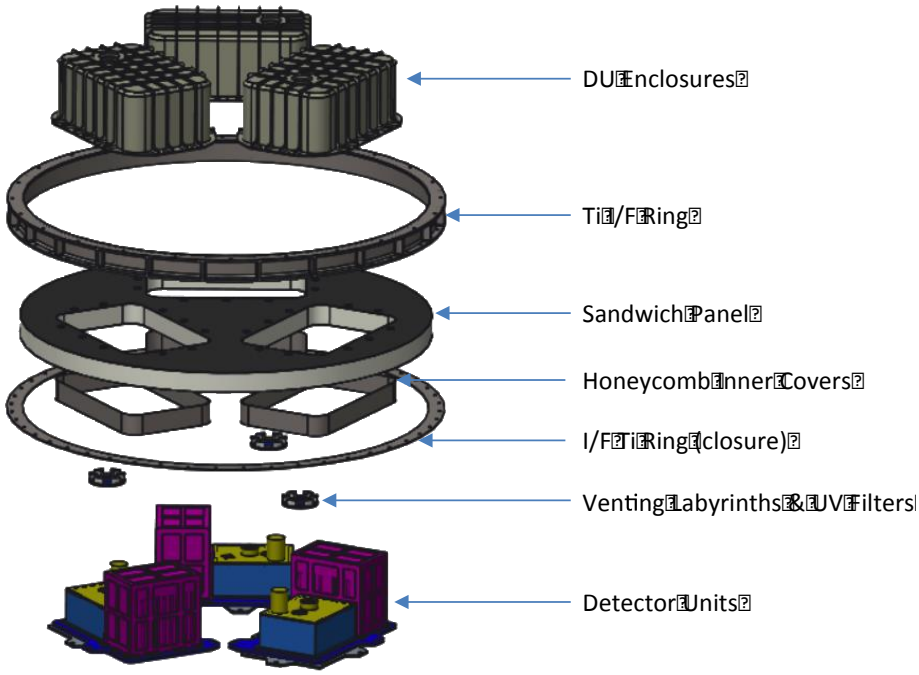

Figure 4-18 Exploded view of the Focal Plane Assembly

Each DU is connected to the Focal Plane Structure (FPS) by means of M5 fasteners of which 6 are related to the GPD. The FPS provides a stable mechanical support for the DUs, for the radiators and the thermal hardware and hosts the mechanical alignment tools. The FPS is composed of a structural Titanium Ring and a composite sandwich panel. The sandwich panel has a honeycomb core (Nomex an Aramid Fibre) and two Carbon Fibre Reinforced Plastic (CFRP) skins, of 1 mm thickness, which serves as interface and placement for the DUs. The panel includes the inserts and the Honeycomb Inner Covers which protects the DU from any contamination due to the cuts in the honeycomb. A Titanium ring acts as a peripheral ring to encapsulate the sandwich FPS with an additional ring acting as its closure. This ring is the interface between the FPS and the metering structure.

This combination of a sandwich panel and a peripheral Ti ring was successfully used in the Coded Mask of the SPI instrument developed for *INTEGRAL* ESA mission. The I/F ring has an external diameter of 1100 mm.

4.4 Stand Alone, End-to-End Ground calibration

The aim of on-ground calibrations will be to verify the compliance of the *XIPE* payload with requirements and characterize its scientific performance. Stand-alone calibration will be dedicated to check, before integration, the performance at the unit level, and they will be performed on each DU and MU (qualification, flight, and spare models). Telescope calibration will be aimed at verifying the operation of the assembly DU/MU with known sources in conditions equivalent to the observation of celestial objects. This is particularly important since *XIPE* will open a new observational window and, as matter of fact, the polarization state of celestial sources is unknown with the exception of that of the Crab Nebula. On-ground and in-orbit calibration are foreseen for *XIPE*.

The DU stand-alone calibrations (Figure 4-19) have the following goal: (1) measuring the modulation factor and, therefore, the response to polarization of the Gas Pixel Detector (GPD) as a function of energy; (2) characterize the energy resolution of the GPD as a function of energy; (3) measure the spatial resolution of the GPD as a function of energy (4) check the absence of spurious polarization (5) characterize the relation between the reconstructed and the expected angle of polarization; (6) map the gain non-homogeneities of the Gas Electron Multiplier (GEM); (7) measure the quantum efficiency of the GPD; (8) measure the GPD dead time; (9) characterize the response of the GPD with the calibration sources mounted on the Filter and Calibration Wheel (FCW) included in the DU. For each detector unit it is foreseen 60 days of total calibration time including contingency and set-up.

The DU stand-alone calibration will be performed with the calibration equipment at INAF-IAPS in a dedicated clean-room.

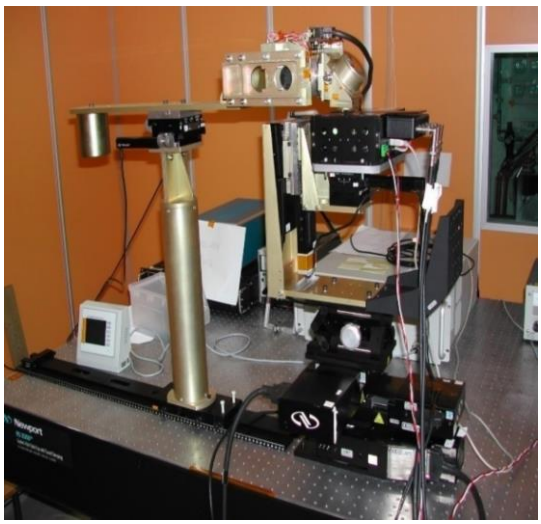

Figure 4-19 Calibration facility (INAF-IAPS).

The MU stand-alone calibration are aimed at (1) measuring the mirror effective area as a function of energy and off-axis direction; (2) measuring the Point Spread Function (PSF) of the mirror as a function of energy and off-axis direction; (3) check influence of single reflections; (4) measuring the vignetting function; (5) measuring the reflectivity of the shells; (6) measuring the scattering; (7) measuring the focal length; The MU stand-alone calibration are responsibility of ESA that takes advantage of the Telescope Advisory Group expertise, whose aim is to establish the accomplishment of test of the Mirror Unit. The MU stand-alone calibration will be performed at PANTER X-ray test facility. The telescope End-to-End calibration, also performed at PANTER X-ray test facility are aimed at (1) characterizing any effect on the polarization state of radiation due to the grazing-incidence reflection on and off-axis up to the systematic limit in sensitivity; (2) measuring the effective area of the telescope to relate the measured counting rate to the absolute flux of the observed source; (3) measure the angular resolution of the telescope as a function of energy and off-axis direction. The telescope End-to-End calibration are responsibility of DLR and it will be performed prior the delivery to ESA for the integration activity. The anticipated duration for each MU and telescope is 5 weeks.

4.5 Interfaces between Payload and Spacecraft

The mechanical interface between the Payload and the spacecraft consist of: (1) Mirror Assembly mounting Structure (for what concern the MU) as interface to the Metering Structure; (2) Interface Ring (for what concern the Focal Plane Structure) as interface of the Metering Structure (3) Six fixations on the bottom plate the mechanical interface of ICU to the SVM.

The electrical and data interface to the spacecraft is provided by the ICU. It will follow the full Space-Wire standard from electrical interfaces and cable design to the data transmission with the CFDP protocol. In addition, the ICU will receive a time signal from the satellite's GPS system. The ICU will receive 4 x 28 V unregulated power (nominal and redundant = 8 in total) from the satellite. Moreover, the ICU will receive 8 additional dedicated lines for redundancy switching, status and safety (nominal and redundant = 16 in total).

4.6 Payload MAIT and telescope Alignment

The mechanical assembly and alignment procedure is performed and validated at Instituto Nacional de Tecnica Aereospacial (INTA) with the Structural Thermal Model (STM) of the FPA and DUs. The STM models will then be accommodated into the satellite STM, together with the dummy ICU. The environmental test of the DUs and FPA will also be carried out at INTA. Two sets of GPD, FCW and BEE are then procured. Individual qualification tests are performed for the first set while the second set is integrated by INFN as Qualification Model and tested at the proper level. The DU flight model is integrated and preliminarily bench-tested at INFN-Pi with the FCW the GPD, the BEE and the mechanical case. The flight model FPS is integrated at UV and sent to the Prime after acceptance testing. The DUs are then individually environmental tested at INTA and calibrated at IAPS. After this activity, the instrument, which includes the ICU, is bench tested at INAF-IAPS, prior to the shipping to PANTER for the telescope calibrations. After telescope calibration, the DUs and the ICU are sent to the Prime for integration on the FPS and the spacecraft.

This solution allows to decouple the activity on the FPS from the activity on the DUs and the ICU.

XIPE X-ray telescopes will be integrated by the means of metrology equipment to monitor/control the following aspects for each telescope: (1) the alignment of MU Line of Sight (LoS) with DU LoS; (2) the position of focal spot at the DU center; (3) the position of focal spot inside the gas cell; (4) telescopes co-alignment (MU-boresight, DU-boresight/roll); (5) knowledge of alignment (boresight/roll) of each DU with respect to the Star Tracker (ST).

In principle MUs could be aligned/co-aligned first with respect to the main ST (boresight). After this first step the telescope alignment/positioning can be limited to DUs only. New baseline has adopted on each DU/GPD a three points interface. This solution allows the implementation at prime level of a standard alignment process, basically consisting in three steps: 1) measurement of misalignment of each DU (optical reference) with respect to the satellite reference (e.g. Star-trackers) without shimmies; 2) calculation of calibrated shims; 3) shims insertion on the unit interface; 4) verification of the achieved alignment.

The new baseline for the instrument allows the regulation of the focal spot position in the center of the GPD sensitive area by using its three mounting points. However, a method utilised for mirror shell position during MU manufacturing, such as that uses a Light Emitting Diode (LED) at a focus of an optical mirror to get a parallel beam, could be adopted for the direct verification of focal spot position.

4.7 Resources

4.7.1 Mass

The tables below show the mass budget for the DU, the FPA, and the ICU.

DU					
DU				**TOTAL**	**13.019**
Description	Units considered for Mass	CBE Mass (kg/unit)	DMM %	DMM (kg/unit)	CBE-DME Total
GPD	X1	2.230	20%	0.446	2.676
FCW	X1	1.484	20%	0.297	1.781
BEE	X1	1.850	20%	0.370	2.220
Housing	X1	3.974	29%	1.169	5.143
Harness	X1	1.000	20%	0.200	1.200

FPA					
FPA				**TOTAL**	**75.148**
Description	Units considered for Mass	CBE Mass (kg/unit)	DMM %	DMM (kg/unit)	CBE-DME Total
DU	X3	10.538	24 %	2.481	39.201
I/F Ti Ring	X1	13.200	20%	2.640	15.84
Honeycomb Core+CFRP Skin+Insert+Fastner-Inner Cover	X1	9.056	20%	1.811	10.867
DU Enclosure	X3	2.567	20%	0.513	9.24

ICU					
ICU				**TOTAL**	**10.584**
Description	Units considered for Mass	CBE Mass (kg/unit)	DMM %	DMM (kg/unit)	CBE-DME Total
Housing	X1	1.9	20 %	0.380	2.28
Harness to DU	3x3	0.480	20%	0.576	5.184
Data Processing Board	2	0.700	20%	0.840	1.680
Power Distribution Board	2	0.600	20%	0.720	1.440

4.7.2 Power

The table below shows the ICU and DU power budget.

Description		Units	Power (W)	Margin %	Power/Unit (W)	Total (W)
ICU incl. conv. effic.		X1	18.4	20 %	22.08	22.08
DU incl. conv. effic.		X1	24.3		4.9	29.2
	GPD	X1	6.3	20%	1.3	7.6
	FCW	X1	0.3	20%	0.1	0.4
	BEE	X1	17.7	20%	3.5	21.2

4.7.3 Telemetry

The autonomous generation of the Region of Interest of the ASIC and the zero suppression performed by the Back-End electronics reduces very much the number of pixels per event which on average is about 50. Different on-board compression algorithms can be envisaged. The ICU organizes the data by using a format that transmits for each event the coordinate of only the first of the contiguous pixels in a row and the energy of these contiguous pixel until the next transition is found. The format of the scientific data is the Table 4-3.

Table 4-3 Format of scientific data

Element Description	Bits
Header for each event	
Second counter	28
Microsecond counter	20
ROI upper left pixel coordinates	18
ROI length	18
DU ID	2
Total header	**86**
Information for each pixel	
Marker	1
Energy (coordinates)	12(18)
Total (assuming 50 active pixels and 15 transitions)	**1021**

The most demanding foreseen observation is that of Crab Nebula and pulsar, with a total of 2.2 Mbit/s for 440 Gbit of data computed with an assumed format of 1.2 kbit/s (20 % of contingency). The observing time of 200 ks is needed to study the emission from the pulsar. It may be useful to remind that, thanks to the presence of a diaphragm, the contribution of the much brighter nebula can be reduced.

The telemetry rate allocated for the housekeeping is 4 kbit/s, that of the QLA data is 3 kbit/s; both are much larger than the telemetry data expected by the background rate only.

4.8 Operations

4.8.1 Payload Operation Modes

The payload operation modes are managed by the ICU and with a standard and well-proven configuration. The modes are represented in the Figure 4-20. We recall here that the payload calibration and astrophysical observation both require the same 'observation' mode. Indeed, the configuration of the payload during calibrations is the same of an astrophysical observation with a different position of the filter wheel (chosen accordingly to the particular calibration needed). The operation modes are the following:

- "BOOT", it is the start-up mode at power on,
- "MAINTENANCE" is reserved by ICU to support the in-orbit maintenance program.
- "STANDBY" the ICU moves in STANDBY mode to start the instrument monitoring and control.
- "OBSERVATION" From the point of view of ICU, all instrument calibration and scientific modes are managed into a unique OBSERVATION mode that shall be preventively configured while in STANDBY mode
- "DIAGNOSTIC" to perform specific check for diagnosis purposes
- "TEST" This mode is introduced to implement a merge of STANDBY and OBSERVATION modes.

In both 'Boots' and 'Maintenance' modes the software is patchable.

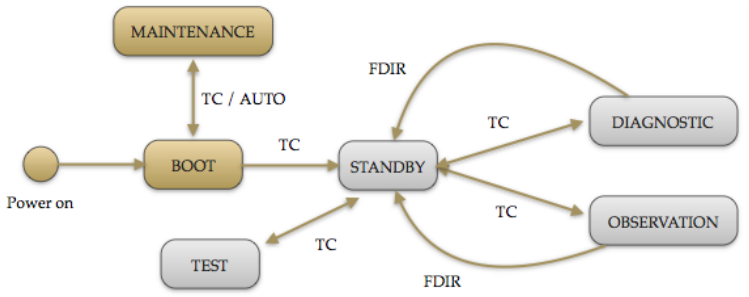

Figure 4-20 Definition of the modes of the payload. In gold the modes with patchable software.

4.8.2 Inflight Calibration

The *XIPE* payload will be calibrated also in orbit (Table 4-4). There are three kinds of calibration. The first one is *electrical* and it is aimed at measuring the pedestal noise of the GPD. The second one is the *physical* calibration of the DU. It uses the set of calibration sources mounted on the FCW with the aim of: (1) monitoring the modulation factor and energy resolution of the GPD; (2) check for the presence of spurious polarization due to, e.g., any anisotropy in the distribution of the background; (3) monitor the gain of the GEM (to be recovered by changing the GEM high voltage, if necessary); (4) map periodically the GEM gain non-homogeneities. Telescope calibrations will be dedicated to monitor the angular resolution, the alignment, and the single reflection component of the PSF. The third kind of calibration is the *astrophysical* one, using celestial sources (e.g., the Crab) to check the performances, verify the absence of any spurious polarization (with clusters of Galaxies), and cross-calibrate *XIPE* with other X-ray observatories.

We also plan to perform astrometric calibrations to check and calibrate the telescope astrometry. This will be performed either using two sources within a single pointing or observing extended source and comparing (e.g. cross calibrating) with the corresponding smoothed *Chandra* image.

4.9 Heritage & Technological Readiness Levels

The *XIPE* instrument team has considered the proposal of devices in his baseline concept with design solutions based on technologies of TRL 6, minimum.

Table 4-4 In-Orbit Electrical and physical Calibration

Calibration type	Frequency	Real time duration (ks) per DU
Modulation factor	every month	5.0
Absence of spurious modulation & gain monitoring	every 3 months	20.0
Mapping GEM energy 1	every 3 months	15.0
Mapping GEM energy 2	every 6 months	20.0
Pedestals	every 6 months	0.1
Crab Nebula (polarized source)	every 6 months	part of the observing plan
Cluster of Galaxies (unpolarized source)	every 6 months	part of the observing plan
Crab Nebula or Cas A (cross calibration)	every 1 year	part of the observing plan

The assessment study goal is to consolidate the proposal technology status by the means of a technology roadmap, consisting in the development of breadboards set to ascertain the adequacy of the selected technologies.

In particular, the critical element of the Gas Pixel Detector has been subjected to all environmental test (thermal, thermal vacuum, sinusoidal and random vibrations). Radiation tests were also performed. Iron ions (500 MeV/Nucleons) irradiated the GPD, while operating, corresponding to 40 years in equatorial orbit without damaging or degrading the performances. The ASIC was also irradiated with ions of different energies/nucleon to search for Single Event Upset (SEU) and latch-up events. The observed Single Event Effects (SEE), when the radiation in the orbit of *XIPE* is considered, indicates a negligible expected rate (by orders of magnitude). In the design of the BEE we, anyhow, consider a latch-up protection circuit and the regular load of the register. Leak test are also performed on a GPD after being subjected to all the environmental test. Therefore, the TRL 6 is well justified.

The BEE is a direct derivation of the laboratory Data Acquisition system that operated already in vacuum and in thermal chambers. It will comprise all space qualified for ADC (12-bit) components and FPGA (Microsemi Rad-Hard FPGA, RTAX2000S). A TRL of 6 is therefore justified.

In principle, all critical parts of the FCW have flight heritage and as such exceed the TRL level of 6. However, the holder wheel itself as an assembly can't claim this heritage nor TRL level of 6. During the adoption phase of *XIPE*, TRL of the FCW needs to be enhanced from the breadboard functionality of TRL 4 to the flight qualification standard of TRL 6. In order to achieve this, a flight representative holder wheel needs to be subjected to the relevant mechanical and thermal test environments as well as a life test. The life test requirements are relatively limited as not many operations are foreseen during the life of the instrument. Filter wheel rotations in the order of 1500 are foreseen at present which is not a challenging requirement as the member of *XIPE* team has filter wheels in a good working state in orbit. Indeed, the MSSL filter wheel design as it flies on XMM-Optical Monitor and on *Swift* have been operating since 1998 and 2004 and are still working without a problem having performed more than 150'000 rotations to this date. The position repeatability for the filters achieved is +/- 100 micron, which translates to 10 arc-min. There is no launch stop required for the *XIPE* filter and calibration wheel as the worm wheel stops rotation during launch and the wheel is stiff enough out of plane to minimise wear on the gears during vibrations.

The ICU baseline processor for the ICU data processing board is currently the GR712RC, a dual-core LEON3FT SPARC V8 processor, which is space quality level and flight proven. Flash NAND memories are the highest density memories qualified for space applications. The radiation tolerant stacks require a power supply of 3.3V. Based on the robust SLC NAND FLASH technology they feature endurance of 100K Write/Erase cycles per sector and 10-years data retention time. Moreover, they are indicated for the use in space.
The Focal Plane Support Items are based on a design well-proven by SPI on-board Integral and also for this item the TRL is 6.

5 Mission design

Table 5-1 below summarises the *XIPE* mission architecture.

Orbit	Nominal: LEO, circular 550 km altitude, 5.6 deg inclination
Launch vehicle	VEGA-C
Ground Stations	15-m ESTRACK Kourou (KOU-1) or 10-m ASI Malindi (MAL-1)
Observation strategy	Target Pointings with slews between targets
Field of Regards	half of the sky at any given time
Lifetime	3 yrs nominal with consumables sized for 2 yrs extension
Disposal	Controlled re-entry into Earth atmosphere
Total delta-V	220 m/s including margins

Table 5-1 Summary of Mission architecture

5.1 Mission Analysis

5.1.1 Launcher Characteristics

The mission and systems are designed for a launch with a VEGA-C vehicle with the PLA 1194 VG adapter. VEGA-C will replace VEGA at the time of launching *XIPE*. VEGA-C has a payload mass performance above 2000 kg including adapter, in the *XIPE* orbit, allowing for very comfortable mission margin over the SC maximum wet mass.

The fairing of VEGA-C has a diameter of about 3 m compared to VEGA's 2.4 m and a slightly larger height, which allow for accommodation of the three 4-m focal length Telescopes.

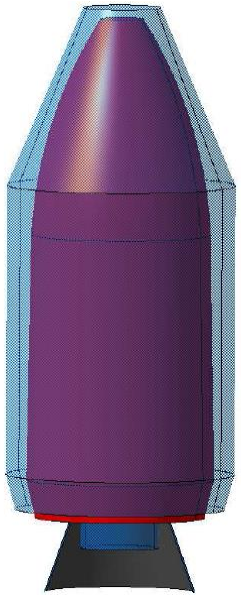

Figure 5-1 VEGA-C fairing (blue) in comparison to VEGA fairing (purple)

5.1.2 Orbit

XIPE will be placed directly into an equatorial Low Earth Orbit (LEO), with an inclination <6° and altitude ~550-630km. There are no seasonal constraints on the launch date. This orbit provides near-complete shielding of the spacecraft by the geomagnetic field against damaging solar particle events and Galactic cosmic rays, together with a low and stable detector background, as demonstrated in missions such as *BeppoSAX*.

The inclination value is the lowest that can be reached by a Launch from Kourou without requiring the Launch Vehicle to perform an orbit plane change (dog-leg manoeuvre). The altitude choice depends on several factors which are discussed in the following sections, but none are especially driving.

5.1.3 Eclipses

There are eclipses of about 35 minutes every orbit. The spacecraft design allows operation of the payload during eclipses, and duration changes by only 10s per 50km altitude change, and is not driving.

5.1.4 Orbit decay

The mission shall comply with ESA debris avoidance regulations which require that the Spacecraft re-enters into the Earth atmosphere within 25 years from end of operations. This sets the higher bound of the possible altitude range to around 630 km. The lower bound is defined by the minimum

mission lifetime requirements. When the initial altitude is 550 km, assuming no orbit maintenance manoeuvres, the orbit decays to 450 km over 8 years, predicted using the ECSS Sample Solar Cycle for the reference atmosphere. If, during the 3 years of nominal lifetime, the altitude is kept within ± 10 km around its nominal value, the decay time increases by one year at a small delta-V cost. Therefore, any altitude between 550 km and 630 km may be in principle, selected trading maintenance delta-V vs mission extension capabilities.

In the *XIPE* orbit, a debris collision avoidance risk of 1 in 10,000 can be tolerated with less than one manoeuvre per year. To allow for some margin a total ΔV of 1 m/s is sufficient for collision avoidance manoeuvres for 5 years independently of the orbit altitude.

5.1.5 Ground station coverage

Figure 5-2 shows the mean contact time *XIPE* will have with low-latitude ground stations for different orbit altitudes. The higher the altitude the longer is the average contact. Also the closer the ground station is to the equator the longer is the coverage, although the differences are small. Worst case data rates have been sized for the ESA-provided Kourou station, although an ASI contribution for Malindi has been proposed. For occasional critical high data volume observations, access to additional commercial station passes (e.g. Singapore) can be considered. For costing purposes use of a single and the same Ground Station for science data and SC housekeeping downlink during the operational phase has been baselined.

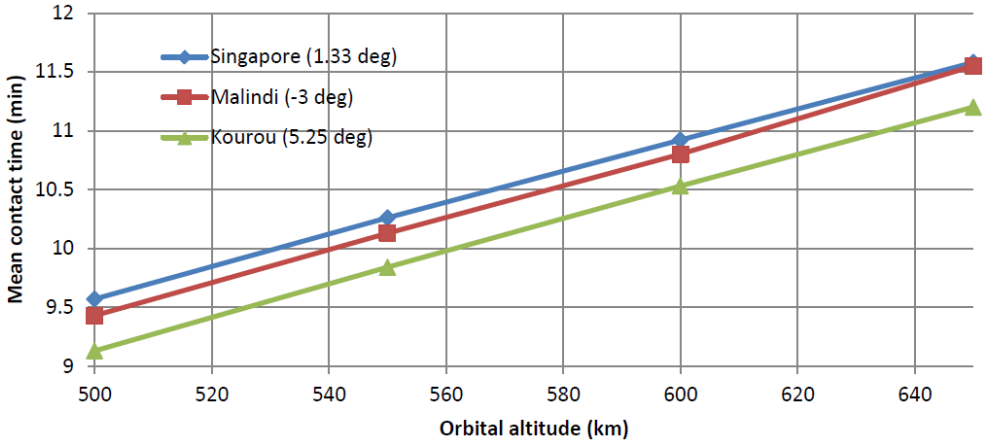

Figure 5-2 Mean contact time of a satellite in a 6º-inclination circular orbit with low-latitude ground stations and South Atlantic Anomaly interference.

5.1.6 South Atlantic Anomaly Pass

The low altitude and inclination serve to minimise the van Allen trapped charged particles seen by the SC, avoiding especially the South Atlantic Anomaly (Figure 5-3). A thorough study of the populations and effects of these two sources of trapped protons has been conducted during the assessment phase (by the Payload Consortium, industry and ESA) using AP8/AP9 and Petrov radiation models (including comparison with previous missions in LEO, e.g. *BeppoSAX*).
Present simulations show that for an altitude of 550 km, the fraction of the orbit exposed to >100 MeV protons is about 5% of the orbital time. This increases by a few percentage points at 630 km. However, there is a significant spread in results depending on the model used.
ESA is currently performing an activity where results from actual spacecraft measurements in the Van Allen belt regions crossed by *XIPE* will be used to tune the existing model, potentially reducing uncertainties.

5.1.7 Mission End of Life

If an uncontrolled re-entry is baselined at end of mission, the casualty risk on ground due to remaining spacecraft fragments is close to the mandatory limit of 10^{-4}. Therefore, the Spacecraft is designed conservatively for a controlled de-orbit.

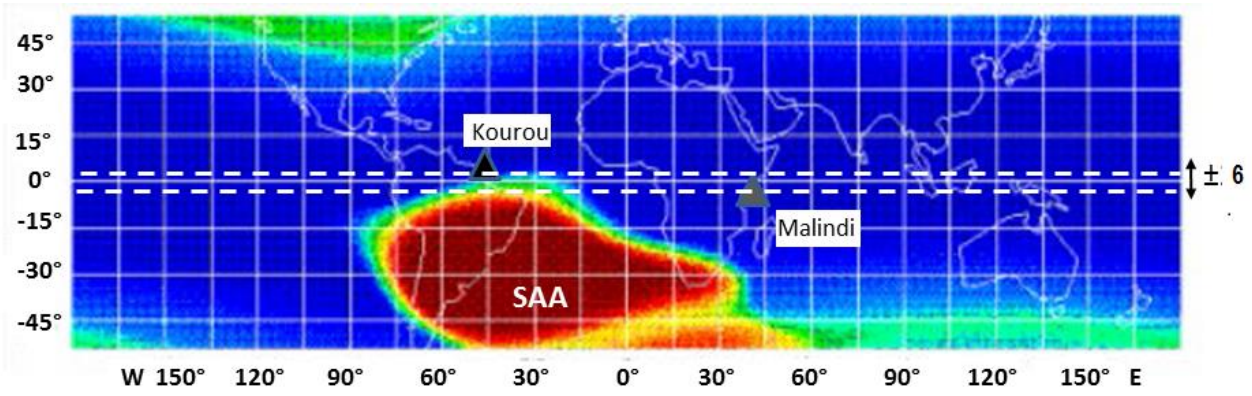

Figure 5-3 The XIPE orbit with inclination <6° excludes almost all regions of high charged particle background (e.g. SAA)

This can be achieved by a sequence of propulsive manoeuvres lowering progressively the orbit perigee. The perigee of the last full orbit cannot be too low because the spacecraft needs to be fully controlled and quite large aerodynamic torques will be experienced at altitudes below 200 km. For a strategy where the total deorbiting is split in 4 burns, the starting altitude is 630 km (worst case) and a total thrust of ~30N is available on-board, the required ΔV is ~190ms^{-1}. This totally dominates the propellant budget.

5.1.8 Mission Phases

The operational phase of the mission has been scoped for LEOP of ~3 days, a satellite and payload commissioning lasting ~ 3 months. It is proposed to execute a Calibration and Performance Verification phase which includes and initial Science Demonstration, lasting 2 months. A total Operational Phase of 3 years includes a final deorbit phase of about 1 month.

5.1.9 Observation concept and mode of operation

The Observation strategy of *XIPE* consists of consecutive slews and long exposure pointings to target sources on the basis of the science plan which is updated at regular intervals. Between target observations, the plan includes also short pointings to specific sources for monitoring purpose. These pointings have a distribution and a timeline such to optimise the mission efficiency.

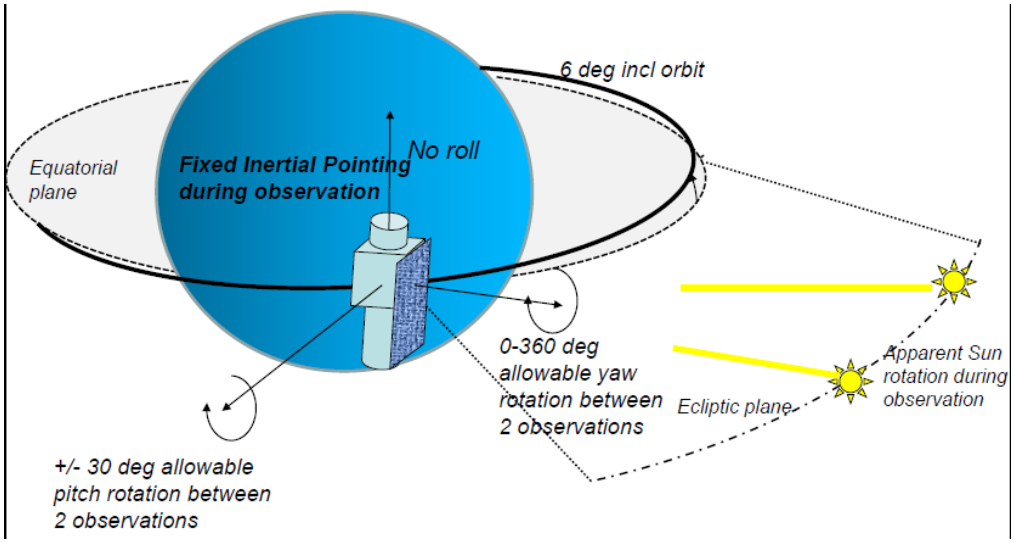

Figure 5-4 XIPE pointing

The science plan is interrupted in the case of Target of Opportunity triggers or in case the safety of the Spacecraft is at risk (collision warning, safe mode). After termination of the event that has caused the interruption, the plan is autonomously resumed by the SC. The initial mission analysis, demonstrating a target

availability of ~65% for a field of regard of ½ sky, has been folded with a mock observation plan, including core science targets and a range of specimen guest observer targets in different science classes. This results in about 80-days margin against the nominal science duration of 30 months.[1]

During the operational phase, the spacecraft supports a single payload operational mode. The payload always generates data to the bulk memory, except in high background regions, where the detector high voltage can be lowered. Depending on the spacecraft architecture, either all S-band or S-band with a X-band downlink capability are possible. Depending on overheads and coding schemes, a 6 Mbps telemetry rate is achievable. With 14 daily passes of >8 minutes' duration (worst case lowest altitude to Kourou), a total daily downlink of ~40 Gbits can be expected. X-band allows an increase to a downlink data rate of 10.3 Mbps.

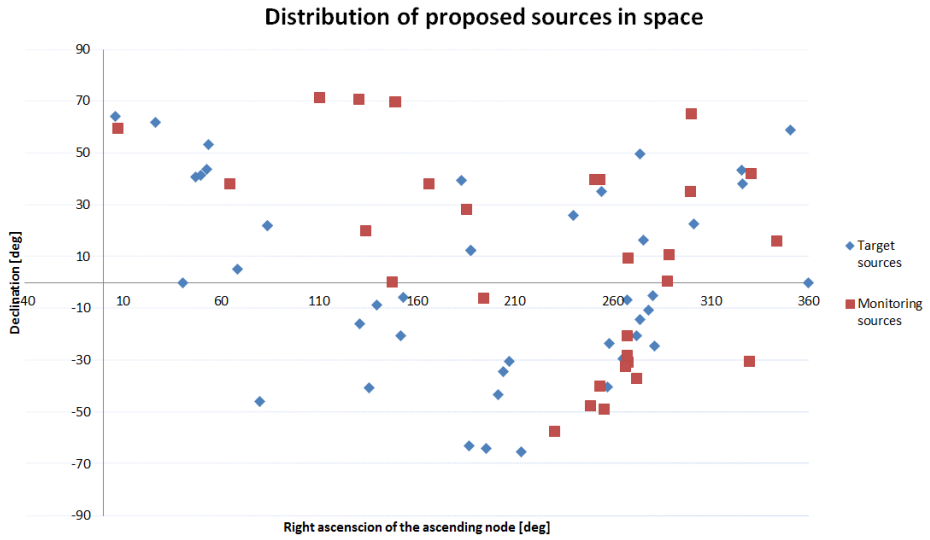

Figure 5-5 Initial selection of target sources

From the mock observing plan it has been determined that a handful of targets can exceed the nominal downlink rate, and it will be arranged that (for example Crab Nebula) the data will be stored to the mass memory and subsequently downlinked. In almost all cases the required data latency requirement of 7 days is easily met with rare exceptions leading to about 10 days. For those cases, additional ground stations could be temporarily rented to reduce latency.

5.2 Spacecraft Design

5.2.1 Satellite Overview

The key aspects of the design of the *XIPE* spacecraft (SC) are driven by the Payload requirements and, in particular, by the accommodation of the long telescope tube (*metering structure*) and its associated thermo-elastic stability and by pointing performance. Both factors contribute to the achievement of the nominal angular resolution and the required effective area. The avionics, Attitude control, and electrical systems are based on a Low Earth Orbit (LEO) platform developed for Earth Observation and for commercial programmes which provides cost savings in hardware procurement and AIV/AIT.

The key aspects of design of the *XIPE* SC are driven by the accommodation of the long telescope tube, the need to maintain its absolute temperature (20°C at EoL to achieve the nominal angular resolution), associated thermal stability, and pointing and availability requirements.

During the Assessment Phase two SC designs were derived by industry teams, leading to different concepts of the bus design but substantially, with similar architecture (see Figure 5-6). Both industrial designs satisfy all

[1] In addition to the nominal science observations, the analysis of mission planning has included occultation periods where the spacecraft will slew to selected "monitoring" targets to check for interesting source state changes.

key mission requirements, and there is very good confidence that a mission profile satisfying the overall science requirements will be achieved.

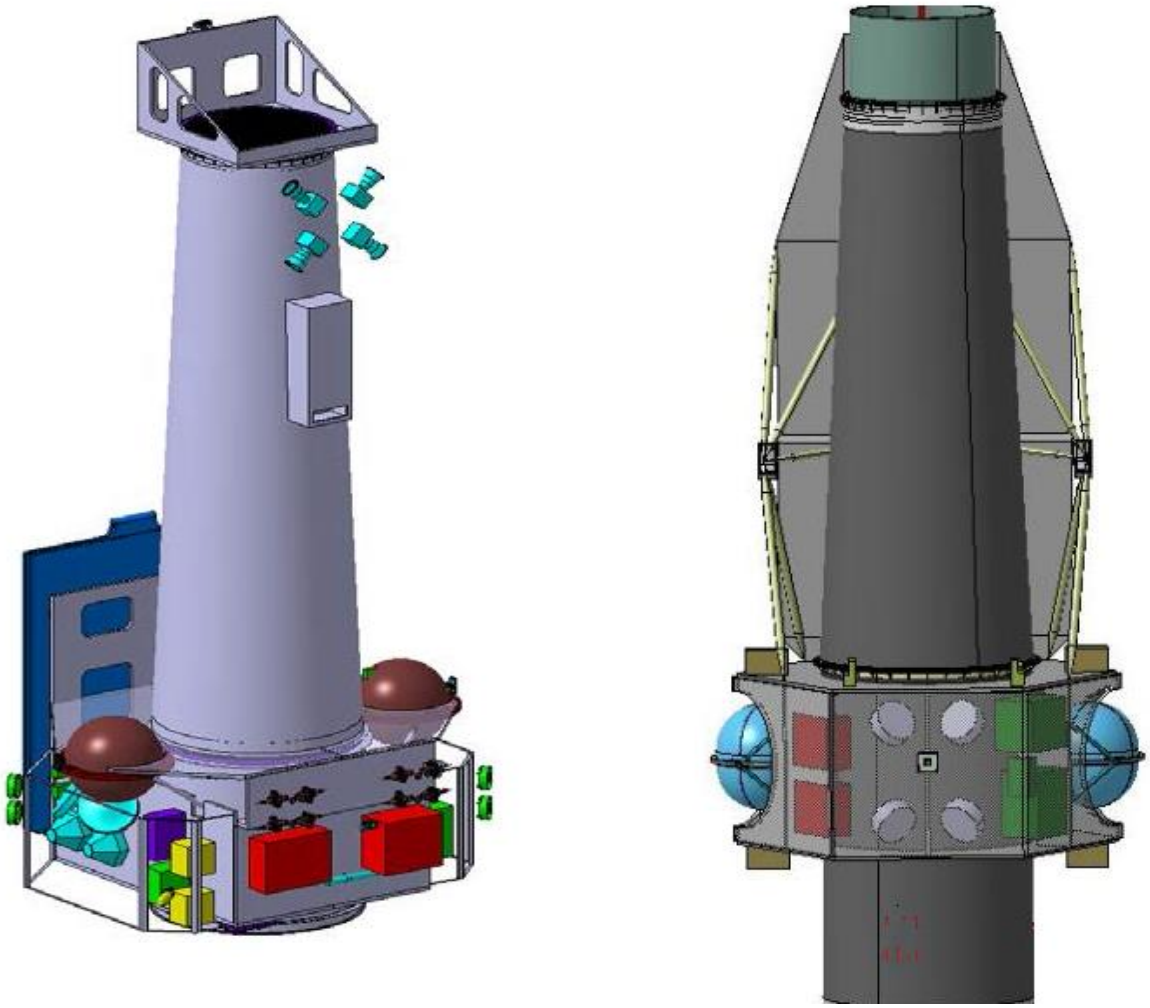

Figure 5-6 View of the XIPE spacecraft configuration proposed by two contractors. The main differences include the location of SVM along the tube, deployable or fixed solar panels.

5.2.2 Satellite Configuration

The SC is divided into a Payload and a Service Module (PLM and SVM). The PLM is composed of the three Mirror Units with their common mounting structure, the Telescope Tube and the Focal Plane Assembly. Clearly the SC is dominated in scale by the telescope tube.

5.2.3 Mechanical Design

The satellite mechanical design is dominated by the conical telescope tube defined by the 4m focal length. The service module will surround the structure supporting the 3 mirrors, and will be located above the launch vehicle adapter. The focal plane platform will be accommodated at the other end of the telescope tube.

The solar panel will be either configured as a single body-mounted fixed panel or composed of two parts with one deployed after launch.

The SC design includes a sunshield for the Focal Plane Assembly; while the Mirrors are placed inside the SVM so to avoid Sun impingement at all times. This permits SC pitch angles within ±30° from the Sun direction, so ensuring a Field of regard corresponding to ½ of the sky at any given time of the mission.

The ESA-supplied mirror units will be integrated into a support platform, and furnished with thermal hardware,

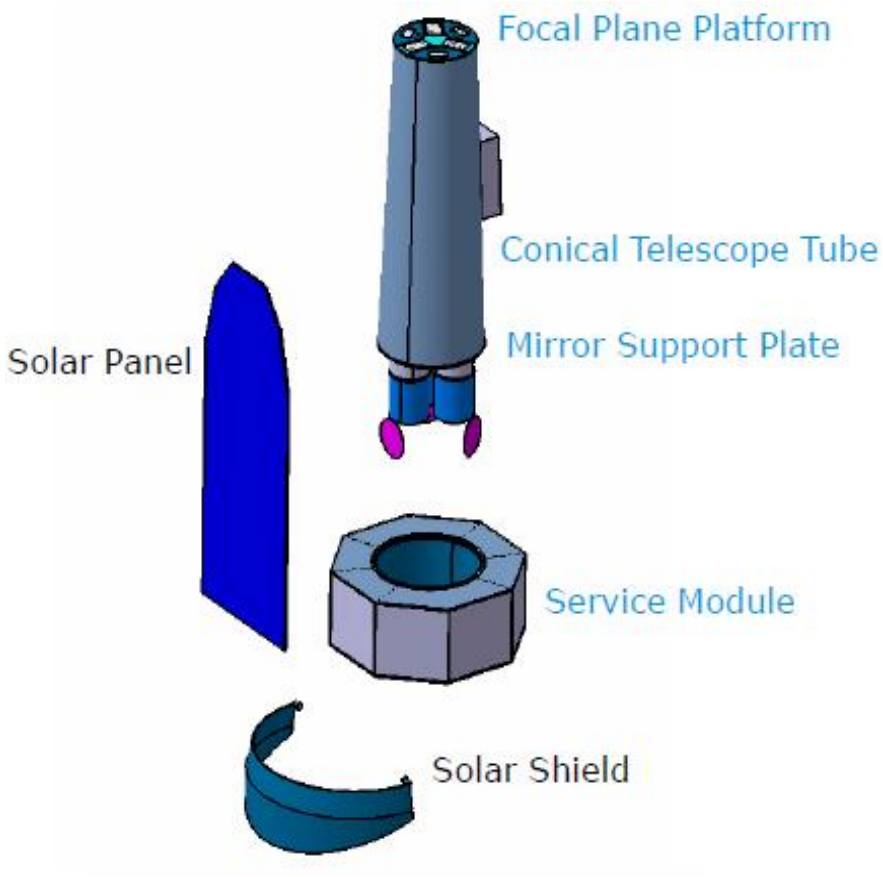

Figure 5-7 Break out of major satellite components.

particularly baffles, and a deployable cover that prevents contamination during AIV and launch.

The three detector units and associated electronics will be provided by the instrument consortium as pre-integrated boxes that allow for expedited installation and alignment onto the focal plane support structure. Thermal control of the platform and the interface ring to the fixed conical telescope tube will be provided by industry.

A preliminary modal analysis has confirmed compliance with launcher stiffness requirements, Specific tailoring of CFRP laminate of the Telescope Tube minimizes the longitudinal CTE, so fulfilling the required stability. An analysis has led to locate the Star Tracker Assembly at the high end of the Metering Tube, close to the Focal Plane Assembly. This guarantees low angular resolution error due to relative misalignment between the Telescope line of sight and the Star Tracker boresight and good knowledge of polarisation angle with respect to celestial coordinates due to sufficient proximity to the detectors.

5.2.4 Thermal Control Design

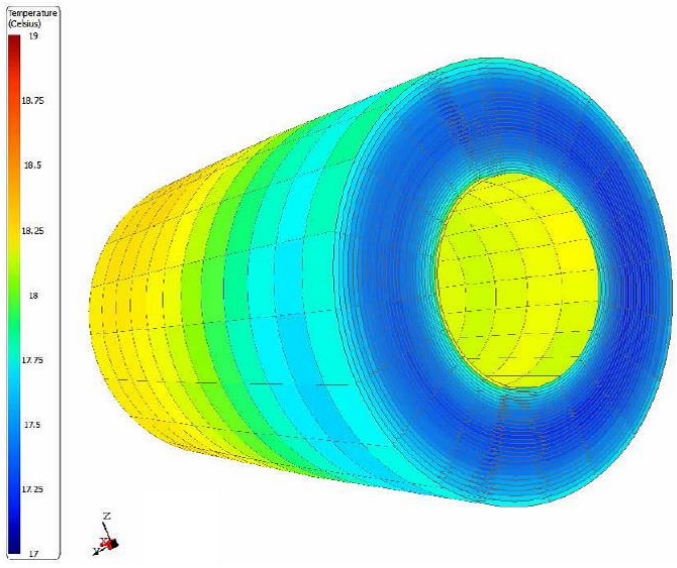

Figure 5-8 Example of distribution of temperatures across Mirror Unit.

The thermal design is a key aspect for the *XIPE* system, in order to satisfy the science requirements. The detector and mirror absolute temperatures will be defined within the range 5°C to 25°C, with a detector temporal stability required of ±1°C during measurements. The most severe requirement is to maintain the temperature spatial gradient across each Mirror Unit within 1°C in longitudinal direction and 1°C in radial direction during pointing times. These are challenging as a consequence of continuous change between sun illumination and eclipse phase. Modelling must also account for Earth IR and albedo input on the whole S/C and on the effects of the open Mirror covers.

The thermal control of the mirrors is based on the concept to create a warm environment that radiatively controls the optics temperature. To this aim, Mirror Units are provided with

thermal baffles actively controlled by means of SW-controlled heaters. The total power required to maintain Mirrors' thermal stability is about 150 W. The Telescope Tube is wrapped with MLI to minimise thermal gradients across that could generate distortions and affect the mission angular resolution performance. The Focal Plane is kept constantly in shadow from the Sun but receive variable thermal inputs from the Earth along the orbit.

The SVM thermal control is fully passive and presents no critical issues.

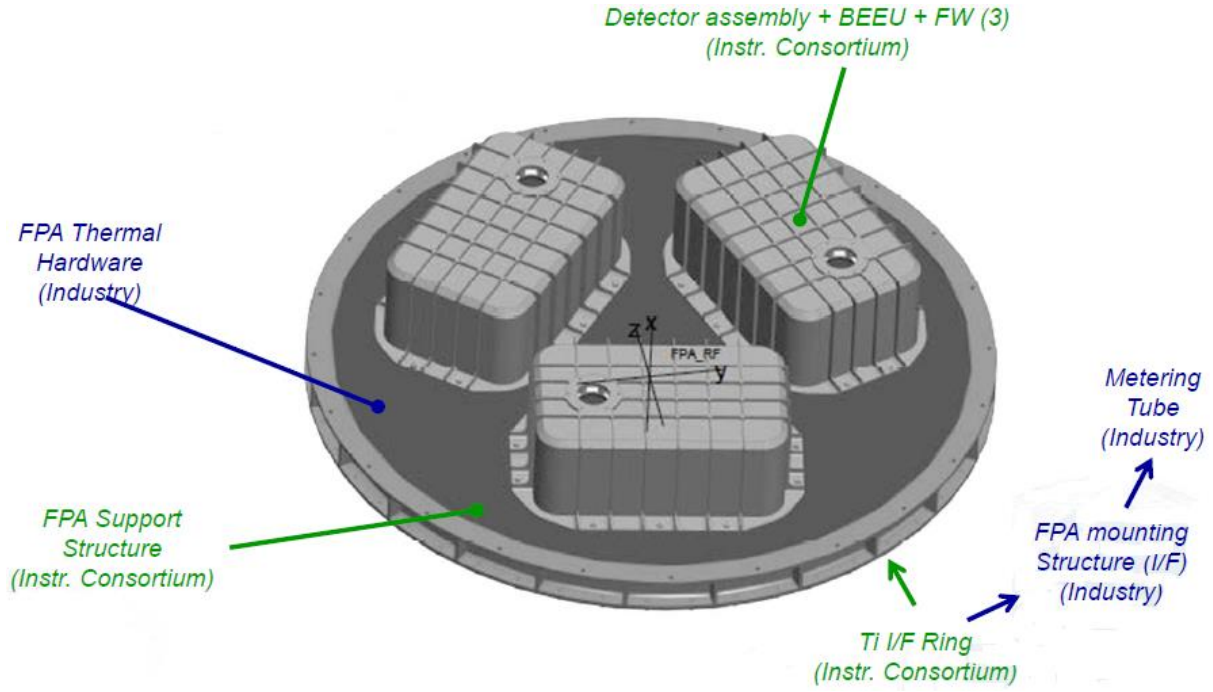

Figure 5-9 The instrument support platform. Indicating responsibilities for different sub-systems. The three focal plane detector systems are supplied as integrated boxes that include front-end electronics, filter/calibration wheel. Reference optical alignment cubes are used to allow industry to position each box at the correct (x,y,z) focal position.

5.2.5 Attitude Control System

The main requirements on the Attitude Control System are:

- provide Relative Knowledge Error (RKE) <5 arcsec at 2σ over 2 Ms to satisfy angular resolution requirement;
- provide Absolute Knowledge Error (AKE) <10 arcsec at 2σ to comply with astrometric requirement;
- provide Absolute Pointing Error (APE) <90 arcsec at 3σ to limit vignetting and reduction of Total effective area.

These are moderate requirements that can be achieved by a 3-axis stabilized, STR-based system.

A solution of 4 STR Optical Heads has been proposed, aligned at 90° in one plane and canted out of plane.

Two Optical heads shall always be in Tracking to ensure performance. Taking all possible orbit and observation possibilities, the probability of 3 STR blinding occurring is as low as ~3%, and is assumed this can be accommodated by mission planning steps.

Periodic calibration of STR to instrument alignment must accommodate thermal deformation. Calibration needs to consider each STR separately for its to different alignment on its mounting bracket.

Attitude is controlled by Reaction Wheels (RW) that will be quasi-continuously desaturated by Magnetic Torquers (MTQ). Despite the poor force law in equatorial orbit a reasonable system performance is obtained with ~150Am-2 MTQ.

Analysis of the disturbance torques has shown that gravity gradient and aerodynamic forces are driving and require reaction wheels with capacity >45 Nms. Such wheels also provide SC slew agility of a few deg/min Monopropellant Thrusters are used for de-tumbling at separation, for Safe Mode, collision avoidance, orbit maintenance and de-orbiting functions.

The ACS includes a GPS receiver that is used for orbit determination but also to provide time synchronization to the Instrument electronics better than 4 μs. This allows determination of time of X-ray photon arrival to the detector with an error less than 8 μs. Periodic calibration of STR to instrument alignment must accommodate thermal deformation. Calibration needs to consider each STR separately for its to different alignment on its mounting bracket. Driving requirements: include a knowledge error of 3 arcsec (95%) to be achieved by the calibration approach. This must be stable or repeatable over the mission duration, but also over time scales associated with cadence of calibration. All the while, a Relative Knowledge Error is specified for 7 arcsec, and an Astrometric Accuracy of 10 arcsec, 95% absolute value is needed. The scenarios simulated include checking for duration: of at least one orbit to verify for eclipse transition cases, and a frequency that covers both cold and hot cases.

5.2.6 Electrical Power System Architecture

The dimensions of a Vega-C fairing practically limit the extent of any plausible fixed solar array configuration to ~9 m^2 which is compatible with the Power needs. The platform and payload will operate and be powered continuously for the whole orbit, including eclipses. The sizing case for the Solar Array is the observation mode with the transmitter ON and the Mirror heaters fully operational. This amounts to about 1 kW load.

To avoid losses in efficiency, the power bus uses unregulated voltage around 28 V also for interfacing the instrument. A trade-off has been considered between a MPPT solar array regulator (which makes best use of the extra energy available from the cold solar array on every eclipse exit), and Direct Transfer Energy which is simpler in architecture. MPPT has been chosen.

Standard battery configurations in serial/parallel strings have been identified, providing ~3 kWh of power, in a package <30 kg.

The standard industry LEO platforms offer Power Control & Distribution Units compatible with the needs of the mission.

Due to the high number of heaters which require SW control, a specific Remote Terminal Unit (also called Thermal Management Unit) needs to be included in the SC electrical architecture. There is wide heritage for this unit from several space missions.

5.2.7 Data Handling Architecture

The DH will provide sufficient data storage to prevent data loss through up to 7-day Ground outages. It provides adequate data handling resources for OBC handling of telemetry and telecommands to and from Ground Control Stations, and offers autonomous FDIR capabilities.

Large scale Solid State Memory provides around 1 Tbit of data capacity for science and HK with 100% margin.

Interfaces over a redundant SpaceWire link to the Instrument Control Unit have been baselined for payload data transfer. An additional PPS (Pulse Per Second) line may be offered to transfer the synchronisation signal from platform OBC to Instrument Control Unit.

5.2.8 Telecommunications Telecommanding and Tracking

Science data volume varies considerably with the target source flux. The most demanding source is the Crab nebula with a science data telemetry rate of ~1.5 Mbit/s and a required exposure time of 200 ks. However, most of the sources have data rates a few orders of magnitude lower, even in the case of exposure times of 2000 ks. The average data volume is ~1 Gbit/day. The Quick Look data and the platform and instrument telemetry do not contribute significantly to the data budget.

In principle, a simple S-up/S-down TT&C system is suitable for the mission. This provides about 3 Mbps downlink rate and it allows coping with the 7-day data availability requirement for more than 80% of the

sources. For the remaining cases, data time to ground can be shortened either by adding ground station passes from another equatorial station or switching to an S-up/S-X-down with the addition of a Payload Data Transmitter in X-band. This will increase the downlink data rate to up to 8 Mbps. The choice of S- or X-band transmitters architecture can be defined later, subject to choice of most suitable platform. The selected transponder includes RF tracking capability as Doppler Measurement using coherent RF link and ranging.

5.2.9 Budgets

The tables below show the *XIPE* mass and power budgets. Compared with Vega launch capability to equatorial LEO of 2 tonnes, the *XIPE* estimated mass has a very comfortable margin.

Table 5-2 Consolidated Mass budget (synthesised from parallel studies)

Subsystem	Best Estimate (kg)	Maturity Margin
Mirror Assy	230	20
FPA	70	12
Instrument Control Unit	10	1
NGRM	3	0.3
Telescope Tube	130	25
SVM Structure	165	25
Thermal Control	25	5
Data Handling	30	3
GNSS	7	.1
Solar Array	39	3
Power SS	45	5
Harness	40	7
S band Tx	10	1
AOCS	74	5
Propulsions	39	4
Total	917	115
Dry Mass	**1032**	
Propellant	160	
Wet Mass	**1192**	
System Margin	238	
Total	**1430**	*+LVA 78kg*

Table 5-3 Consolidated Power budget (synthesised from parallel studies)

Subsystem	Best Estimate Normal Pointing Mode (W)
TTC	30
AOCS	135
Data Handling	90
Power Syst	40
SVM Thermal	110
PLM Thermal	220
Instrument	90
Sub-Syst Total	**715**
Harness Loss	30
PCDU Loss	70
Syst Margin 30%	240
Total	**1050**

6 Ground Segment

The Ground Segment (GS) provides the means and resources to manage and control the mission via telecommands, to receive and process the telemetry from the satellite, and to disseminate and archive the generated products. In Figure 6-1, the elements of the *XIPE* GS and the data flow between them is illustrated. The two main elements are the Mission Operations Ground Segment (OGS, light red) and the Science Operations Segment (SGS, light blue). The OGS consists of the Mission Operations Centre (MOC) and the ground stations, which receive the telemetry from the spacecraft (S/C, grey). The SGS consists of the Science Operations Centre (SOC), a Science Data Centre (SDC), and an Instrument Operations Centre (IOC). The development and operations of the SDC and IOC is assumed to be on national funds, provided by the *XIPE* consortium.

A typical *XIPE* observing schedule will consist of long observations up to 4 Ms. Mission planning is thus assumed to be dominated by 1-month ahead planning. The MOC provides Planning Skeleton information while the SOC generates the final timeline that the MOC uplinks to the spacecraft via ground stations. Each 1-month timeline may be revised on 1-week time scales, responding to short-term constraints imposed by, e.g., ground station passes.

The mission is designed to be able to interrupt the timeline during execution, e.g., to observe Targets of Opportunity (ToOs) with a relaxed response time that only requires ground operations during office hours. It is assumed that an autonomous on-board system will be available that allows spacecraft operations to be performed based on input from the SOC, thus target coordinates and observation duration. A feasibility study is under way, led by ESOC, to develop a system that will perform Autonomous ToO on-board on ground request. This study's aim is to improve the ToO planning efficiency.

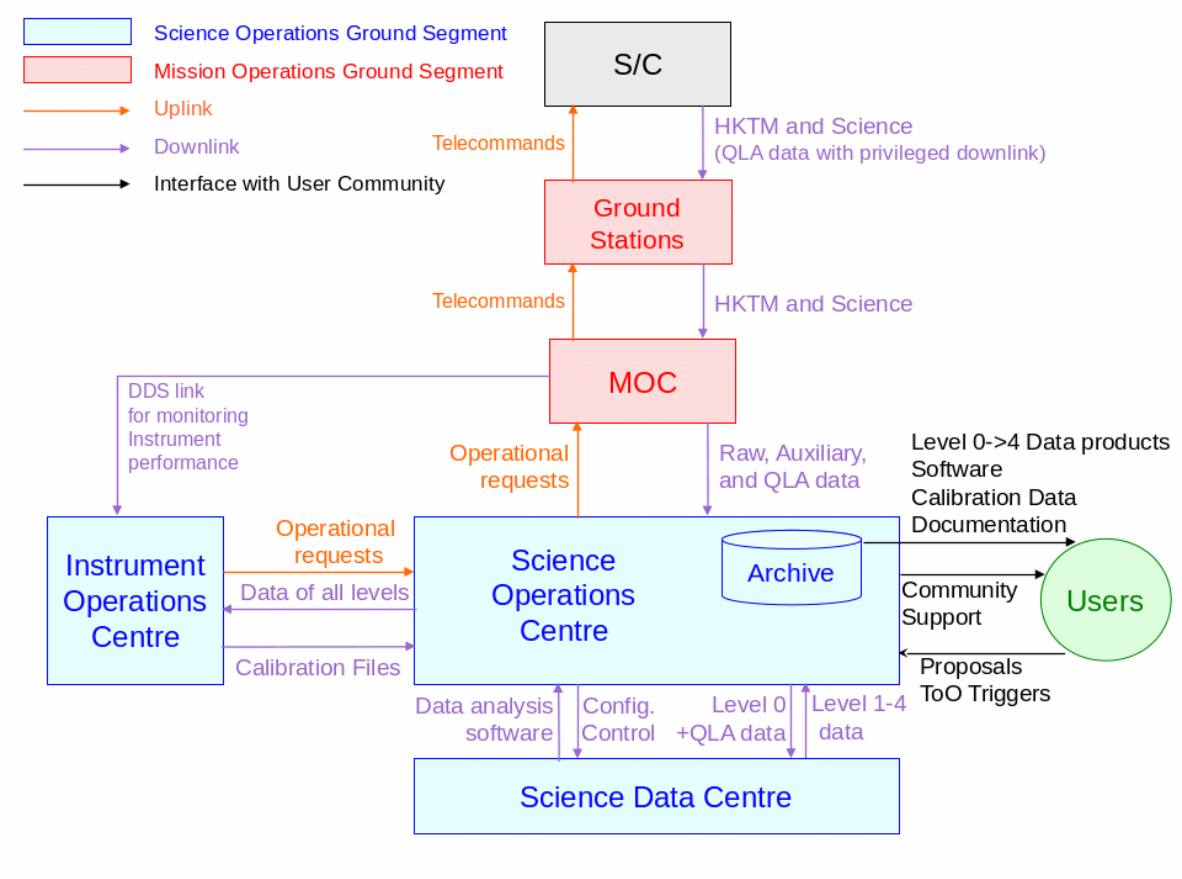

Figure 6-1 Overview of the XIPE Ground Segment elements, including the data flow between them.

Since some variable sources can only be triggered from X-ray observations, the mission design will allow the SOC to schedule short monitoring observations between long observations or during Earth blocks. This monitoring programme can consist of up to 350 snapshot (300 second-long) observations of pre-selected

variable targets per year. Their purpose is to obtain X-ray brightness and some spectral characteristics that scientists can use to trigger ToOs. Since the desired source state is only temporary, the brightness and spectral information needs to be available before final data products are available, and for this reason quick look analysis (QLA) data will be produced on board and downlinked via privileged downlink channels. They will be analysed by the SDC who can then derive triggers for deeper ToO observations. QLA data may be made publicly available so the community can derive triggers independently of the SDC. This will be decided at a later stage based on Science Management Plan (SMP) policy.

The following data products have so far been defined for the *XIPE* mission:

- **Raw data**: Science telemetry plus (preliminary) auxiliary data (e.g., electrical calibration data, orbit prediction files, housekeeping data) that have been produced on board. Science data are currently foreseen (TBD) to be in FITS format following the CFDP protocol.
- **Level 0**: Raw data removed of any communication artefacts (e.g., headers, duplicated data, etc.) and with applied on-board corrections (e.g. corrections of the pixel to pixel gain). Output is a generic events file in binary FITS format including all recorded events in each GPD detector. The FITS files still contain the full information on the tracks measured by the detectors, i.e. the photoelectron emission direction is not yet reconstructed.
- **Level 1**: Photon list with the reconstructed photoelectron direction, photon absorption point, energy and time of arrival. Note that a number of calibrations have to be applied to derive this information, including the overall detector gain calibrations. Photoelectron tracks are no longer available in the FITS file.
- **Quick look data**: A set of preliminarily science data such as light curves, spectra, images, and modulation curves for the central source in each observation. The QLA data are produced on board by the *XIPE* ICU and are downlinked with high priority, requiring at most 3 kbps TM rate. They provide a quick means to assess the observation output without the need of processing all the observation data. While QLA data are obsolete once level 3 data are available, they will be included in the (legacy) archive for permanent storage.
- **Level 2**: Level 1 data with all corrections applied (such as aspect correction, time calibration, barycentric corrections) and remaining instrument-specific calibrations (such as good-timing information) to level 1 data. Output is cleaned FITS event files for each GPD detector. The data will be organized per exposure/pointing.
- **Level 3**: a set of pre-defined science products (examples: light curves, energy and power spectra, photon lists, and polarization measurements) extracted for each observation, eventually combining the information derived from all exposures/pointings that constitute an observation.
- **Level 4**: Data containing enhanced, higher level, scientific products derived from Level 3 data, such as catalogs of sources, historical measurements of the flux, combined multi-wavelength spectral energy distribution and polarization. More level 4 data products may be defined during the course of the mission.

6.1 Operational Ground Segment

The Mission Operations Centre will be responsible for the spacecraft operations. This is described below together with the functioning of the ground stations and the spacecraft operations.

6.1.1 Ground Station

The ground stations network to be used consists of the ESTRACK 15 m ground station Kourou and the ESA Augmented Network Malindi. Both X and S band communications are considered, depending on the mission profile. During the nominal operations phase, ground station utilization has been studied assuming one contact per orbit using Kourou, and several passes per year are assumed with external stations. During LEOP phase, extended coverage is assumed with at least two ground station passes per orbit.

	longitude (deg)	average contact time (min)	daily contact time (min)	station passes per day
Malindi	-3,00	11,51	158,81	14
Kourou	5,25	11,23	153,84	14

Table 6-1 Ground Station Coverage at 650km/5.6^0 i

	longitude (deg)	average contact time (min)	daily contact time (min)	station passes per day
Malindi	-3,00	9,48	135,56	14
Kourou	5,25	9,16	130,10	14

Table 6-2 Ground Station Coverage at 500km/5.6^0 i

6.1.2 Mission Operation Centre

The European Space Operations Center (ESOC) will be the MOC for the *XIPE* mission and will prepare a ground segment including all facilities, hardware, software, documentation, the respective validation, and trained staff, which are required to conduct the mission operations.
The MOC is responsible for the commanding of the spacecraft and instruments, including overall mission planning, for ensuring the spacecraft safety and health, for provision of Flight Dynamics support including determination and control of the satellite's orbit and attitude, and intervention in case of anomalies. The MOC performs all communications with the satellite through the ground stations for the upload of the platform and payload telecommands (based on the observation schedule provided by the SOC, see below), and reception of the downloaded telemetry data. They are also responsible for collecting the science data and its transmission to the SOC, along with the raw telemetry, housekeeping and auxiliary data. Due to the non-continuous coverage, the spacecraft will mainly be controlled via off-line operations.
Anomalies will typically be detected by the MOC only during the passes which are manned by Spacecraft Controllers. After the initial spacecraft commissioning, all telecommands required to carry out the mission will normally be loaded in advance on the Mission Timeline for later execution.
The mission planning cycle will include the platform and payload activities, including ToO operations. It will be performed during office hours. The spacecraft will be able to continue nominal operations without ground contact for a period of up to 7 days.
On-board Control Procedures will allow autonomous execution of complex procedures, including decision loops which the GS cannot support due to the limited ground coverage. The MOC will provide telecommand history and other auxiliary data (including attitude history, time calibrations and barycentric corrections) to the SOC.
The MOC will be in charge of up-linking the ToO requests coming from the SOC. This activity will be implemented as part of the mission planning cycle and loaded to the spacecraft during a next available ground station pass.
The MOC will be in charge of planning collision avoidance maneuvers requiring input from FDS and Space Debris Office (SDO) experts and approval from Spacecraft Operations Manager and Mission Management. The planning of a collision avoidance maneuver should start at latest 12 and 24 hours before the conjunction event. Usually the firing is executed at least one orbit before the conjunction, if performed few revolutions before the encounter the required ΔV drops significantly.
The orbit determination will be carried out using the GNSS receiver on-board (and range/Doppler during GNSS long outages). The Flight Dynamics Team will also support trajectory and maneuver optimization: the maneuver performed for LEOP and the orbit maintenance maneuver (once in the lifetime of the mission).

6.2 Science Ground Segment

6.2.1 Science Operation Centre (SOC)

ESA's European Space Astronomy Centre (ESAC), near Madrid, Spain, will host the Science Operations Centre (SOC). It will be the primary point of contact to the MOC for providing detailed operational requests, and it will plan the payload operation activities. The SOC is also the single point of contact for the scientific user community. The SOC operates a helpdesk as communication interface with the community but delegates

issues related to data analysis software, data processing, data quality and data characteristics to the SDC. Issues related to calibration and instruments are delegated to the IOC.

The overall SOC activities are the following:

- Proposal Handling and organisation of AOs - full responsibility of the SOC;
- (Payload) mission planning – full responsibility of the SOC;
- Raw to Level 0 data processing – the development, validation, and maintenance of the pre-processing software is a responsibility of the IOC; the integration and running is the responsibility of the SOC;
- *XIPE* Science Data Archive at ESAC – full responsibility of the SOC (with support from the ESAC Science Data Centre, ESDC);
- User Support – the SDC is responsible for issues related to analysis software, data processing, data quality and data characteristics; the IOC for issues related to calibration and instruments, the SOC is responsible for the rest.

During the development phase, the SOC will be responsible for configuration control and to overview all the software development carried out by the SDC. About two years before launch, the SOC will start organising Operations Rehearsals involving all elements of the Science Ground Segment (SGS) to identify any problems well ahead of launch.

Although the Science Data Centre will perform all the data processing from level 0 to level 4, the SOC will, on irregular time scales, perform the same data processing steps by the scientists in the team in order to maintain expertise in the SOC and to verify that pipeline data are reproducible with public tools.

During the Operations phase, the SOC will organise the Announcements of Opportunity (AO) process. This involves preparing and publishing documentation, making announcements to the community, supporting the community during proposal preparation, organising the peer review (Time Allocation Committee, TAC), and circulating the final decisions (based on the TAC recommendations) to the proposers. The SOC further prepares the approved observations for scheduling. At the start of each observing cycle, the SOC prepares a long-term plan that assures that the approved observing programme can be performed until the end of each observing cycle. Detailed time lines will be generated on a monthly basis in terms of medium-term schedules that may be modified every week. Within a latency period of 7 days (for 80% of observations) after end of each observation, the SOC will receive raw and consolidated auxiliary data from the MOC and will convert them to level 0 data within a maximum of 4 days after consolidated auxiliary data are available. They will be ingested into the archive from where the SDC (see next section) will pick them up to produce higher-level science data products within 24 hours after level 0 data are available. The SOC has full responsibility of the archive which will be operated as close as possible to the design of the legacy archive. Only during the Post Operations Phase (POP) will the SOC be involved in science validation of data products before ingesting the final products into the legacy archive. During nominal, extended, and post-operations phases, the SOC will provide User Support by making available all relevant documentation about instrumentation, calibration, User Guides, etc. The SOC will operate a Helpdesk as the primary communication interface to the scientific community while the SDC and IOC will provide technical support on request.

6.2.2 Science Data Centre (SDC)

The Science Data Centre (SDC) will be established through national funding and is assumed to be led by the Data Centre for Astrophysics at the University of Geneva (UoG), Switzerland. The *XIPE* SDC will be built on the heritage of previous missions (e.g., *INTEGRAL*) and will be organized as a consortium of different institutes, providing each the needed man power to cover certain tasks. The SDC effort will be led by the SDC PI, coordinating the activities of all participating entities, ensuring the successful completion of all tasks and the timely delivery of all products. At present, it is expected that the SDC will cover and be held responsible for the following activities:

1. Production of all software needed for the processing of the mission data, as well as the daily processing, analysis, and exploitation of all *XIPE* data (the only exception is the software needed for the processing of the raw telemetry into the level 0 data that is provided by the IOC).
2. Packaging of the software in order to facilitate the distribution to the science community.

3. Daily processing of the level 0 data into the level 1, 2, 3, and 4 data.
4. Verification of the X-ray emission status of all *XIPE* targets through the usage of the QLA data ("sky monitoring")
5. Assist SOC in user support for what concerns the data processing, analysis, and exploitation. The SDC will also organize in collaboration with the SOC dedicated workshops for the training of scientists to the usage of the *XIPE* software and the manipulation of the mission data products. As part of this activity, the SDC will also train the SOC personnel in the usage of the *XIPE* software in order for them to be able to check the pipeline products and assist the SDC in the science validation of the data.

About 2 years before launch, the SDC will provide training to the SOC to ensure that all data analysis steps can also be performed by SOC scientists and that the final documentation is clear enough to be followed by any scientist in the world-wide community. This will be verified during Operations Rehearsals taking place during the last 2 years of the Development Phase. During the Nominal Operations Phase (NOP), the SDC will perform the pipeline processing of science data, starting from level 0, using exclusively publicly available software and only the calibration data that are also accessible to the public, and deliver the products to the SOC for archiving and distribution. The science data processing and re-processing will include all necessary calibrations provided by the IOC. The SDC is expected to lead the data processing software maintenance. As part of routine data processing, the SDC also performs systematic trend analysis[2], production of value-added products, catalogues, surveys. The SOC and the IOC support the SDC in the quality control of the science data. The SOC feeds all data products into the Science Archive.

The SDC will support the IOC in the instrument calibration activities, and assists the SOC in providing user support related to analysis software, data processing, data quality and data characteristics. Also, in collaboration with the IOC and the SOC, the SDC contributes to the testing and validation of new releases of the archive and the overall SGS operational system.

6.2.2.1 XIPE Software production

The production of all *XIPE* software by the SDC comprises:

1. The processing pipelines, routinely used to perform the processing from level 0 to level 1, 2, 3, and 4 data;
2. The interactive tools that are needed to calibrate and clean level 1 data, generate level 2 data and to further process level 2 data into level 3 and 4 data;
3. The visualization and tools needed to check the QLA products produced on-board by the *XIPE* ICU (i.e. the Quick Look Software);
4. The environmental software that is needed by the SDC to pipeline-processing data in the SOC archive (all products will be stored in the same archive).
5. The polarization models for both extra Galactic and Galactic sources.

It shall be remarked that the level 0 data are the lowest level products made available to the science community. The raw telemetry will not be distributed, even though this will be kept available in the SOC archive to be used (if needed) by the SDC and the IOC personnel. In order to maximize the exploitability of the *XIPE* data, the images of the track imprinted by the X-ray photons on the GPD detectors will be distributed within the FITS structure of the level 0 data. From these tracks, it will be possible to derive the direction of emission of the photoelectron and the polarization measurements by using a number of instrument specific algorithms. The algorithms are already available as of today and have been developed by the *XIPE* instrument team based on a number of independent inputs and control samples, derived from data acquired in the lab and dedicated Monte Carlo simulations. The instrument team considers that any possible attempt from the community to modify these algorithms during the *XIPE* operational phase should be discussed and coordinated with the

[2] All standardized reduction processes directed at trend analysis can be run at the SDC as part of their systematic pipeline processing. But it is understood that an in-depth evaluation of trends in the instrument characteristics will have to be done by the IOC, who will also use the interactive capabilities of the data processing system in the course of this activity.

instrument team in order to have a proper validation and assessment of the correctness of the results. We note that it is still considered very useful to keep separated the level 0 and level 1 data, as the IOC might want to reprocess the level 0 data into newer level 1 data if improved methods to reconstruct the photoelectron emission direction from the tracks are developed during the course of the mission or even in the post operation phase.

All software and calibration data needed to process the *XIPE* level 0 data into higher data level will be made publicly available to the community through the SOC archive. The environmental software, being dedicated to the reserved access of the SDC to the SOC archive for the retrieval of data to be daily processed, will not be distributed to the community. The pre-processing software to reduce raw data into level 0 data that will be provided by the IOC will be installed at SOC for automatic running and daily processing operations. These will not be distributed to the community.

It is important that (at least some of) the pipelines for the daily processing make use of the same tools developed for the interactive analysis, as to minimize the duplication of efforts and optimize the man power required for the software production. At present, we plan to use for the pipeline the interactive tools run in a specific sequence and with a pre-defined parameter file in such a way that a standard and coherent set of level 2, 3, and 4 data can be extracted for all *XIPE* observations during the entire mission lifetime. A complete re-processing of all data to obtain an updated version of this standard set of products can be carried out from time to time when significantly updated calibrations will be available.

The SDC will also take care of the integration of all tools and relevant pipelines into a unique software data package, in order to facilitate the software distribution, installation, and usage for the science community. The required documentation will also be written and made available to the community through the SOC archive.

As part of the overall software development effort, the SDC will also develop the polarization models, which will be used to convert the modulation curves measurements into polarization measures. As it is currently done for the usual X-ray spectral analysis with developed spectral models made available to the community in Xspec, we plan to do something similar for the polarization. The polarization models will be developed by specialists in different classes of sources (divided mainly in the two large classes of extra Galactic and Galactic sources) and distributed to the community in order to obtain polarization measurements from the modulation curves provided as outputs of the standard or customized *XIPE* data processing.

In our current plan all pipelines to process level data from 0 to 4 are developed by the UoG. These pipelines will make use of the interactive tools which production is led by the ASI Science Data Center (ASDC) in Italy. The production of the level 4 data will also require the usage of the same interactive tools, but since these data are generated later and not on the same timescale as the data level 1,2, and 3, we currently plan to have the Observatory of Strasbourg to lead this activity and the preparation of the level 3 → level 4 pipeline. The quick look software production will also be led by the Observatory of Strasbourg. The overall development of the polarization models will be coordinated by the University of Tuebingen (IAAT) in Germany, with a substantial contribution of the University of Valencia (UV) participating into the development of the polarization models especially suited for extra Galactic sources.

6.2.2.2 Sky monitoring

As part of its observing program, *XIPE* will also monitor roughly once per day (on a best effort basis) a certain number of sources that are identified as critical targets to achieve the *XIPE* science goals are supposed to be observed once they enter a particularly interesting state. We cannot guarantee at present that an X-ray monitoring scanning the sky in the interesting energy band will be available at the time of *XIPE*, and thus this monitoring program needs to be included as part of the mission Mock Observing Plan (MOP).

The targets of interest for *XIPE* change their emission states on timescales of several days to weeks. For this reason, the activity of the quick look of the mission data can be carried out on relaxed timescales and there is no need to impose the availability of the data on-ground on timescales shorter than a few days. However, in order to give the possibility to the SDC to check the emission state of the sources being monitored, as well as verifying the quality of the ongoing observation, it has been decided to implement in the instrument ICU the capability to produce on-board a number of quick look products. These include images, lightcurves, rate-meters, and modulation curves for all sources being observed by *XIPE* (including nominal targets, as well as the short monitoring observations). The QLA data will be downloaded from the S/C using a dedicated virtual

channel and made available to the SDC in the SOC archive as soon as the downlink is completed. Note that the QLA products do not need further reprocessing on the ground but some validation could still be needed.

The SDC will make use of the QLA to:

- Check the status of the monitored sources
- Check the status of the normal observations to scientifically validate the data and verify that all data parameters are nominal (contributing to the overall effort of the instrument health checks)

It is expected at present that the QLA products will be replaced as soon as the level 3 data products extracted from the consolidated data that are made available. However, the QLA data will also be made public when available, in order to maximize the involvement and interest of the international scientific community in the mission. In principle, the QLA data of the monitoring observations can be made publicly available as soon as they are downlinked, providing a historical record of the X-ray emission from many sources with rapid access (the QLA data do not need to be further reprocessed – note that this is also expected to be provided through the level 4 data making use of publicly available level 3 data). QLA products from proprietary observations can be made available to the corresponding PI in order to allow scientists to quickly assess the status of the observation they were granted. These products can be made public when the proprietary time expires (usually one year). These details will be discussed later in the future mission phases. Details on the distribution of the QLA data is clearly not driving the design of the SGS. The QLA data will also be stored in the XSDA (*XIPE* Science Data Archive) for completeness.

At present, the SDC consortium plan to share among all participating institutes the task of the sky monitoring. Scientists will be on a rotating shift in all institutes (one at a time) in order to ensure the most efficient possible follow-up in case an interesting event is discovered or any instrument anomaly emerges.

6.2.3 Instrument Operations Centre (IOC)

The Instrument Operations Centre will be established at the institute of the *XIPE* instrument PI and will be the hub for collecting and maintaining expertise and knowledge about the *XIPE* instrument hardware and software. It includes all aspects of calibration and operational support for the instrument as part of the *XIPE* SGS. As such the IOC will be led by the instrument PI and collect contributions (in terms of man power) from all institutes that develop the instrument hardware.

During the *XIPE* development phase, the IOC will:

- provide support to ESA for payload system integration on the spacecraft
- organize the on-ground campaigns to characterise and calibrate the *XIPE* instrument response
- analyse ground calibration data and maintain an archive of results for transfer to the SOC (including the pre-flight calibration data)
- provide the support to MOC, SOC, and SDC related to the instrument on-board software, including support for testing
- support the MOC in the development of instrument specific procedures in the Flight Operations Plan
- develop the instrument data base
- develop and maintain a *XIPE* simulator, which will permit the end user to evaluate the exposure time needed to obtain measurements of the polarization angle and degree for a pre-defined source with established emission properties in the *XIPE* energy band (this tool will also be included by the SOC as part of their package distributed to the community in order to support the calls for observational proposals)
- develop and maintain the instrument specific algorithms that will be particularly important to process the raw telemetry into level 0 and level 1 data. For the latter, the key algorithm will be the one computing the photoelectron emission direction from the tracks recorded by the GPD detectors.
- develop the software to process the raw telemetry into level 0 data (to be installed and run at SOC).
- develop the on-board software within the ICU to produce Quick-Look Analysis (QLA) products.

- be consulted by the SDC to develop the instrument specific data analysis software for pipeline and interactive processing.

During the mission operations, the IOC will:

- maintain the instrument database
- maintain the instrument on-board software
- maintain the pre-processing software (raw telemetry → level 0 data) installed at SOC
- perform the instrument health monitoring and trend analyses by using all relevant data products produced by the SOC and SDC. To monitor the instrument performance, a DDS (Data Dissemination System) link will send the instrument performance information directly from the MOC to the IOC. In addition, the SOC will have remote access to instrument performance data.
- provide help and support in case of any anomaly detected by the MOC, SOC, and SDC during the data reception, processing, and QLA
- provide improved and updated in-flight calibrations, to be ingested into the SOC archive and made available to the community
- Assist SOC answering instrument-specific queries from the community.

Given the current approach to the *XIPE* instrument development, it is expected that the IOC effort will be led by INAF-IAPS, with a major contribution from INFN-Pisa and INFN-Torino. Additional contributions are planned from all institutes leading the different sub-systems, e.g. the Space Research Center in Poland (CBK), the Mullard Space Science Laboratory in the United Kingdom (MSSL/UCL), IAAT, UV, and the Royal Institute of Technology in Sweden (KTH, especially for the instrument background characterization). In order to build up and maintain the relevant instrument expertise in the SOC, IOC activities are supported by a Calibration/Instrument Operations Scientist (sometimes also called "Liaison/Disciplinary Scientist"). This role will be fully funded by ESA and co-located 50%/50% during the Development Phase (DP) and 25%/75% during the Nominal/Extended Operations Phase (NOP/EOP) at IOC and SOC, respectively.

6.3 *XIPE* Data-Flow and Processing Strategy

The data flow of the *XIPE* mission is sketched in Figure 6-2. In the current organization of the *XIPE* GS the raw telemetry is downlinked to the ground from the spacecraft through the ground station and collected at the MOC. As the QLA products generated on-board are downlinked through a dedicated virtual channel, these data take priority over the rest of the telemetry, even though their limited size is not expected to impact on the normal telemetry transfer. Both the QLA and the nominal telemetry are transferred to the SDC as soon as available at SOC, together with all relevant auxiliary files produced at MOC.

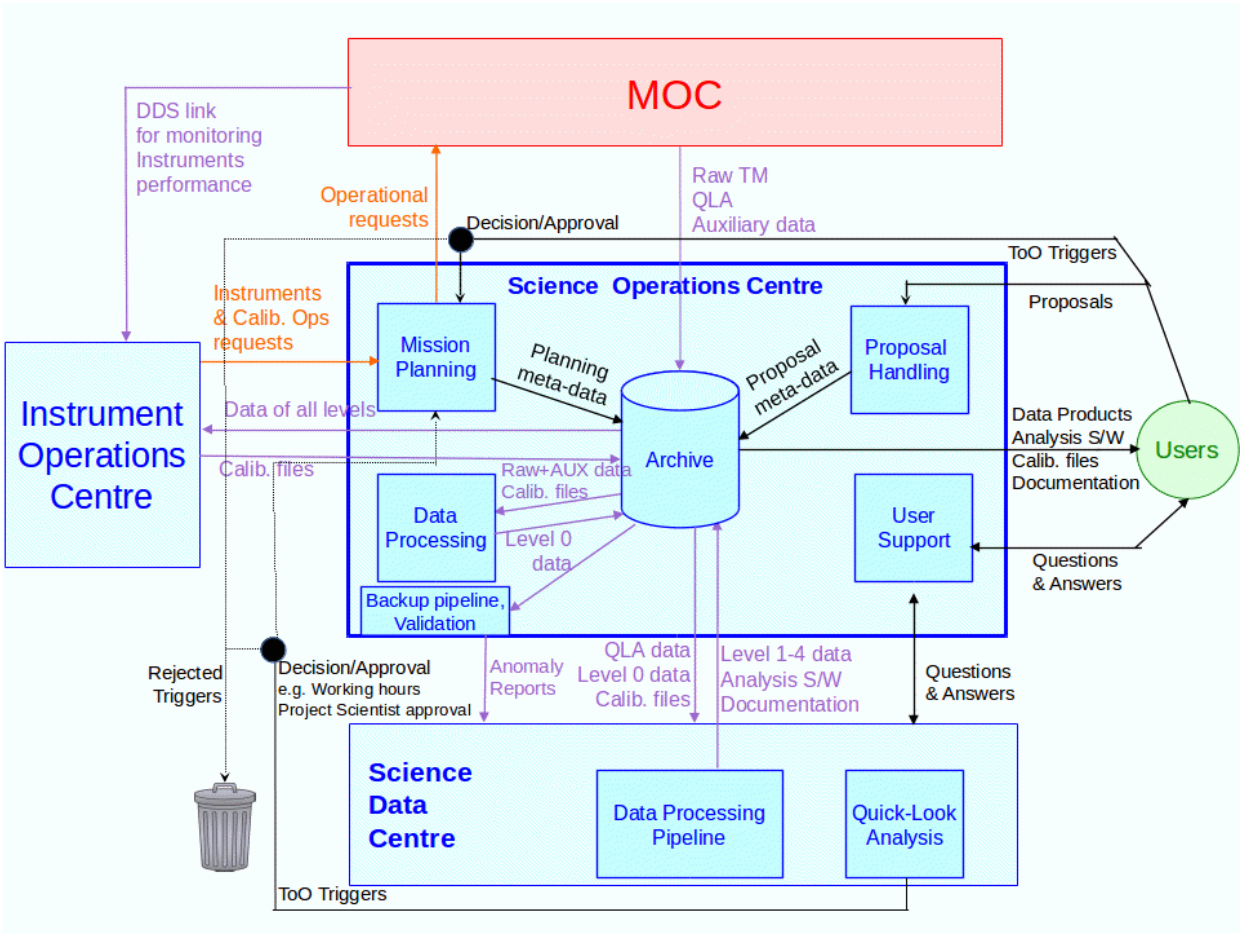

Figure 6-2 Overview of the XIPE Science Operations Ground Segment, including the operational interactions.

The QLA products do not need any further processing, and are thus made immediately available to the SDC to perform QL activities. There is not a requirement imposed on the timescale for making the QLA products available at the SDC, neither there is one on the completeness of these data. The QLA products do not drive the SGS design. If some QLA products are lost due to transmission issues, no recovery action is planned. The QLA data will be used by the SDC to alert the SOC in case any interesting event is spotted and they will be made immediately public to the community to increase its involvement in the mission (it is possible that some validation will be needed by the SDC before they can eventually be made public).

The normal telemetry will first be processed locally at SOC in order to produce the level 0 data. The level 0 data are the lower level products that will be made available to the science community and that can be further processed and analysed with the public *XIPE* software and calibration data. The raw telemetry will anyway be stored in the SOC archive and made available to the SDC and the IOC to perform deeper data/instrument investigations, if needed. The usable level 0 are expected to be produced at SOC within a maximum delay of 7 days from the observation (for 80% of the cases at least), driven by the availability of the flight dynamic data from the MOC. Once produced, the level 0 data will be accessed by the SDC in order to produce remotely the level 1, 2, 3, and 4 data with the *XIPE* processing pipelines. All products of this processing will be stored and made available to the community through the *XIPE* archive at SOC (the XSDA, *XIPE* Science Data Archive). The level 0 data can be re-processed by the science users at any time, using the publicly available software that will incorporate the same executables adopted for the production of the pipelines (the latter will however use a pre-defined set of parameters in a dedicated parameter files). It is expected that the QLA data described before for all observations will be superseded once the level 3 data obtained out of the SDC processing are available. They are anyway stored in the XSDA for completeness (they might be needed in case any anomaly is found in these data and deeper investigations have to be carried out by the SDC and the IOC).

It is expected that during the mission lifetime, the IOC will produce from time to time updated instrument calibration files. These will always be stored into the *XIPE* archive at SOC and used for both the SDC and the general scientific user processing of the data. All software and calibration documentation will always be

available within the SOC *XIPE* archive. If improved algorithms for the reconstruction of the tracks are developed by the IOC, a new version of level 1 data can be produced in the archive (or by the end users using the publicly available software) and then all data can be re-processed to re-obtain updated level 2, 3, and 4 data at any time during the mission lifetime, as well as during the post operation phase.

At present we expect that the level 4 data include for *XIPE*:

- A catalogue of all detected sources (this is expected to be a useful product because *XIPE* will perform deep observations of many regions, possibly providing in the soft energy domain a deeper survey than other X-ray missions in at least a few of these regions);
- A multi-wavelength characterization of all detected and serendipitous X-ray sources, produced by cross-correlating the *XIPE* catalogue with catalogues in many other energy domains;
- A historical record for each detected source of the flux, spectral energy distribution, X-ray timing properties, and (if possible) polarization measurements.

The level 4 data will likely be generated by combining publicly available level 3 data and thus the production of level 4 data is not expected to occur daily on the same timescale and frequency as the other level 1,2, and 3 data. The UoG is currently expected to lead the production of level 1, 2, and 3 data, while the production of level 4 data is planned to be led by the Observatory of Strasbourg (where a long standing expertise in the production of multi-wavelength catalogues is available).

6.4 *XIPE* Ground Segment Timeline

The timeline for the set-up of the fully functional SDC and IOC has been agreed with ESA to match their current plans for the ESA led GS elements. The *XIPE* consortium plans to start developing the SDC and the IOC already in 2019, beginning mostly with the definition of a detailed software development plan and coding standards with the SOC. The software development will start in the SDC and IOC around 2020, with a preliminary software package delivery to SOC already in 2022 in order to allow early tests concerning especially the pre-processing of the raw telemetry into level 0 data. This early delivery will also allow SOC personnel to be properly trained in the usage of the software from the beginning and with large margins compared to the SGS overall tests planned to start two years ahead of launch (including "operations rehearsals"). The SDC and IOC will be fully functional and staffed at the time of these tests. The payload calibration activities on-ground are planned to be organized by the IOC already in 2021, in order to produce as early as possible, the pre-flight calibration data to be used during the SGS tests and the preliminarily software package verifications/tests. Apart from the nominal operations phase when all agreed tasks of the SDC and IOC will be accomplished, we are also planning two years of post-operations when the IOC and the SDC will support the SOC into preparing the final version of the XSDA, containing the most updated payload calibrations, processed data, and software packages (to remain as legacy products of the mission).

7 Management

7.1 Project management

XIPE is envisaged as an ESA mission with contributions from ESA Member States and therefore the 'usual' project management approach for ESA missions will be followed.

ESA management: The overarching responsibility for all aspects of the *XIPE* mission rests with ESA's Directorate of Science and its director (D-SCI). During the development phase, ESA will appoint a Project Manager, who is responsible for implementing and managing ESA's activities during this phase. This work will cover all industrial activities (procurement of the spacecraft, procurement of X-ray telescopes, integration of the spacecraft and instruments, testing, the launch campaign and also the early in-orbit phase). After commissioning, the ESA Mission Manager assumes responsibility for operations of the spacecraft, its payload, and the ground segment.

The *XIPE* Project Scientist is ESA's interface with the scientific community for all scientific matters. A *XIPE* Science Team (XST) will be set up by the Agency (with some representatives of the instrument consortium but also with external scientists) following the normal practice of the Agency. The XST advises the Project Scientist (who chairs the team). The Project Scientist advises the Project Manager during the development phase on all issues that affect the scientific performance of *XIPE*, and advises the Mission Manager during operations on all issues that affect the scientific output of the mission.

Payload management: The Payload consortium will provide the payload. All members of this consortium have a long track record and have in the past provided instruments for successful high-energy missions (*XMM-Newton*, *Chandra*, *BeppoSAX*, *INTEGRAL*, *AGILE*, *ROSAT*, *Swift*, *NuSTAR*) and as such have the right level of expertise. During the early phase of the Definition Phase activities, the ESA management team will work to secure multilateral agreements. These will be established between ESA and the Payload Consortium funding agencies to formalise the commitments and deliverables of all parties. A *XIPE* Steering Committee with representatives from the national funding agencies and ESA will then be set up to oversee the activities of the Payload Consortium and the timely fulfilment of the obligations of all parties to the Multilateral Agreement (MLA).

A *Science Data Centre* has been conceived as part of the consortium and is responsible for ensuring suitable pipeline processing tools for the science data to produce standard products for ingestion into the archive at ESA. Whereas the full responsibility of the timely delivery of the instruments and the SDC rests with the PI who is supported by the co-PIs and the PI of the SDC, a consortium council will meet twice a year. In this council all contributing institutes are represented taking into account the relative size of the contributions and this body will advise the PI in case of conflicts or resource adjustments.

7.2 Procurement and member state contributions

XIPE is planned as an ESA-only mission, with only a small non-critical contribution from the Tsingua University (China). The Payload and the contribution to the Science Ground Segment will be provided by the *XIPE* Consortium, supported by the ESA Member States, with the noticeable exception of the X-ray optics for which ESA-funded manufacturing is planned, while the testing and end-to-end calibration of the focal plane instruments with the telescope will be supported by the *XIPE* consortium, and carried out at the PANTER facility (provided as part of the German contribution to the project).

Table 7-1 Overview of member state contributions

Italy	Consortium PI, Instrument PI, and Project Office GPD manufacturing and characterization Back-End electronics design & manufacturing DU assembly design & manufacturing Filter and calibration wheel calibration set design & manufacturing *XIPE* Instrument calibration plans & strategy Malindi Ground Station Telescope calibration advisory team lead AIVT activities at system level Instrument operation center lead SDC contribution
Spain	*XIPE* co-PI FPSI design and manufacturing Thermal hardware Test and assembly facilities SDC contribution
United Kingdom	*XIPE* co-PI Consortium thermo-mechanical aspects of all *XIPE* payload elements Filter and calibration wheel design and manufacturing
France	SDC contribution
China	Filter and calibration wheel filters design & manufacturing Mixture/pressure/drift-length of the Gas Cell fine tuning

Germany	*XIPE* co-PI ICU design & Manufacturing ICU software EGSE provision SDC contribution PANTER facility for X-ray tests
Switzerland	*XIPE* co-PI *XIPE* SDC PI and Project Office *XIPE* SDC engineering, software development, data processing
Poland	*XIPE* co-PI Power boards design & manufacturing
Sweden	*XIPE* background characterization

7.3 Mitigation actions for top risks

In the framework of the XPOL preliminary study the risk assessment has been performed since MSR taking into account the Instrument baseline of *XIPE* proposal and the outcomes of ESA CDF study.

Most of the identified *XIPE* Instrument medium risks are typical of a phase A project.

The high risk areas, peculiar of this mission, are all related to an early conceptual Instrument baseline, not yet based on a complete preliminary design assessment. The outcomes of the XPOL risk assessment is a risk mitigation plan, which has been considered in the Instrument trade-off analysis as well as DDV and test plan. As example of this risk mitigation plan in Table 7-2 reports four top level risks identified in the risk analysis.

At the completion of XPOL assessment study we can consider all the identified high risks overcome by the implementation of the mitigation design and management solutions in a consolidated XPOL baseline. Such baseline variation, which is also relevant the Prime level activities, have been widely deepen with ESA and the two industries in charge of the *XIPE* assessment studies.

Table 7-2 Top level risks and mitigation strategy (already on-going)

Risk	Cause	Mitigation Actions
Internal DU Calibration sources do not allow a satisfactory calibration	Unsatisfactory in source repositioning	- Implementation of local metrology inside DU to measure the position of calibration source; - Implementation of a high precision encoder on FWC to define the relative position of Calibration sources.
Date of the instrument/units delivery not respected	DU, BEEU & ICU integration need more effort	- Verify the instrument integration pipe-line starting from the bread-board activities; - Development of ICU EM; - Organise the environmental verification of produced hardware in a centralised fashion, with expert personnel and testing facilities.
Utilization of radiactive sources for calibration impacts the satellite integration schedule	Radiation sources have to be mounted/dismounted from the DU because not admitted during ground operations	- FPA Architecture that can allow the DU accessibility at satellite integrated level; - DU architecture that can allow a easy and quick replacement of radiative sources.
GPD Thermal stability not achieved	Underestimation of thermal control efficiency	- Development of GPD B/B be tested in thermal environmental; - Implementation of GPD Flight Representative in the satellite STM; - Development of DU QM.

7.4 Schedule

The *XIPE* schedule is consistent with a launch date at 2026 with the appropriate margins. Given the currently high TRL of the different payload components, no item is currently expected to be on the critical path. Figure 7-1 reports the XPOL phase B/C/D master schedule which identifies the main tasks, milestones and deliveries for each XPOL unit model. The XPOL master schedule is summarised as follow:

- The XPOL milestones are synchronised with the mission level milestone while the delivery dates are in compliance with ESA reference dates.
- The detailed design definition of the *XIPE* Instrument will start from the finalization of the high level (Instrument level) specification and Experiment Interface Document. Starting from these documents, lower level specifications (unit level, equipment level) will be prepared by the *XIPE* consortium responsible and agreed with the PI.
- The *XIPE* Consortium will develop or procure the various items to be collected by the Institutes responsible for the integration at unit and FPA level.
- DU and ICU Units will be characterised, calibrated and tested at environmental condition prior the delivery to the PI (INAF-IAPS) for the instrument E2E testing and calibration at the INAF facility, equipped with polarised X-ray sources.
- In parallel with DU and ICU the Focal Plane Structure will be integrated and tested.
- After the detector calibration at the INAF X-ray facility, the DU and ICU, will be delivered to the MPE-PANTER facility for combined test and calibration with the Mirror Units using X-rays.
- The current planning considers INTA as a centralised HUB for the environmental test of DU, FPA STM and FPA structure.
- During XPOL accommodation on satellite FM, the performance will be monitored by the means of the internal sources and the alignment stability will be verified.

ID	Task Name	Duration
1	**Mission Phase B1**	**502 days**
7	**Mission Phase B2/C/D**	**1741 days**
15	**XPOL Phase B1**	**502 days**
16	Activation of Institutes in-kind activities	60 days
17	Consortium Activities KO	0 days
18	Industrial Contractor activation	156 days
19	Instrument baseline refinement	201 days
20	AIV/AIT and procurement organization	201 days
21	B/B Development	201 days
22	Margin	240 days
23	**XPOL Phase B2/C/D**	**1742 days**
24	XPOL Phase B2/C/D KO	1 day?
25	Instrument System Requirement Review (I-SRR)	0 days
26	Instrument Preliminary Design Review (I-PDR)	0 days
27	Instrument Critical Design Review (I-CDR)	0 days
28	Instrument Qualification Review (I-QR)	0 days
29	Instrument Final Acceptance Review (I-FAR)	45 days
30	**XPOL Phase B2/C/D Master Activities**	**1203 days**
31	LLI Procurement	398 days
32	B/B Test completion	398 days
33	XPOL Detailed Design refinement	839 days
34	Part, Material & EEE procurement	545 days
35	XPOL Calibration Facility Design Refinement	398 days
36	XPOL Calibration Facility set-up	415 days
37	XPOL AIT/AIV	557 days
38	XPOL Test @ XPOL/Panter x-ray facilities	415 days
39	**XPOL STM Development**	**196 days**
40	Integration of DU Dummies/STM & Environmental Tests	155 days
41	Integration of FPA Support Item STM	155 days
42	Integration of FPA composite STM & Environmental Tests	42 days
43	Integrated FPA STM Delivery to ESA Prime	0 days
44	Integration & Test of ICU Dummy	195 days
45	ICU Dummy Model delivery to ESA Prime	0 days
46	**XPOL ICU AVM Development**	**238 days**
47	Integration of ICU AVM	90 days
48	ICU AVM Test	72 days
49	ICU AVM HW/SW Integration	72 days
50	ICU AVM Delivery to ESA prime	0 days
51	**XPOL DU/ICU QM Development**	**340 days**
52	Integration of DU QM and qualification test campaing	180 days
53	Development of DU GSE	180 days
54	DU QM & GSE delivery to XPOL Calibration Facility	0 days
55	Integration of ICU QM and qualification test campaign	180 days
56	Development of ICU GSE	180 days
57	ICU QM & GSE Delivery to XPOL Calibration Facility	0 days
58	XPOL QM (DU&ICU QM) E2E test & Cal. @ Instr. Cal. Facility	99 days
59	XPOL QM I-QR & Delivery to Panter X-ray facility for Tel. E2E test	0 days
60	Combined XPOL/MU QM test at x-ray Panter facility	60 days
61	**XPOL FM & FS Development**	**377 days**
62	AIV/T of ICU FM & FS & Environmental Tests	332 days
63	ICU FM Delivery to XPOL Calibration Facility	0 days
64	ICU FS Delivery to XPOL Calibration Facility	0 days
65	AIV/T of DUs FM/FS & Environmental Tests	332 days
66	DU FMs Delivery to Calibration Facility	1 day
67	DU FS Delivery to Calibration Facility	0 days
68	E2E test & calibration of DU FMs @ XPOL Calibration Facility	60 days
69	ICU+DUs FM set-up @ XPOL Calibration Facility	15 days
70	E2E test & calibrationl of ICU+Dus FM @ XPOL Calibration Facility	37 days
71	ICU+DU FMs & GSE to ESA for E2E Calibration @ Panter/DU & IC	0 days
72	XIPE Telescope FS E2E Calibration at Panter x-ray facility	44 days
73	DU FMs and ICU FM Delivery to Prime for integration on satellite	0 days
74	E2E test & calibration of DU & ICU FS @ XPOL Calibration Facility	44 days
75	DU+ICU FS delivery to ESA Prime/ DU & ICU FS FAR	0 days
76	Integration of FPA Support Item FM	210 days
77	Integration of FPA with DU dummies & Environmental Tests	66 days
78	FPA FM (including spare parts kit) Delivery to ESA Prime / FPA FA	0 days

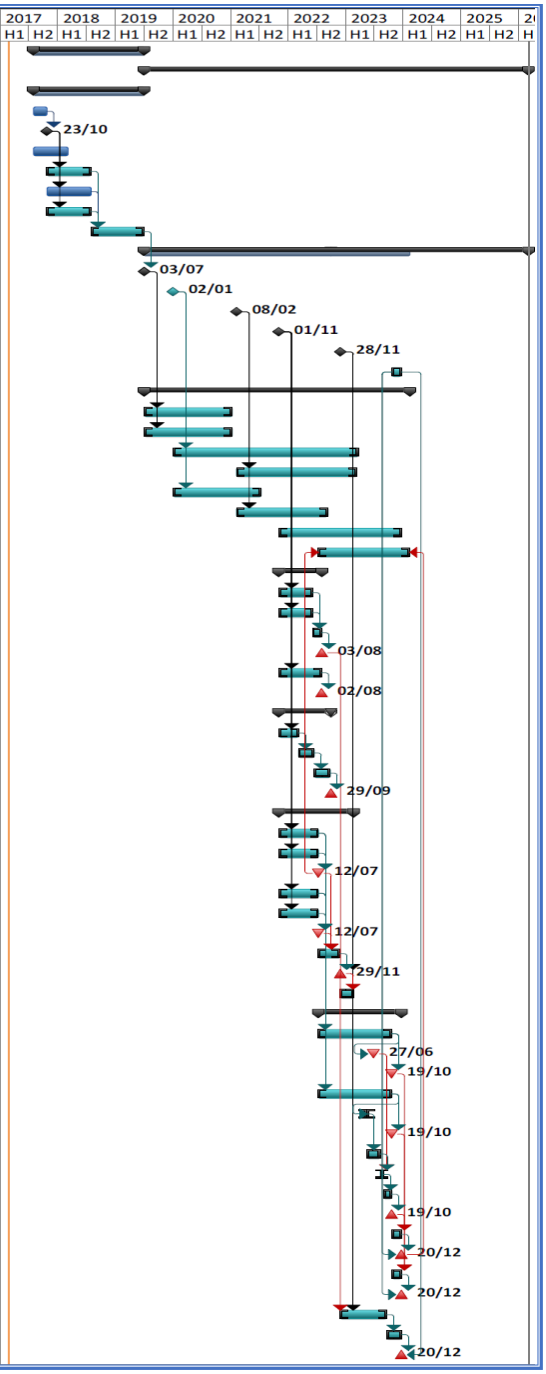

Figure 7-1 XPOL Master Schedule

7.5 Science Management

We have demonstrated convincingly that a comprehensive and coherent science investigation can be accommodated within the baseline mission duration. There is a comfortable margin of time available for investigations not yet considered and which would be part of an on-going Guest Observer programme. The consumables margin for the spacecraft is further evidence that unexpected sensitivity estimates or completely new landscape for science discoveries can be accommodated with modest increase in further AO cycles.

A detailed Science Management Plan has not yet been defined. In this section we describe the basic principles of the Science Management Plan with a focus on the allocation of observing time. The prime goal of the science management plan is to ensure the best possible scientific results for the mission which implies that the best

scientists should have a key role. At the same time there should be a reasonable return to the member states that have funded the instruments. This leads to the following approach:

1. *XIPE* will operate as an observatory. Observing time will be open to the world-wide scientific community and allocated via annual Announcement of Opportunities (AOs) and scientific peer review organized by the SOC.

2. Time will be allocated to the core science goals of the mission as some of the core scientific goals of the *XIPE* cannot be achieved by aggregating a number of individual GO proposals. So it is proposed to devote a fraction of total observing programme to *Key Projects* to ensure a co-ordinated approach to a sub-set of the science goals. A separate AO will be executed for the formation of *Key Project* Teams during the implementation phase. Before this call it will be decided with the ESA Advisory Groups for which topics a key project will be established (and how much time will be reserved). The topics for the key projects will be set by ESA based on advice from the science advisory team closer to the launch. For these core science goals proposals can be submitted by individual scientists or groups of scientists. This is open to the scientific community and does not require an involvement in the instrumentation. Again, based on peer review, the key project teams will be selected.

3. A fraction of the total observing time will be allocated to the instrument consortium to ensure a reasonable return for their investment. The fraction will be decided by ESA. This time will be evenly distributed over the total mission duration. This helps to guarantee that the instrument teams remain actively involved in the optimisation and calibration of the instruments following their delivery to ESA. The instrument teams' observing proposals will participate in the Observing Time Allocation Committee (OTAC) selection process as for any external scientist, but it is envisaged that they will receive a guaranteed fraction of the time if they do not achieve it based on the quality of their proposal (the instrument team proposals will have priority over higher ranked observation proposals till the fraction reserved for the instrument teams is achieved). This ensures that the top level ranked proposals will be executed irrespective of the instrument involvement but the lower ranked proposals might be substituted for proposals of the instrument teams in case the instrument proposals do not already fill their fraction based on science ranking only.

4. Targets of Opportunity can be proposed by the scientific community and the ESA Project Scientist will decide about this (eventually after consulting the relevant members of the OTAC). Depending on the nature of the ToO either the one-year proprietary data rule can be applied or the data will be made available to the science community in general.

5. The standard 1-year proprietary data rights are assumed for the *XIPE* observations (from the point level 1 data are available). After this period all data become public.

6. For the QLA data no proprietary rights will apply and this data could be made available to the community on a much shorter time scale (to be discussed and decided at later mission phases).

8 Communications and Outreach

ESA will be responsible for planning and coordinating education and outreach activities related to *XIPE*, with the support of the *XIPE* consortium. An outreach and education plan will be developed and executed jointly by ESA and the consortium. The following guidelines apply to ESA missions:

- ESA leads and coordinates the execution of all education and outreach activities within the data rights framework of the mission;
- For the purpose of public relation activities, the consortium will provide to ESA unlimited access to all processed and analysed data, even during their proprietary period (if applicable); this material will anyway follow the data rights policy for matters concerning scientific publication purposes;
- Members of the consortium have a duty to support ESA with regards to education and outreach;
- ESA gives credit to members of the consortium regarding scientific and technical results, when applicable.
- The consortium has the duty to exploit the outreach and educational potential of *XIPE*. The contributions from national funding agencies to the science exploitation phase will include resources to develop plans and produce education and outreach material such as high quality website, children booklets, secondary school material, press releases, popular science-level material, animations and simulations, audio-visual kits, etc.… As appropriate, the consortium members will develop locally targeted educational material, and cultivate local contact points to broaden the Europe-wide network of outlets for the public relations activities.

The SDC plans to develop additional tools to facilitate the access of the science community to *XIPE* legacy data products, as well as simplified tools to allow citizen to visualize the variable *XIPE* X-ray sky, explore source behaviours and flag interesting events, provide target advocacy and participation, connect with public robotic telescope networks etc. During the mission implementation phase the consortium will gather feedback from existing citizen science projects to better understand the lessons learned on engagement, tools, interfaces and data production. This will be used to inform the *XIPE* outreach programme for maximising the participation and expediting the websites to be ready near launch.

9 References

[1] Abdo, A.A., et al. 2009, ApJ, 707, L142

[2] Abdo, A.A., et al. 2010, ApJ, 722, 520

[3] Abubekerov, M. K., et al. 2008, ARep, 52, 379

[4] Agudo, I., et al. 2011, ApJ, 735, L10

[5] Agudo, I., et al. 2012, IJMPCS, 8, 299

[6] Agudo, I., et al. 2014, A&A, 566, A59

[7] Ajello, M., et al. 2010, Ap.J., 725, 1688

[8] Alexander, K. D., et al. 2016, ApJ, 819, 25

[9] Amelino-Camelia, G. 2004, New J. Phys., 6, 188

[10] An, H., et al. 2014, ApJ, 793, 90

[11] Angelakis, E., et al. 2012, JPhCS, 372, 012007

[12] Angelakis, E., et al. 2016, in press (arXiv:1609.00640)

[13] Antonucci, R., et al. 1993, ARA&A, 31, 473

[14] Bachetti, M., et al. 2014, Nature, 514, 202

[15] Balman, S. 2005, ApJ 627, 933

[16] Basko, M. M. & Sunyaev, R. A. 1976, MNRAS, 175, 395

[17] Bassan, N., et al. 2010, JCAP, 5, 010

[18] Begelman M. C. & Sikora, M. 1987, ApJ, 322, 650

[19] Bell, A. R. 2004, MNRAS, 353, 550

[20] Bellazzini, R., et al. 2007, NIMPA, 579, 853

[21] Bellazzini, R., et al. 2006, NIMPA, 566, 552

[22] Beloborodov, A. M. & Thompson, C. 2007, ApJ, 657, 967

[23] Berger, E., et al. 2012, ApJ, 748, 36

[24] Blandford, R. D. & Payne, D. G 1982, MNRAS, 199, 883

[25] Blandford, R. D. & Znajek, R. L. 1977, MNRAS, 179, 433

[26] Blandford, R., et al. 2014, Nuclear Physics B Proc.Supp., 256, 9-22

[27] Bloom, J. S., et al. 2011, Sci, 333, 203

[28] Bogovalov, S. V., et al. 2005, MNRAS, 358, 705

[29] Brenneman, L. W., et al. 2014, ApJ, 781, 83

[30] Brown, G. C., et al. 2015, MNRAS, 452, 4297

[31] Bucciantini, N., et al. 2005, A&A, 443, 519

[32] Burrows, D. N., et al. 2011, Natur, 476, 421

[33] Burwitz, V., et al. 2014, SPIE, 9144, 1

[34] Bykov, A. M., et al. 2009, MNRAS, 399, 1119

[35] Caiazzo, I. & Heyl, J. S. 2016a, in preparation

[36] Caiazzo, I. & Heyl, J. S. 2016b, in preparation

[37] Caiazzo, I. & Heyl, J. S. 2016c, in preparation

[38] Campana, R., et al. 2013, ExA, 36, 451

[39] Cara, M., et al. 2013, ApJ, 773, 186

[40] Cash, W., 1979, ApJ, 228, 939

[41] Cburazov, E., et al. 2017, MNRAS, 465, 45

[42] Celotti, A. & Matt, G. 1994, MNRAS, 268, 451

[43] Celotti, A. & Matt, G. 1994, MNRAS, 268, 451

[44] Cenko, S. B., et al. 2012, ApJ, 753, 77

[45] Chatterjee, R., et al. 2008, ApJ, 689, 79

[46] Chatterjee, R., et al. 2012, ApJ, 749, 191

[47] Churazov, E., et al. 2017, MNRAS, 465, 45

[48] Churazov, E., et al. 2010, MNRAS, 404, 1165

[49] Churazov, E., et al., 2002, MNRAS, 330, 817

[50] Connors, P. A., et al. 1980, ApJ, 235, 224

[51] Coppi, P. 1999, ASP, 161, 375

[52] Cordier, B., et al. 2015, arxiv:1512.03323

[53] Costa, E., et al. 2001, Nature, 411, 6838

[54] Cotroneo, V., et al. 2007, SPIE, 6688, 0

[55] Covino, S. & Götz, D. 2016, arxiv:1605.03588

[56] Cropper, M., et al., 1999, MNRAS 306, 684

[57] Dean, A. J., et al. 2008, Science, 321, 1183

[58] Del Zanna, L., et al. 2004, A&A, 421, 1063

[59] Donnarumma, I. & Rossi, E. 2015, ApJ, 803, 36

[60] Donnarumma, I., et al. 2015, PoS (AASKA14), 054

[61] Dovčiak, M., et al. 2008, MNRAS, 391, 32

[62] Dovčiak, M., et al. 2011, ApJ, 731, 75

[63] Drake, J. J., et al. 2008, ApJ, 678, 385

[64] Durant, M., et al. 2013, ApJ, 763, 72

[65] Elwert, G. & Haug, E. 1970, Solar Physics, 15, 234

[66] Emmanoulopoulos, D., et al. 2014, MNRAS, 439, 3931

[67] Ercolano, B., et al. 2008, ApJ, 688, 1315

[68] Ezuka, H. & Ishida, M. 1999, ApJS 120, 277

[69] Fabian, A. C., et al. 2002, MNRAS, 335, 1

[70] Fabian, A. C., et al. 2012, MNRAS, 424, 217

[71] Fabiani, S., et al. 2014, ApJS, 212, 25

[72] Fabiani, S., et al. 2013, AdSpR, 49, 143

[73] Farrell, S. A., et al. 2009, Nature, 460, 73

[74] Favata, F. & Schmitt, J. H. M. M. 1999, A&A, 350, 900

[75] Fender, R., et al. 2015, PoS (AASKA14), 051

[76] Fender, R. 2001, MNRAS, Volume 322, 31

[77] Ferguson, D. C. 1973, ApJ 183, 977

[78] Ferguson, D. C. 1976, ApJ 205, 247

[79] Fernández, R. & Davis, S.W. 2011, ApJ, 730, 131

[80] Fischer, A. & Beuermann, K. 2001, A&A 373, 211

[81] Forot, M., et al. 2008, ApJL, 688, 29

[82] Foschini, L., et al. 2006, A&A, 453, 829

[83] Foschini, L. 2014, IJMP CS 28, 1460188

[84] Foschini, L., et al. 2015, A&A 575, A13

[85] Fragile, P. C., et al. 2007, ApJ, 668, 417

[86] Fürst, F., et al. 2013, ApJ, 779, 69

[87] Gambini, R., & Pullin, J. 1999, Phys. Rev. D, 59, 124021

[88] Gastaldello, A., et al. ApJ, 800,139 (2015)

[89] Gehrels, N., et al. 2004, ApJ, 611, 1005

[90] Ghosh, P., et al, 2013, arXiv1301.5514

[91] Gilfanov, M. 2010, The Jet Paradigm, Springer-Verlag Berlin, 794, 17

[92] Gladstone, J. C., et al. 2009, MN- RAS, 397, 1836

[93] Goosmann, R. W., et al. 2014, AdSR, 54, 1341

[94] Goosmann, R. W. & Matt, G. 2011, MNRAS, 415, 3119

[95] Götz, D., et al. 2014, MNRAS 444, 2776

[96] Harding, A. K. & Lai, D. 2006, RPPh, 69, 2631

[97] Helder, E., et al. 2012, SSR, 173, 369

[98] Helder, E. & Vink, J. 2008, ApJ, 686, 1094

[99] Heisenberg, W. & Euler, H. 1936, Z. Physik, 98, 714

[100] Heitler W., 1954, Intern. Series of Monographs on Physics, Oxford: Clarendon, 1954, 3rd ed.

[101] Hellier, C., et al. 1998, MNRAS 297, 526

[102] Hellier, C. & Mukai, K. 2004, MNRAS, 352, 1037

[103] Herold, D. 1979, PhRvD, 19, 2868

[104] Heyl, J. S. & Hernquist, L. 1997, Journ. Phys. A, 30, 6485

[105] Heyl, J. S. & Shaviv, N. J. 2000, MNRAS, 311, 555

[106] Heyl, J. S. & Shaviv, N. J. 2002, Phys. Rev. D, 66, 023002

[107] Heyl, J. S. & Hernquist, L. 2005, MNRAS, 362, 777

[108] Hoormann, J. K., et al. 2016, PhRvD, 93, 4020

[109] Ingram, A., et al. 2009, MNRAS, 397, 101

[110] Ingram A., et al. 2015, ApJ, 807, 53

[111] Israel, G., et al. 2008, ApJ, 685, 1114

[112] Israel, G., et al. 2016, in press (arXiv160907375I)

[113] Jaeckel, J. & Ringwald, A. 2010, Ann. Rev. Nucl. Part. Sci., 60, 405

[114] Jiang, Y.-F., et al. 2014, ApJ, 796, 106

[115] Jorstad, S., et al. 2005, AJ, 130, 1418

[116] Jourdain, E., et al. 2012, ApJ, 761, 27

[117] Kallman, T., et al 2015, ApJ, 815, 53

[118] Kara, E., et al. 2016, in press (arXiv:1606.06736)

[119] Kennel, C. F. & Coroniti, F. V. 1984, ApJ, 283, 710

[120] Kiehlmann, S., et al. 2016, A&A, 590, 10

[121] Kluzniak, W. & Lasota, J.-P. 2015, MNRAS, 448, 43

[122] Komarov, S. V., et al., in press (arXiv:1604.08669)

[123] Komissarov, S. S. & Lyubarsky, Y. E. 2003, MNRAS, 344, 93

[124] Komossa, S. 2015, JHEAP, 7, 148

[125] Kontar, E. P., et al. 2011, SSRev., 159, 301

[126] Koyama, K., et al. 1996, PASJ, 48, 249

[127] Kraus, M., et al 2003, ApJ, 590, 424

[128] Krawczynski, H. 2012, ApJ, 754, 133

[129] Krawczynski, H., et al. 2013, arXiv:1303.7158v1

[130] Lamb, D. Q. & Masters, A. R. 1979, ApJ, 234, 117

[131] Larionov, V., et al. 2010, A&A, 510, 93

[132] Larionov, V. M., et al. 2016, Galaxies, 4, 43

[133] Laurent, P., et al. 2011, Science, 332, 438

[134] Leahy, D. A., et al. 2008, ApJ, 672, 1119

[135] Leahy, D. A., et al. 2011, ApJ, 742, 17

[136] Leahy, D. A., et al. 2009, ApJ, 691, 1235

[137] Levan, A., et al. 2011, Sci, 333, 199

[138] Liberati, S., & Maccione, L. 2009, Ann. Rev. Nucl. Part. Sci., 59, 245

[139] Lister., M. L., et al. 2016, ApJ, 152, 12

[140] Lo, K. H., et al. 2013, ApJ, 776, 19

[141] Lodato, G. & Rossi, E. M. 2011, MNRAS, 410, 359

[142] Lynden-Bell, D. 1969, Nature, 223, 690

[143] Lyubarsky, Y. E. 2002, MNRAS, 329, 34

[144] Maccarone, T. 2005, MNRAS, 360, 68

[145] Maiani, L., et al. 1986, Phys. Lett. B, 175, 359

[146] Marcowith, A., et al. 2016, Reports on Progress in Physics, 79, 4

[147] Marin F., et al. 2015, A&A, 576, 19

[148] Marin, F., et al. 2014, MNRAS, 441, 3170

[149] Marinucci, A., et al. 2016, MNRAS, 456, 94

[150] Marin, F., et al. 2016, A&A, 591, 23

[151] Marin, F., et al. 2012, MNRAS, 426, 101

[152] Marinucci, A., et al. 2014, ApJ, 787, 83

[153] Markevitch, M., et al. 1993, Nature, 364, 40

[154] Markoff, S., et al. 2005, ApJ, 635, 1203

[155] Markowitz, A. G., et al. 2014, MNRAS, 439, 1403

[156] Marscher, A. P. 2014, ApJ, 780, 87

[157] Marscher, A. P. & Gear, W. K. 1985, ApJ, 298, 114

[158] Marscher, A. P., et al. 2008, Nature, 452, 966

[159] Marscher, A. P., et al. 2010, ApJL, 710, 126

[160] Massaro, E., et al. 2006 A&A, 459, 859

[161] Mastrano, A., et al. 2013, MNRAS, 434, 1658

[162] Matt, G. 2004, A&A, 423, 495

[163] Matt, G. 1993, MNRAS, 260, 663

[164] Mattingly, D. 2005, Living Rev. Relativity, 8, 5

[165] McNamara, A., et al., 2009, MNRAS, 395, 1507

[166] McNamara, A. L., et al. 2008b, MNRAS 383, 962.

[167] McNamara, A. L., et al. 2008a, MNRAS 386, 2167

[168] Meszaros, P. & Ventura, M. 1979, PhRvD, 19, 3565

[169] Mészáros, P. & Nagel, W. 1985, ApJ, 299, 138

[170] Mèszáros, P., et al. 1988, ApJ, 324, 1056

[171] Metzger, B. et al. 2015, ApJ, 806, 224

[172] Middleton, M. J., et al. 2015, MNRAS, 447, 3243

[173] Migliari, S., et al. 2002, Science, 297, 1673

[174] Mignani, R. P., et al. 2016, MNRAS, in press

[175] Miller, M. C. & Lamb, F. K. 2015, ApJ, 808, 31

[176] Miller, L., et al. 2009, MNRAS, 399, 69

[177] Miniutti, G. & Fabian, A. C. 2004, MNRAS, 349, 1435

[178] Miniutti, G., et al. 2007, PASJ, 59, 315

[179] Mirabel, I. & Rodríguez, L. 1999, ARA&A, 37, 409

[180] Mirabel, I. & Rodríguez, L. 1994, Nature, 371, 46

[181] Morales-Rueda, L., et al. 2002, MNRAS, 329, 597

[182] Moran, P., et al. 2013, in press (arXiv1302.3622)

[183] Muleri, F., et al. 2010, NIMPA, 620, 285

[184] Muleri, F., et al. 2008, NIMPA, 584, 149

[185] Muleri, F., et al. 2016, SPIE, 9905, 99054

[186] Mundell, C. G., et al. 2013, Nature, 504, 119

[187] Muno, M., et al. 2007, ApJ, 656, 69

[188] Mushtukov, A. A. 2015, MNRAS, 454, 2539

[189] Nakamura, Y. & Shibata, S. 2007, MNRAS, 381, 1489

[190] Nättilä J., et al. 2016, A&A, 591, 25

[191] Nenkova, M., et al. 2008, ApJ, 685, 147

[192] Nobili, L., et al. 2008, MNRAS, 386, 1527

[193] Olmi, B., et al. 2015, MNRAS, 449, 3149

[194] Osten, R. A, et al. 2007, ApJ, 654, 1052

[195] Pacciani, L., et al. 2003, SPIE, 4843, 394

[196] Paragi, Z., et al. 2015, PoS (AASKA14), 143

[197] Pareschi, G., et al. 2004, SPIE, 5488, 481

[198] Parker, M. L., et al. 2014, MNRAS, 443, 1723

[199] Pasham, D. R., et al. 2014, Nature, 513, 74

[200] Patruno, A. & Watts, A. 2012, arXiv:1206.2727

[201] Petropoulou, M., et al. 2015, MNRAS, 448, 2412

[202] Phinney, E. S. 1989, Natur, 340, 595

[203] Ponti, G., et al. 2010, ApJ, 714, 732

[204] Porth, O., et al. 2014, MNRAS, 438, 278

[205] Porth, O., et al. 2013, MNRAS, 431, 48

[206] Poutanen, J. 2008, AIP, 1068, 77

[207] Poutanen, J. & Gierlinski M. 2003, MNRAS, 343, 1301

[208] Poutanen, J., et al. 1994, ApJS, 92, 607

[209] Poutanen, J., et al. 2014, MNRAS, 442, 3777

[210] Prandoni, I. & Seymour, N. 2015, PoS (AASKA14), 067

[211] Psaltis, D., et al. 2014, ApJ 787, 136

[212] Pshirkov, M. S., et al. 2016, Phys. Rev. Lett. 116, 191302

[213] Raban, D., et al. 2009, MNRAS, 394, 1325

[214] Radhakrishnan, V. & Cooke, D.J. 1969, Astrophysics Letters, 3, 225

[215] Raiteri, C., et al. 2012, A&A, 545, A48

[216] Rees, M. J. 1988, Natur, 333, 523

[217] Reis, R. C. & Miller, J. M. 2013, ApJ, 769, 7

[218] Revnivtsev, M., et al. 2004, A&A, 425, 49

[219] Risaliti, G., et al. 2002, ApJ, 571, 234

[220] Rosen, S. R., et al. 1988, MNRAS 231, 549

[221] Rovelli, C. & Speziale, S. 2003, Phys. Rev. D, 67, 064019

[222] Russell, D. & Shahbaz, T. 2014, MNRAS, 438, 2083

[223] Salvaterra, R., et al. 2009, Nature, 461, 1258

[224] Sauli, F., et al. 1997, NIMPA, 386, 531

[225] Saxton, C. J., et al. 2012, MNRAS, 422, 1625

[226] Saxton, C., et al. 2005, MNRAS, 360, 1091

[227] Sazonov, S.Y., et al. 2002, MNRAS, 333, 191

[228] Schmitt, J. H. M. M. & Favata, F. 1999, Nature, 401, 44

[229] Schmitt, J. H. M. M., et al. 2003, A&A, 412, 849

[230] Schnittman, J. D. & Krolik, J. H. 2009, 701, 1175

[231] Schnittman, J. D. & Krolik J. H. 2010, ApJ, 712, 908

[232] Schnittman, J. D. & Krolik J. H. 2013, ApJ, 777, 11

[233] Schweizer, T., et al. 2013, MNRAS, 433, 3325

[234] Schwinger, J. 1951, Physical Review, 82, 664

[235] Shakura, N. I, & Sunyaev, R. A 1973, A&A, 24, 337

[236] Shakura, N. I. & Sunyaev, R. A. 1973, A&A, 24, 337

[237] Sironi, L., & Spitkovsky, A. 2014, ApJL, 783, 21

[238] Slowikowska, A., et al. 2009, MNRAS, 397, 103

[239] Smith, R. K., et al. 2001, ApJ, 556, 91

[240] Soffitta, P., et al. 2013, NIMPA, 700, 99

[241] Spiga, D. & Cotroneo, V. 2010, SPIE, 7732, 2

[242] Spiga, D., et al. 2011, A&A, 529, 18

[243] Stark, R. F. & Connors, P. A. 1977, Nature, 266, 429

[244] Strohmayer, T. E. & Kallman, T. R. 2013, ApJ, 773, 103

[245] Suleimanov V., et al., 2011, ApJ, 742, 122

[246] Sunyaev, R., et al. 1993, ApJ, 407, 606

[247] Sutton, A. D., et al. 2013, MNRAS, 435, 1758

[248] Takei, D., et al., 2015, ApJ 801, 92

[249] Tanaka, Y., et al. 1995, Nature, 375, 659

[250] Tanvir, N. R., et al. 2009, Nature, 461, 1254

[251] Taverna, R., et al. 2014, MNRAS, 438, 1686

[252] Taverna, R., et al. 2015, MNRAS, 454, 3254

[253] Testa, P., et al. 2008, ApJ, 675, 97

[254] Thompson, C. & Duncan, R.C. 1995, MNRAS, 397, 763

[255] Thompson, C., et al. 2002, ApJ, 574, 332

[256] Titarchuk L., et al. 2009, ApJ 700, 1831

[257] Toma, K., et al. 2012, PhRvL, 109, 1104

[258] Trümper, J. E., et al. 2013, ApJ, 764, 49

[259] Turolla, R., et al. RPPh, 78, 116901

[260] Valinia, A., et al. 2000, ApJ, 543, 733

[261] Van Adelsberg, M. & Lai, D. 2006, MNRAS, 373, 1495

[262] van den Eijnden J., et al. 2016, MNRAS, 458, 3655

[263] Van Velzen, S., et al. 2011, ApJ, 741, 73

[264] Van Velzen, S., et al. 2016, Science, 351, 62

[265] Ventura, M. & Meszaros, P. 1979, ApJ, 233, 125

[266] Viganò, D., et al. 2012, J. Phys. Conf. Ser., 342, 012013

[267] Viironen K. & Poutanen J. 2004, A&A, 426, 985

[268] Volpi, D., et al. 2008, A&A, 485, 337

[269] Vrielmann S., et al. 2005, A&A, 439, 287.

[270] Warner, B. 1995, Cataclysmic Variable Stars, Cambridge Univ. Press

[271] Weisskopf, M. C., et al. 2010, SPIE, 7732, 7732

[272] Weisskopf, M. C., et al. 2000, ApJ, 536, 81

[273] Weisskopf, M. C., et al. 1978, ApJL, 221, 13

[274] Weisskopf, M. C., et al. 1978, ApJL, 220, 117

[275] Weisskopf, M. C., et al. 1977, ApJ, 215, 65

[276] Weisskopf, V. S. 1936, Kongelige Danske Vidensk-aberns Selskab, Mathematisk-Fysiske Meddelelser, 14, 1

[277] Wiersema, K., et al. 2012, MNRAS, 421, 1942

[278] Wiersema, K., et al. 2014, Nature, 509, 201

[279] Wijnands, R., et al. 2005, ApJ, 619, 492

[280] Wilms, J., et al. 2001, MNRAS, 328, 27

[281] Woelk, U. & Beuermann, K. 1996, A&A, 306, 232

[282] Wu, K., et al. 1994, ApJ, 426, 664

[283] Wykes, S., et al. 2015, MNRAS, 447, 1001

[284] Yang, X.-J., et al. 2011, A&A, 11, 457

[285] Zane, S., et al. 2016, SPIE, 9905, 99054

[286] Zauderer, A., et al. 2011, Nature, 476, 425

[287] Zauderer, A., et al. 2013, ApJ, 767, 152

[288] Zdziarski, A., et al. 2004, MNRAS, 351, 791

[289] Zhang, H. & Böttcher, M. 2013, ApJ, 774, 18

[290] Zhang, H., et al. 2014, ApJ, 789, 66

[291] Zhang, H., et al. 2015, ApJ, 804, 58

[292] Zhang, H., et al. 2017, in preparation

[293] Zhuravleva, I. V., et al. 2010, MNRAS, 403, 129

10 List of Acronyms

AD	Applicable Document
AFE	Agency Furnished Equipment
AGN	Active Galactic Nuclei
AIV	Assembly Integration & Verification
AIT	Assembly Integration & Test
ALP	Axion-like particle
AMP	Accreting millisecond pulsar
ASI	Agenzia Spaziale Italiana (Italian Space Agency)
BEE	Back-End Electronic
BMB	BEE Back-Plate and Mother Board
CBK	Space research Center Poland
CDR	Critical Design Review
CFDP	CCSDS File Transfer Protocol
CV	Cataclismic Variable
DAQ	DAQ e pre-processing board
DP	Data Processing & I/F Board
DTM	DU Thermal & Mechanical I/F
DU	Detector Unit
DUH	DU Housing
DWI	Deviation Work Item
ECSS	European Cooperation for Space Standardisation
EGSE	Electrical Ground Support Equipment
EM	Electrical Model
EMC	Electro-Magnetic Compatibility
ESA	European Space Agency
ESD	Electro Static Discharge
FPA	Focal Plane Assembly
FDE	FPA DU Enclosure and Shielding
FAR	Final Acceptance Review
FCB	FCW control drivers board
FCL	FCW Lid
FCP	FPA Composite Plane
FCW	Filter & Calibration Wheel
FCO	Functional Check-Out
FCS	Filter & Calibration Set
FEM	Finite Element Model
FM	Flight Model
FoV	Field of View
FoR	Field of Regard
FPR	FPA Interface Ring
FR	Flight Representative
FSI	FPA Support Items
FS	Flight Spare
FSS	FPA Support Structure
FTC	FPA Thermal control
FRR	Flight Readiness Review
GAM	GPD ASIC Miniboard
GPD	Gas Pixel Detector
GPT	GPD Peltier & Thermal I/F
GR	General Relativity
GRB	Gamma-ray Burst
GSE	Ground Support Equipment
HEW	Half Energy Width
HID	Harness ICU to DU
HVB	HV Power Board
HW	Hardware
ICU	Instrument Control Unit
ICA	Instrument Control Unit Case

I/F	Interface
I/O	Input/Output
IOC	Instrument Operation Center
INAF	Istituto Nazionale di Astrofisica
INFN	Istituto Nazionale Fisica Nucleare
INTA	Instituto Nacional de Técnica Aeroespacial
KO	Kick Off
LEO	Low Earth Orbit
LIV	Lorentz Invariance Violation
LOS	Line Of Sight
LVB	DC/DC & LV Power Board
MAIT	Mechanical AIT
MDP	Minimum Detectable Polarization
MM	Mirror Module
MOC	Mission Operation Center
MPE	Max-Planck-Institute für Extraterrestrische Physik
MRB	Material Review Board
MSSL	Mullard Space Science Laboratory
MTQ	Magnetic Torquers
NCR	No Conformance Report
OGSE	Optical Ground Support Equipment
OGS	Operational Ground Segment
OTAC	Observing Time Allocation Committee
PA	Product Assurance
PM	Power Distribution and Memory Board
PDR	Preliminary Design Review
P/L	Payload
PLM	Payload Module
PTB	Peltier Thermal Control Board
PVS	Procedure Variation Sheets
PWN	Pulsar Wind Nebula
QED	Quantum electrodynamics
QLA	Quick Look analysis
QM	Qualification Model
QPO	Quasi Periodic Oscillation
RFW	Request For Waiver
RFD	Request For Deviation
RPP	Rotation powered pulsars
S/C or SC	Spacecraft
SDC	Science Data Center
SED	Spectral Energy Distribution
SGS	Science Ground Segment
SKA	Square Kilometer Array
SMBH	Supermassive black-hole
SNR	Supernova Remnant
SOC	Science Operation Center
SVM	Service Module
TDE	Tidal Disruption Event
ToO	Target of Opportunity
UCL	University College London
ULX	Ultra-luminous X-ray source
UoG	University of Geneva
UV	University of Valencia
XPOL	*XIPE* Instrument
XRN	X-ray Reflection Nebula
XRP	X-ray pulsar
WD	White Dwarf